



MODELIZATION, SIMULATION AND DESIGN OF MICRO-ELECTRO-MECHANICIZED SYSTEMS (MEMS) PRECONCENTRATORS FOR GAS SENSING
Roser Inglés Bort

ISBN: 978-84-694-0327-3
Dipòsit Legal: T-198-2011

ADVERTIMENT. La consulta d'aquesta tesi queda condicionada a l'acceptació de les següents condicions d'ús: La difusió d'aquesta tesi per mitjà del servei TDX (www.tesisenxarxa.net) ha estat autoritzada pels titulars dels drets de propietat intel·lectual únicament per a usos privats emmarcats en activitats d'investigació i docència. No s'autoritza la seva reproducció amb finalitats de lucre ni la seva difusió i posada a disposició des d'un lloc aliè al servei TDX. No s'autoritza la presentació del seu contingut en una finestra o marc aliè a TDX (framing). Aquesta reserva de drets afecta tant al resum de presentació de la tesi com als seus continguts. En la utilització o cita de parts de la tesi és obligat indicar el nom de la persona autora.

ADVERTENCIA. La consulta de esta tesis queda condicionada a la aceptación de las siguientes condiciones de uso: La difusión de esta tesis por medio del servicio TDR (www.tesisenred.net) ha sido autorizada por los titulares de los derechos de propiedad intelectual únicamente para usos privados enmarcados en actividades de investigación y docencia. No se autoriza su reproducción con finalidades de lucro ni su difusión y puesta a disposición desde un sitio ajeno al servicio TDR. No se autoriza la presentación de su contenido en una ventana o marco ajeno a TDR (framing). Esta reserva de derechos afecta tanto al resumen de presentación de la tesis como a sus contenidos. En la utilización o cita de partes de la tesis es obligado indicar el nombre de la persona autora.

WARNING. On having consulted this thesis you're accepting the following use conditions: Spreading this thesis by the TDX (www.tesisenxarxa.net) service has been authorized by the titular of the intellectual property rights only for private uses placed in investigation and teaching activities. Reproduction with lucrative aims is not authorized neither its spreading and availability from a site foreign to the TDX service. Introducing its content in a window or frame foreign to the TDX service is not authorized (framing). This rights affect to the presentation summary of the thesis as well as to its contents. In the using or citation of parts of the thesis it's obliged to indicate the name of the author.

Roser Inglés Bort

MODELIZATION, SIMULATION AND DESIGN
OF MICRO-ELECTRO-MECHANICAZED
SYSTEMS (MEMS) PRECONCENTRATORS FOR
GAS SENSING.

DOCTORAL THESIS

Directed by Jose Luis Ramirez

Department of Electronic, Electrical
and Automatic Control Engineering



UNIVERSITAT ROVIRA I VIRGILI

Tarragona
2010

UNIVERSITAT ROVIRA I VIRGLI
MODELIZATION, SIMULATION AND DESIGN OF MICRO-ELECTRO-MECHANICAZED SYSTEMS (MEMS) PRECONCENTRATORS
FOR GAS SENSING
Roser Inglés Bort
ISBN:978-84-694-0327-3/DL:T-198-2011

UNIVERSITAT ROVIRA I VIRGLI
MODELIZATION, SIMULATION AND DESIGN OF MICRO-ELECTRO-MECHANICAZED SYSTEMS (MEMS) PRECONCENTRATORS
FOR GAS SENSING
Roser Inglés Bort
ISBN:978-84-694-0327-3/DL:T-198-2011

UNIVERSITAT ROVIRA I VIRGLI
MODELIZATION, SIMULATION AND DESIGN OF MICRO-ELECTRO-MECHANICAZED SYSTEMS (MEMS) PRECONCENTRATORS
FOR GAS SENSING
Roser Inglés Bort
ISBN:978-84-694-0327-3/DL:T-198-2011



UNIVERSITAT
ROVIRA I VIRGILI

ESCOLA TÈCNICA SUPERIOR D'ENGINYERIA
DEPARTAMENT D'ENGINYERIA ELECTRONICA, ELÈCTRICA I AUTOMÀTICA

Avinguda dels Països Catalans, 26
Campus sescelades
43007 Tarragona
Tel. (977) 55 96 10
Fax (977) 55 96 05
e-mail: secelec@etse.urv.es
<http://www.etse.urv.es/DEEEA/>

I STATE that the present study, entitled "MODELIZATION, SIMULATION AND DESIGN OF MICRO-ELECTRO-MECHANICAZED SYSTEMS (MEMS) PRECONCENTRATORS FOR GAS SENSING", presented by Roser Inglés Bort for the award of the degree of Doctor, has been carried out under my supervision at the Department of Electrical, Electronic and Automatic Control Engineering of this university, and that it fulfils all the requirements to be eligible for the European Doctorate Award.

Tarragona, 26th July 2010

Doctoral Thesis Supervisor

Dr. José Luis Ramírez Falo

UNIVERSITAT ROVIRA I VIRGLI
MODELIZATION, SIMULATION AND DESIGN OF MICRO-ELECTRO-MECHANICAZED SYSTEMS (MEMS) PRECONCENTRATORS
FOR GAS SENSING
Roser Inglés Bort
ISBN:978-84-694-0327-3/DL:T-198-2011

Als meus, en especial als més petits:
Pau, Cesar, Jordi, Izan, Lidia, Miquel i Marina

A Iván,
por el tiempo que te he robado

UNIVERSITAT ROVIRA I VIRGLI
MODELIZATION, SIMULATION AND DESIGN OF MICRO-ELECTRO-MECHANICAZED SYSTEMS (MEMS) PRECONCENTRATORS
FOR GAS SENSING
Roser Inglés Bort
ISBN:978-84-694-0327-3/DL:T-198-2011

Agraïments

Voldria agrair a la Universitat Rovira i Virgili l'oportunitat que m'ha ofert al concedir-me la beca sense la qual no hagués estat possible aquest treball. També voldria agrair a tota la gent que ha fet possible el desenvolupament d'aquest treball, per tal de no deixar-me a ningú voldria fer-ho de manera general.

En primer lloc, no puc deixar de nomenar al meu tutor Jose Luis Ramirez per haver-me guiat, escoltat i animat tots aquests anys, especialment en els moments més difícils. Així com a la resta de professors del grup i del departament que m'han ajudat durant aquestos anys.

A tots els companys del grup MINOS, que han deixat la seva petjada en el camí per fer-nos més fàcil el viatge als que anem darrera i a tots els que han fet amb mi aquest viatge. Espero haver estat bona companya de viatge i haver deixat un bon llegat als que vénen darrera.

A Raul Calavia i a tots els tècnics que han fet molt menys dura l'àrdua feina. A Anne Marié Gué i a tots els companys del LAAS que van fer la meva estada molt profitosa i hem van ajudar en tot moment. A Isabel Gràcia i els companys del CNM que m'han ajudat en la fabricació dels dispositius.

Finalment, a la família i amics que han estat sempre al meu costat oferint-me el seu amor i la comprensió i paciència que més he necessitat.

Moltes gràcies a tots,

UNIVERSITAT ROVIRA I VIRGLI
MODELIZATION, SIMULATION AND DESIGN OF MICRO-ELECTRO-MECHANICAZED SYSTEMS (MEMS) PRECONCENTRATORS
FOR GAS SENSING
Roser Inglés Bort
ISBN:978-84-694-0327-3/DL:T-198-2011

Resumen

Hoy en día, la normativa sobre gases que son tóxicos a muy bajas concentraciones se está haciendo muy estricta. Por esta razón, los dispositivos que permiten la detección de estos gases a bajas concentraciones se están investigando cada vez más. En este marco, los preconcentradores están tomando un papel importante.

En esta tesis se hace un estudio sobre preconcentradores planos fabricados en silicio, con la idea de poder integrarlos con el sistema sensor. Estos preconcentradores se han simulado para comprender mejor su funcionamiento. Se ha hecho un estudio para conseguir una óptima homogenización de temperatura en el área calentada y así obtener un pico de desorción estrecho.

Se han desarrollado nuevos diseños con calefactores optimizados. También se han fabricado membranas grandes para poder depositar más material adsorbente y así incrementar la capacidad de concentración. Los nuevos diseños han sido fabricados y caracterizados para validar las simulaciones y poder crear un modelo que sirva para probar nuevas ideas de diseño evitando los largos y costosos procesos de fabricación.

Abstract

Nowadays the allowed limits of volatiles that are toxic at very low concentrations are becoming restrictive. For this reason, preconcentrators which let detection at low levels are becoming more important and its study is increasing.

In this thesis, our aim is to design a planar preconcentrator in silicon technology, in order to be able to design in the same substrate the preconcentrator and the sensor system. Simulations have been developed to study its behaviour. A good homogenisation temperature is needed in order to obtain big concentrations in a narrow desorption peak.

We will develop new designs which improve homogenisation temperature. Also, a large area is needed in order to have more adsorbent material which ensures more concentration. New design have been fabricated and characterized. Experimental results validate our simulations and let us to develop future designs avoiding time and cost fabrication.

UNIVERSITAT ROVIRA I VIRGLI
MODELIZATION, SIMULATION AND DESIGN OF MICRO-ELECTRO-MECHANICAZED SYSTEMS (MEMS) PRECONCENTRATORS
FOR GAS SENSING
Roser Inglés Bort
ISBN:978-84-694-0327-3/DL:T-198-2011

Publication List

International Conferences

1. Roser Inglés, Jose Luis Ramírez, Xavier Vilanova, Xavier Correig, Eduard Llobet, **Electro-thermal simulation of preconcentration membranes using finite elements tools**, *Gas and Radiation Sensors: Characterisation. Properties. Thin film based sensors*, July 7-9 2008, Salamanca (Spain), **Poster**.
2. Roser Inglés; Jordi Pallarés; Jose Luis Ramirez; Eduard Llobet, **Fluid Flow Simulation of Preconcentration Membranes Using Finite Elements Tools**, *Comsol Conference 2009*, October 14-16 2009, Milano (Italia), **Poster**, Proceedings of the Comsol Conference Milan 2009 ISBN: 978-0-9825697-0-2
3. Roser Inglés, Jordi Pallarés, Jose Luis Ramirez, **Improving sample flow in planar preconcentrator**, *International Conference on Computational and Mathematical Methods in Science and Engineering*, June 26-30 2010, Almeria (Spain), **Oral presentation**, Proceedings of the 2010 International Conference on Computational and Mathematical Methods in Science and Engineering. ISBN 13: 978-84-613-5510-5
4. Roser Inglés, Jordi Pallares, Isabel Gràcia, Anne Marié Gué, Jose Luis Ramírez, **Electro-thermal simulation and characterization of preconcentration membranes**, *Eurosensors XXIV*, September 5-8, 2010, Linz, Austria, **Poster**, Proceedings Eurosensors XXIV.
5. Roser Inglés, Jordi Pallares, Isabel Gràcia, Anne Marié Gué, Jose Luis Ramírez, **Electro-thermal simulations to improve heater design in preconcentration membranes**, *Therminic*, October 6-8, 2010, Barcelona, Spain, **Poster**, Therminic Proceedings.

UNIVERSITAT ROVIRA I VIRGLI
MODELIZATION, SIMULATION AND DESIGN OF MICRO-ELECTRO-MECHANICAZED SYSTEMS (MEMS) PRECONCENTRATORS
FOR GAS SENSING
Roser Inglés Bort
ISBN:978-84-694-0327-3/DL:T-198-2011

Figure list

Figure I.1: Papers with topic “preconcentrator” in Web of science (*July 2010)	8
Figure I.2: Comparison of the analyte concentration and time constant in micromachined and conventional preconcentrators[3].....	9
Figure I.3: Schematic of a suspended-membrane-type gas sensor: a) top view; b) side view[6].....	10
Figure I.4 Schematic of a suspended-membrane-type gas sensor: a)top view; b) side view[6].....	11
Figure I.5: Schematic of micro-hotplates without (s) and with (b) Si island. [16].....	12
Figure I.6: Photograph (real view) and schematic cross section of simple meandered microheater resistor [23]	13
Figure I.7: Microhotplate with a silicon plug [24].....	14
Figure I.8: Principal layers of a microhotplate that is fabricated in CMOS technology and used as a micropreconcentrator.[27].....	14
Figure I.9 Novel loop-shaped [11].....	14
Figure I.10: Schematic drawing of the ‘S shaped sensor and polysilicon heater (top view) [30]	15
Figure I.11: Pt double spiral resistor [9]	15
Figure I.12: Simulated power consumption for three different membranes versus the membrane size at 350 °C average temperature.[40].....	17
Figure I.13: Simulated temperature across the chip for membranes with (—) and without silicon plug. 0.0 corresponds to 0 °C and 1.0 to the maximum temperature in °C.[40]	17
Figure II-1: Initial design: a) A view from the top of the membrane b) A cross sectional view of the membrane.....	24
Figure II-2: Heat evacuation	27
Figure II-3: Piece of silicon with air in the bottom.....	27
Figure II-4: Piece of silicon with air in the bottom. Red line defines next temperature profile	28
Figure II-5: Temperature profile with two different heat flux	28
Figure II-6: Temperature distribution of the whole system	29
Figure II-7: Temperature distribution on plane x-y	29
Figure II-8: Temperature profile in the x axis (red line in Figure II-6)	30
Figure II-9: Temperature profile in the y axis (red line in Figure II-7)	30
Figure II-10: Temperature distribution of the whole system (10 V).....	31
Figure II-11: Temperature distribution on plane x-y (10 V).....	31
Figure II-12: Temperature profile in the x axis (10 V) (red line in Figure II-10).....	32
Figure II-13: Temperature profile in the y axis (10 V) (red line in Figure II-11).....	32
Figure II-14: Contact between membrane and silicon bulk.....	33
Figure II-15: Initial design	34
Figure II-16: Localization points	34
Figure II-17: Dynamic response initial design.....	35
Figure II-18: x-y temperature distribution for initial design.....	35
Figure II-19: Temperature profile along diagonal for initial design.....	36
Figure II-20: Area where $\Delta T < 15$ K. (Red line will be used to compare this area).....	37
Figure II-21: Area comparison.....	37
Figure II-22: Power consumption as a function of distance from the heater to the edge membrane	38
Figure II-23: Design “4 heaters”	39
Figure II-24: x-y temperature distribution “4 heaters”	39
Figure II-25: Area where $\Delta T < 15$ K (4 heaters)	40
Figure II-26: Area where $\Delta T < 25$ K (4 heaters)	40

Figure II-27: Area where $\Delta T < 30$ K (4 heaters)	41
Figure II-28: Design “around the oval”	41
Figure II-29: x-y temperature distribution “around the oval”	42
Figure II-30: Area where $\Delta T < 15$ K (Around the oval).....	42
Figure II-31: Area where $\Delta T < 25$ K (Around the oval).....	43
Figure II-32: Area where $\Delta T < 60$ K (Around the oval).....	43
Figure II-33: Design “15-30-60-80”	44
Figure II-34: x-y temperature distribution “15-30-60-80”	44
Figure II-35: Area where $\Delta T < 15$ K (15-30-60-80).....	45
Figure II-36: Area where $\Delta T < 25$ K (15-30-60-80).....	45
Figure II-37: Temperature profile along the diagonal for new designs	46
Figure II-38: Red line defines the diagonal profile.....	48
Figure II-39: Initial design with a silicon plug thickness 5 μm	48
Figure II-40: Initial design with a silicon plug thickness 10 μm	49
Figure II-41: Temperature profile along the diagonal initial design with silicon plug.....	49
Figure II-42: Dynamic response initial design with different silicon plugs	50
Figure II-43: Silicon plug beneath the 15-30-60-80 heater.....	51
Figure II-44: Temperature profile along the diagonal 15-30-60-80 design with different thickness of silicon plug	51
Figure II-45: Power consumption as a function of distance from the silicon plug to the edge membrane.....	52
Figure III-1: Heater design for membrane 1.5 mm x 5 mm.....	58
Figure III-2: Track thickness for design A for membrane 1.5 mm x 5 mm.....	58
Figure III-3: Separation between tracks in design A for membrane 1.5 mm x 5 mm	58
Figure III-4: Temperature distribution at heater design A, membrane 1.5 mm x 5 mm.....	59
Figure III-5: Heated area within a difference of 25 K at heater design A, membrane 1.5 mm x 5 mm	59
Figure III-6: Diagonal profile along the diagonal heater design A membrane 1.5 mm x 5 mm	60
Figure III-7: Second heater design for membrane 1.5 mm x 5 mm.....	60
Figure III-8: Track thickness for design B for membrane 1.5 mm x 5 mm.....	61
Figure III-9: Separation between tracks in design B for membrane 1.5 mm x 5 mm.....	61
Figure III-10: Temperature distribution at heater design B, membrane 1.5 mm x 5 mm.....	61
Figure III-11: Heated area within a difference of 25 K at heater design B, membrane 1.5 mm x 5 mm	62
Figure III-12: Diagonal profile along the diagonal heater design B, membrane 1.5 mm x 5 mm.....	62
Figure III-13: Comparison between two heaters designed for membrane 1.5 mm x 5 mm	63
Figure III-14: Heater design for membrane 2 mm x 4.5 mm.....	64
Figure III-15: Track thickness for design A for membrane 2 mm x 4.5 mm.....	64
Figure III-16: Separation between tracks in design A for membrane 2 mm x 4.5 mm	64
Figure III-17: Temperature distribution at heater design A, membrane 2 mm x 4.5 mm.....	65
Figure III-18: Heated area within a difference of 25 K at heater design A, membrane 2 mm x 4.5 mm	65
Figure III-19: Diagonal profile along the diagonal heater design A, membrane 2 mm x 4.5 mm ...	66
Figure III-20: Second heater design for membrane 2 mm x 4.5 mm.....	66
Figure III-21: Temperature distribution at heater design B, membrane 2 mm x 4.5 mm.....	67
Figure III-22: Heated area within a difference of 25 K at heater design B, membrane 2 mm x 4.5 mm	67

Figure III-23: Diagonal profile along the diagonal heater design B, membrane 2 mm x 4.5 mm.....	68
Figure III-24: Comparison between two heaters designed for membrane 2 mm x 4.5 mm	68
Figure III-25: Heater design for membrane 3 mm x 3 mm.....	69
Figure III-26: Temperature distribution at heater design, membrane 3 mm x 3 mm	69
Figure III-27: Heated area within a difference of 25 K at heater design, membrane 3 mm x 3 mm ..	70
Figure III-28: Diagonal profile along the diagonal heater design, membrane 3 mm x 3 mm	70
Figure III-29: Temperature distribution heater design A membrane 1.5 mm x 5 mm with a silicon plug	73
Figure III-30: Temperature distribution heater design B membrane 1.5 mm x 5 mm with a silicon plug	73
Figure III-31: Heated area with a difference of 25 K heater design A membrane 1.5 mm x 5 mm ..	74
Figure III-32: Heated area with a difference of 25 K heater design B membrane 1.5 mm x 5 mm ..	74
Figure III-33: Diagonal temperature profiles both heaters design membrane 1.5 mm x 5 mm with a silicon plug.....	74
Figure III-34: Temperature distribution heater design A membrane 2 mm x 4.5 mm with a silicon plug	75
Figure III-35: Temperature distribution heater design B membrane 2 mm x 4.5 mm with a silicon plug	75
Figure III-36: Heated area with a difference of 25 K heater design A membrane 2 mm x 4.5 mm ..	76
Figure III-37: Heated area with a difference of 25 K heater design B membrane 2 mm x 4.5 mm ..	76
Figure III-38: Diagonal temperature profiles both heaters design membrane 2 mm x 4.5 mm with a silicon plug.....	76
Figure III-39: Temperature distribution membrane 3 mm x 3 mm with a silicon plug.....	77
Figure III-40: Heated area with a difference of 25K membrane 3 mm x 3 mm	77
Figure III-41: Diagonal temperature profiles membrane 3 mm x 3 mm with a silicon plug.....	77
Figure IV-1: Mask wafer design	82
Figure IV-2: Encapsulated membrane	82
Figure IV-3: Infra red camera with multimeter and computer control	83
Figure IV-4: Infra red camera	84
Figure IV-5: Multimeter and circuit for T8 encapsulated devices.....	84
Figure IV-6: Initial design. Infra red camera image at ambient temperature	85
Figure IV-7: Initial design. Post-processed image at ambient temperature.....	88
Figure IV-8: Experimental set up for temperature dependence extraction.....	89
Figure IV-9: Membrane 1 mm x 3 mm encapsulated. Resistance versus voltage.....	90
Figure IV-10: Membrane 1 mm x 3 mm encapsulated. Maximum temperature versus voltage.	90
Figure IV-11: Membrane 1 mm x 3 mm non encapsulated. Resistance versus voltage.....	91
Figure IV-12: Membrane 1 mm x 3 mm non encapsulated. Maximum temperature versus voltage.	91
Figure IV-13: Membrane 1.5 mm x 5 mm encapsulated. Resistance versus voltage.....	92
Figure IV-14: Membrane 1.5 mm x 5 mm encapsulated. Maximum temperature versus voltage. ...	92
Figure IV-15: Membrane 1.5 mm x 5 mm non encapsulated. Resistance versus voltage.....	93
Figure IV-16: Membrane 1.5 mm x 5 mm non encapsulated. Maximum temperature versus voltage.	93
Figure IV-17: Membrane 2 mm x 4.5 mm encapsulated. Resistance versus voltage.....	94
Figure IV-18: Membrane 2 mm x 4.5 mm encapsulated. Maximum temperature versus voltage. ...	94
Figure IV-19: Membrane 2 mm x 4.5 mm non encapsulated. Resistance versus voltage.....	95
Figure IV-20: Definition of x and y axis.....	96

Figure IV-21: Temperature profile along x axis	96
Figure IV-22: Chip 2 heater A. Temperature profile x applying 12 V	97
Figure IV-23: Chip 2 heater B. Temperature profile x applying 12 V	97
Figure IV-24: Chip 3 heater B. Temperature profile y applying 15 V	98
Figure Annex -1: Chip 2 heater A. Infrared camera image applying 10 V	103
Figure Annex -2: Chip 2 heater A. Post-processed image applying 10 V	103
Figure Annex -3: Chip 2 heater A. Diagonal profile	103
Figure Annex -4: Chip 2 heater B. Infrared camera image applying 12 V	104
Figure Annex -5: Chip 2 heater B. Post-processed image applying 12 V	104
Figure Annex -6: Chip 2 heater B. Diagonal profile	104
Figure Annex -7: Resistance versus voltage chip 2	106
Figure Annex -8: Maximum temperature versus voltage chip 2	107
Figure Annex -9: Chip 2 heater A. Temperature profile y applying 12 V	108
Figure Annex -10: Chip 2 heater A. Temperature profile x applying 12 V	108
Figure Annex -11: Chip 2 heater B. Temperature profile y applying 12 V	109
Figure Annex -12: Chip 2 heater B. Temperature profile x applying 12 V	109
Figure Annex -13: Chip 3 heater A. Infrared camera image applying 15 V	110
Figure Annex -14: Chip 3 heater A. Post-processed image applying 15 V	110
Figure Annex -15: Chip 3 heater A. Diagonal profile	110
Figure Annex -16: Chip 3 heater B. Infrared camera image applying 15 V	111
Figure Annex -17: Chip 3 heater B. Post-processed image applying 15 V	111
Figure Annex -18: Chip 3 heater B. Diagonal profile	111
Figure Annex-19: Resistance versus voltage chip 3	113
Figure Annex -20: Maximum temperature versus voltage chip 3	114
Figure Annex -21: Chip 3 heater A. Temperature profile x applying 15 V	115
Figure Annex -22: Chip 3 heater A. Temperature profile y applying 15 V	115
Figure Annex -23: Chip 3 heater B. Temperature profile x applying 15 V	116
Figure Annex -24: Chip 3 heater B. Temperature profile y applying 15 V	116
Figure Annex -25: Initial design T8. Infrared camera image applying 3V	117
Figure Annex -26: Initial design T8. Post-processed image applying 3V	117
Figure Annex -27: Diagonal profile. Membrane 1 mm x 3 mm. Initial design heater	118
Figure Annex -28: 4 heaters design T8. Infrared camera image applying 6 V	118
Figure Annex -29: 4 heaters design T8. Post-processed image applying 6 V	118
Figure Annex -30: Diagonal profile. Membrane 1 mm x 3 mm. 4 heaters design	119
Figure Annex -31: 15-30-60-80 design T8. Infrared camera image applying 5 V	119
Figure Annex -32: 15-30-60-80 design T8. Post-processed image applying 5 V	119
Figure Annex -33: Diagonal profile. Membrane 1 mm x 3 mm. 15-30-60-80 design	120
Figure Annex -34: Resistance versus voltage chip 4	123
Figure Annex -35: Maximum temperature versus voltage chip 4	124
Figure Annex -36: Initial design. Temperature profile y applying 3V	125
Figure Annex -37: Initial design. Temperature profile x applying 3V	125
Figure Annex -38: 4 heater design. Temperature profile y applying 6V	126
Figure Annex -39: 4 heater design. Temperature profile x applying 6V	126
Figure Annex -40: 15-30-60-80 design. Temperature profile y applying 5V	127
Figure Annex -41: 15-30-60-80 design. Temperature profile x applying 5V	127

Table list

Table I-1: Comparative simulation time	6
Table I-2: Comparison of the experimental measurements with the simulations of the performance of the new sensor design for $T_{\max}=450^{\circ}\text{C}$ [14].....	16
Table II-1: Subdomain parameters.....	24
Table II-2: Boundary conditions.....	25
Table II-3: Distance from the heater to the edge membrane study.....	38
Table II-4: Summary of new design related to the heater area.....	46
Table II-5: Silicon plug influences on initial design.....	50
Table II-6: Comparison difference of temperature with different thick silicon plug. Heater 15-30- 60-80	51
Table II-7: Distance from the silicon plug to the edge membrane study.....	52
Table III-1: New membranes design.....	57
Table III-2: Comparison of different membranes respect membrane, heater and silicon areas	71
Table III-3: Heater design comparison.	71
Table III-4: Comparison of one big membrane with some small ones.....	72
Table III-5: Power consumption membranes 1.5 mm x 5 mm using silicon plug.....	73
Table III-6: Power consumption membranes 2 mm x 4.5 mm using silicon plug.....	75
Table III-7: Power consumption membrane 3 mm x 3 mm using silicon plug	77
Table IV-1: Electric parameters before and after painting the device	86
Table IV-2: Power consumption per unit area and degree.....	98
Table Annex -1: Chip 2 encapsulated in T8	105
Table Annex -2: Chip 3 encapsulated in T8	112
Table Annex -3: Chip 4 encapsulated in T8	121
Table Annex -4: Chip 4 non encapsulated.....	122

UNIVERSITAT ROVIRA I VIRGLI
MODELIZATION, SIMULATION AND DESIGN OF MICRO-ELECTRO-MECHANICAZED SYSTEMS (MEMS) PRECONCENTRATORS
FOR GAS SENSING
Roser Inglés Bort
ISBN:978-84-694-0327-3/DL:T-198-2011

Contents

I.	Introduction.....	1
I.1.	Introduction.....	1
I.2.	Document organization.....	2
I.3.	Objectives.....	3
I.3.1.	Project objectives	3
I.3.2.	Thesis objectives	4
I.4.	Simulation.....	5
I.4.1.	Comsol Multiphysics	5
I.4.2.	Hardware.....	5
I.4.3.	Meshing.....	7
I.4.4.	Electro-Thermal Interaction, Joule Heating.....	7
I.5.	State of the Art	8
I.5.1.	Introduction.....	8
I.5.2.	Technology/Type membranes.....	10
I.5.2.1.	Spider type	10
I.5.2.2.	Membrane type	11
I.5.3.	Membrane efficiency	11
I.5.3.1.	Membrane materials and shape.....	11
I.5.3.2.	Heater materials and shape	13
I.5.4.	Electro thermal simulations	15
I.5.5.	Summary	18
I.6.	References.....	19
II.	Electro-Thermal Simulations	23
II.1.	Introduction.....	23
II.1.1.	Initial preconcentrator design.....	23
II.1.2.	Subdomain and boundary conditions.....	24
II.2.	Simplification hypothesis.....	26
II.3.	Initial heater design simulations.....	34
II.3.1.	Rising time	34
II.3.2.	Temperature homogeneity	35
II.3.3.	Power consumption as a function of distance from the heater to the membrane edge	38
II.4.	Heater design.....	39
II.4.1.	Design 1: 4 heaters.....	39
II.4.2.	Design 2: Around the oval	41
II.4.3.	Design 3: 15-30-60-80	44
II.4.4.	Comparison	46
II.5.	Silicon plug diffuser	48
II.5.1.	Initial design with silicon plug.....	48

II.5.2.	15-30-60-80 design with silicon plug	51
II.5.3.	Power consumption as a function of distance from the silicon plug to the membrane edge	52
II.6.	Conclusions	53
II.7.	References	54
III.	<i>New membranes design.....</i>	57
III.1.	Introduction.....	57
III.2.	Membrane shape and sizes.....	57
III.3.	Heater design	58
III.3.1.	Membrane area: 1.5 mm x 5 mm. Heater area: 1 mm x 4.5 mm A	58
III.3.2.	Membrane area: 1.5 mm x 5 mm. Heater area: 1 mm x 4.5 mm B.....	60
III.3.3.	Membrane area: 2 mm x 4.5 mm. Heater area: 1.5 mm x 4 mm A	64
III.3.4.	Membrane area: 2 mm x 4.5 mm. Heater area: 1.5 mm x 4 mm B.....	66
III.3.5.	Membrane area: 3 mm x 3 mm. Heater area: 2.5 mm x 2.5 mm	69
III.4.	Comparison.....	71
III.5.	Silicon plug in new membranes	73
III.5.1.	Membrane area: 1.5 mm x 5 mm	73
III.5.2.	Membrane area: 2 mm x 4.5 mm	75
III.5.3.	Membrane area: 3 mm x 3 mm	77
III.6.	Conclusions	79
IV.	<i>Electro-Thermal Characterization: Experimental results.....</i>	81
IV.1.	Introduction.....	81
IV.1.1.	Infra red camera parameters.....	83
IV.1.2.	Emissivity adjustment	86
IV.1.2.1.	Physical solution	86
IV.1.2.2.	Post-processing solution	87
IV.2.	Comparison with simulations	89
IV.2.1.	Electro thermal characterization	89
IV.2.2.	Temperature profiles	96
IV.2.3.	Power consumption.....	98
IV.3.	Conclusions	99
V.	<i>Conclusions</i>	101
Annex.....	103
Experimental measurements: Chip 2 (1.5 mm x 5 mm).....	103
Post-processed images	103
Electric characterization.....	105

Temperature profiles	108
Experimental measurements: Chip 3 (2 mm x 4.5 mm).....	110
Post-processed images	110
Electric characterization.....	112
Temperature profiles	115
Experimental measurements: Chip 4 (1 mm x 3 mm).....	117
Post-processed images	117
Electric characterization.....	121
Temperature profiles	125

UNIVERSITAT ROVIRA I VIRGLI
MODELIZATION, SIMULATION AND DESIGN OF MICRO-ELECTRO-MECHANICAZED SYSTEMS (MEMS) PRECONCENTRATORS
FOR GAS SENSING
Roser Inglés Bort
ISBN:978-84-694-0327-3/DL:T-198-2011

I. INTRODUCTION

I.1. Introduction

Nowadays the allowed limits of volatiles that are toxic at very low concentrations are becoming restrictive. Detection must be done at lower levels. One specific case is benzene. It is carcinogenic at repeated parts per billion (ppb) concentrations exposures. It is toxic at concentrations that today's sensors are not able to detect. For this reason, preconcentrators are becoming more important and its study is increasing.

A preconcentrator is a device that has an adsorbent material on top. This material adsorbs volatiles at ambient temperature. When a temperature "desorption temperature pulse" is induced this material desorbs all the volatiles, that will be injected quickly into a detector or a sensor. Volatiles will be in a higher concentration.

Our aim is to design a planar preconcentrator in silicon technology, in order to be able to design in the same substrate the preconcentrator and the sensor system. We will study preconcentrators and sensors developed in silicon technology, in order to know state of the art. Preconcentrators bibliography shows its specifications. A narrow desorption peak is needed in order to obtain big concentrations. A narrow desorption peak is reached having a good homogenisation temperature to heat all the adsorbent material at the same time. Also, a large area is needed in order to be able to have a large amount of adsorbent material.

We will simulate a heater used in our initial design. We will develop new designs which improve preconcentrator behaviour. To obtain a narrow desorption peak homogenisation temperature is necessary. Heater design will be optimised in order to homogenize temperature. The use of a diffuser to homogenise more will be studied. Rapid response is also desirable, but it is not very restrictive taking into account detectors that could be used. A large area is needed in order to have more adsorbent material which ensures more concentration. We will study if it is better to have a large membrane or some small ones in order to increase area.

Finally, we have fabricated some devices in order to measure its behaviour. Experimental results validate our simulations and let us to develop future designs avoiding time and cost fabrication.

I.2. Document organization

This document has been structured in five chapters:

In chapter I objectives of the thesis are defined. We explain simulation software and hardware used. At the end of this chapter, state of the art is presented studying type and efficiency of membranes and electro-thermal simulations reported in bibliography.

In chapter II electro-thermal simulations are explained. Firstly, initial preconcentrator developed before this thesis is defined and simulated. Using these results, new heater designs are proposed to improve its thermal behaviour. Finally, a study of a diffuser is developed.

In chapter III new larger membranes are designed and simulated. Different heaters are simulated and the use of a diffuser is studied.

In chapter IV electro-thermal characterization of fabricated membranes is developed. Using experimental results some simulation parameters are readjusted. A comparison between experimental results and simulations is shown.

In chapter V conclusions are summarized.

Finally, publications developed from this thesis are listed and in Annex all the experimental measurements are shown.

I.3. Objectives

Most part of this thesis is included in CICYT project TEC2006-03671 and both are developed in parallel. For this reason, we want to frame our objectives in the project objectives.

I.3.1. Project objectives

This project is aimed at designing and fabricating a chemical microsystem able to detect traces of toxic gases. The main novelty from the scientific and technological point of view is in the integrated concentrator based on thermal programmed adsorption and desorption, which will enable the detection of toxic species at the ppb level. The detection stage comprises an array of semiconductor gas sensors. The concentrator is based on an adsorption layer deposited on top of one or several membranes with a buried heating resistor. The fabrication of the concentrator should be compatible with the fabrication of the sensor array, so both can share the same Silicon substrate. Seeking to increase its concentration factor, the use of micro and nanoporous template materials acting as supports for gas-absorptive materials will be studied. The compatibility of such templates with membrane fabrication will be studied, too. The concentration stage will not only increase the system sensitivity, but also will confer some selectivity. Therefore, it will be possible to employ the prototype for analysing one or a few target toxic gases, rejecting interfering species. More specifically, the laboratory prototype will be aimed at detecting traces of benzene.

The project is aimed to:

- ✓ Design membranes implemented in silicon having:
 - Large area: The required adsorption capacity is some tens of ppb, so we need a large area to allow the deposition of a sufficient amount of adsorbing material.
 - A good temperature homogeneity and small thermal inertia.
- ✓ Design, fabrication and characterisation of a chemical microsystem to analyse gases (Lab-on-a-chip) aimed at measuring benzene at the ppb level.
- ✓ Deposition of adsorbing materials on nanometric template structures.

My work in this project has been to simulate the preconcentrator in order to improve its behaviour. Preconcentrator has been simulated inside the experimental chamber in order to know experimental behaviour. Electro-thermal, fluid-flow and concentration models have been coupled to study influence between them. A chamber modification was proposed in order to increase concentration during the adsorption phase. It was fabricated and tested obtaining almost twice concentration in the same period of time, as simulation predicted.*

* R. Inglés, J. Pallarés, J. L. Ramirez , **Improving sample flow in planar preconcentrator**, *International Conference on Computational and Mathematical Methods in Science and Engineering*, June 26-30 2010, Almeria (Spain), Proceedings of the 2010 International Conference on Computational and Mathematical Methods in Science and Engineering. ISBN 13: 978-84-613-5510-5

I.3.2. Thesis objectives

In order to use a preconcentrator that can share the same silicon substrate with the sensor, we will design a planar preconcentrator.

A planar preconcentrator is based on an absorption layer deposited on top of one or several membranes with a buried heating resistor. Our aim is to design a heater which ensures homogenisation . If more homogenisation is needed, we will study the use of a diffuser. We will study if it is better to use a big membranes or several small ones.

The thesis objectives are:

- ✓ MEMS (Micro-Electro-Mechanical Systems) membranes state of the art study.
- ✓ Simulation of thermal behaviour of pre-concentration membranes to know its temperature spatial distribution.
- ✓ Simulation of the electro-thermal transient membrane behaviour in order to use it as a preconcentrator .
- ✓ Preconcentrator design in order to improve temperature homogeneity.
- ✓ Design large membranes to obtain more area.
- ✓ Membranes fabrication and electro-thermal characterization in order to validate our simulations.
- ✓ Readjustment of simulations parameters based on characterization.
- ✓ Dissemination of results.

Our principal aim is to define an electro-thermal model which let us to design different heaters and membranes avoiding fabrication time and cost.

I.4. Simulation

I.4.1. Comsol Multiphysics

We will use a finite element tool to simulate the preconcentrator electro-thermal behaviour. Our objectives with this simulations are to design an optimised preconcentrator avoiding the fabrication cost and time in every new idea. For this reason, we will design different preconcentrators looking for the best thermal distribution and quick thermal response.

COMSOL Multiphysics 3.4 has been chosen because this program can couple all this simulations (electro-thermal, mechanics and fluidics) and we can introduce the model of the absorption-desorption behaviour.

I.4.2. Hardware

Finite element simulation uses long time and large computing resources. Using a conventional PC there is no sufficient memory when the mesh elements or the number of degrees of freedom are high (See Table I-1). So, the hardware set up being chosen has been:

- ✓ Sun Fire X4600 M2 x64 server:
 - 4x AMD Opteron Model 8218 processor,
 - 8x 2GB memory
- ✓ RedHat ES 5.1 Enterprise Edition
- ✓ 4 x (2 x 4 GB) memory kit DDR2-667

The Opteron is a dual core, so we have 8 cores available and 48 GB RAM memory. We can see in Table I-1 that, using the proposed hardware set up, simulation time is reduced compared to conventional PC. We can also simulate more models and choose different number of cores used. We have called this hardware 'Prometeu' and Table I-1 shows a comparative between a conventional PC and Prometeu using different numbers of cores.

Computer	Operative System	RAM	Solver	Simulation time (seconds) Parametric 200 points	Simulation time (seconds) Parametric 1000 points	Simulation time (seconds) Parametric 2000 points
Pentium 4 CPU 3,2 GHz	Windows XP profesional Versión 2002 Service Pack 2	2 GB	UMFPACK	2406,938	12146,906	Out of memory
Prometeu	RedHat ES 5.1 Enterprise Edition	8 GB memory kit DDR2-667	UMFPACK	582,356	2987,761	5482,646
Prometeu	RedHat ES 5.1 Enterprise Edition	8 GB memory kit DDR2-667	PARDISO 2 cores	317,897	1627,515	1736,342
Prometeu	RedHat ES 5.1 Enterprise Edition	8 GB memory kit DDR2-667	PARDISO 4 cores	291,250	1485,802	1244,789
Prometeu	RedHat ES 5.1 Enterprise Edition	8 GB memory kit DDR2-667	PARDISO 6 cores	289,516	1465,144	1195,23
Prometeu	RedHat ES 5.1 Enterprise Edition	8 GB memory kit DDR2-667	PARDISO 8 cores	302,693	1435,238	1170,135
			Number of degrees of freedom	15124	15124	49714
			Mesh elements	4957	4957	17035

Table I-1: Comparative simulation time

Using a conventional PC we have a limit due to the available memory. Using just a core in the solver UMFPACK Prometeu is quicker than our conventional PC. Also, using the parallel solver PARDISO with more cores is quicker for complex simulations.

I.4.3. Meshing

A mesh is a partition of the geometry model into small units of simple shapes. In Comsol Multiphysics a default mesh could be created. Default elements are triangular if a 2D simulation is developed and tetrahedral elements if the simulation is 3D. Also a mapped mesh could be created and in this case user define shape elements.

In both cases some parameters could be adjusted:

- ✓ Predefined mesh sizes: it is possible to choose the size of the mesh for each subdomain, boundary or edge in the model. It is interesting to adjust a smaller size in more important parts.
- ✓ Scale geometry before meshing: in this parameter the scale factor for each direction (x,y,z) is adjustable. Scale factors allow us to generate meshes anisotropic, it is useful when there is large aspect ratios in the geometry.

In our case, we have a geometry with large aspect ratios, $\left(\frac{3 \cdot 10^{-3}}{1.2 \cdot 10^{-6}}\right) = 2500$, which force us to use the scale factor. It implies we have really small mesh in z-direction.

Default values are 1.0 in three directions. We adjust 0.01 in x and y-direction and 1.0 in z-direction.

I.4.4. Electro-Thermal Interaction, Joule Heating

The Joule Heating predefined multiphysics coupling combines a Conductive Media DC application mode from COMSOL Multiphysics with the Heat Transfer Module. The interaction is fully coupled in both directions:

- ✓ In the heat transfer application mode, resistive heating appears as a heat source (the resistive heating variable Q_{es} (or Q_{emes}) appears in the Q edit field) and this is calculated by the electric mode.
- ✓ In the Conductive Media DC application mode, the definition of the conductivity σ uses the thermal heating model $1/(\rho_0(1+\alpha(T-T_0)))$, where T is the dependent variable for temperature from the heat transfer application mode. The values for ρ_0 (resistivity at reference temperature), α (temperature coefficient), and T_0 (reference temperature) are adjustable for each material.

It's possible to select steady-state or transient analysis. It will be useful to study thermal distribution on steady state and thermal response on transient analysis.

I.5. State of the Art

I.5.1. Introduction

In this chapter we will review the state of the art of membranes used in MEMS (Micro Electro Mechanical Systems). We will show fabrication technologies, membrane efficiency and electro-thermal simulations developed.

A preconcentrator is a device that has an absorbent material on top. This material adsorbs volatiles at ambient temperature. When a temperature “desorption pulse” is induced, this material desorbs all the volatiles that will be injected quickly into a detector, or a sensor.

Preconcentrators have been much studied last years because limit detection for some volatiles are decreasing quickly. Bibliography related to preconcentrators has increased in recent years.

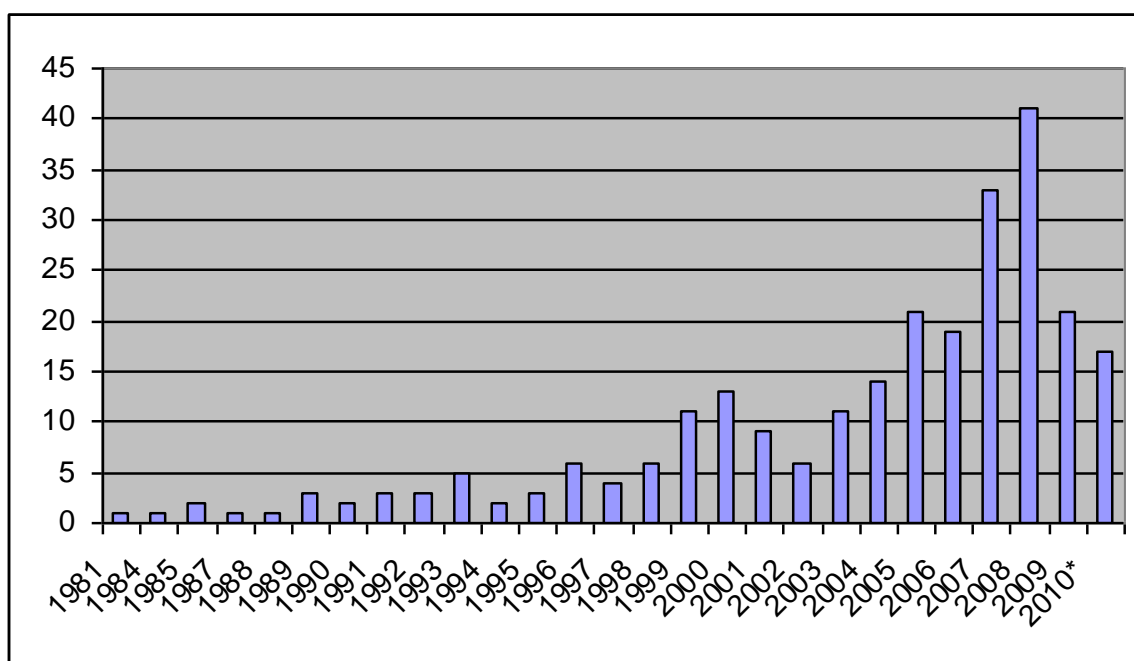


Figure I.1: Papers with topic “preconcentrator” in Web of science (*July 2010)

Desirable features of the preconcentrator device include: [1]

- ✓ Operation at high flow rates
- ✓ Thermal heating with short time constants
- ✓ Selective sampling of the analyte(s) of interest

A high performance MEMS gas preconcentrator should have: [2]

- ✓ Sufficient adsorbent surface area for trapping analytes from the sample stream
- ✓ A small preconcentrator volume and a fast injection speed to achieve the smallest injection volume possible
- ✓ An ability to rapidly heat the sorbent mass to a desired temperature, with low thermal mass for quick heating and cooling
- ✓ Sufficiently good thermal isolation during heating
- ✓

Conventional preconcentrators also called microtraps are characterized by large dead volumes and limited heating efficiency due to their large thermal mass, which subsequently contributes to the delivery of a broad time-width pulse of vapour. Microfabricated preconcentrator reduces the dead volume and thermal mass by delivering a concentrated sample that has a narrow time-width pulse.

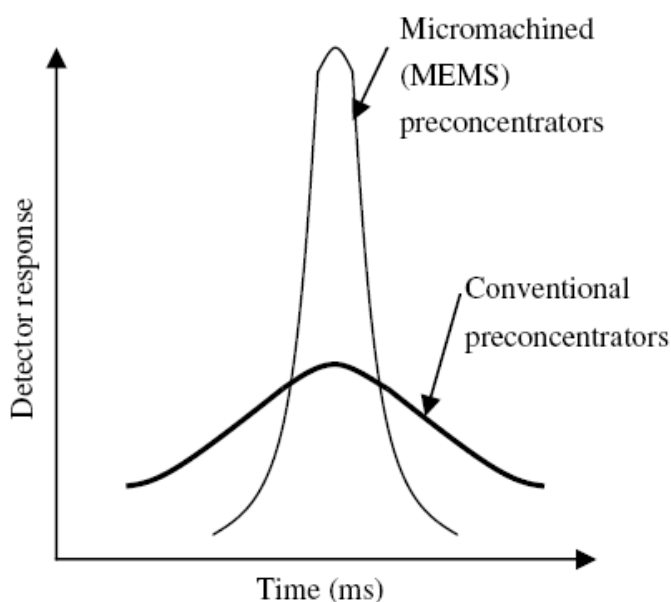


Figure I.2: Comparison of the analyte concentration and time constant in micromachined and conventional preconcentrators[3]

Micromachined preconcentrators are used to enhance the sensitivity of microsensors. Preconcentrators on a silicon substrate can be integrated with a sensor, or a micromachined gas chromatographs (GC) to enhance the signal-to-noise ratio [4].

The applications of micro hotplates, although many and varied, share the same key design requirements: [5]

- ✓ fast response time
- ✓ low power consumption
- ✓ uniform plate temperature
- ✓ scalability

I.5.2. Technology/Type membranes

We study technologies used in sensors because they are the same that used in preconcentrators (what is different is the material deposited, sensors are heated to bring the sensing layer to working temperature and preconcentrator to desorb) and they are more studied than in preconcentrators. Micro machining in silicon is a way to reduce the power consumption and the substrate itself stays nearly at ambient temperature. Control and signal processing can be integrated on the same substrate [6].

Basically there are two different structures for micromachined gas sensors: spider type and membrane type.

I.5.2.1. Spider type

Spider type or suspended-membrane type is shown in Figure I.3. In this device the support beams carry a hotplate with the sensitive layer. Under the hot plate the substrate is etched off to provide for thermal isolation. In this case the etching is performed from the front side.

The advantages of this devices are that this is completely processed from the front side; It's more compatible with CMOS process[6]; This device exhibits high stability against mechanical shocks (the air can flow around the small hotplate and does not need to flow around the whole chip as in the case of the membrane type solution).

One disadvantage of this concept is the limited distance between the hot and the cold parts which is necessarily smaller than the wafer thickness.[7]

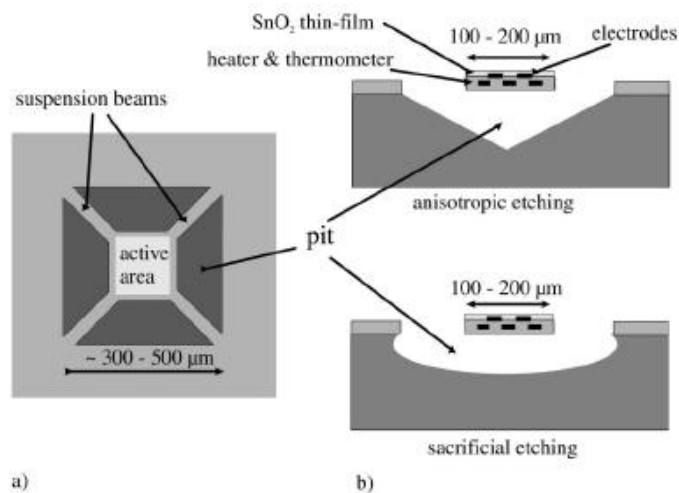


Figure I.3: Schematic of a suspended-membrane-type gas sensor: a) top view; b) side view[6]

I.5.2.2. Membrane type

Membrane type or closed membrane is shown in Figure I.4. It is formed by anisotropic etching of silicon from the backside[6].

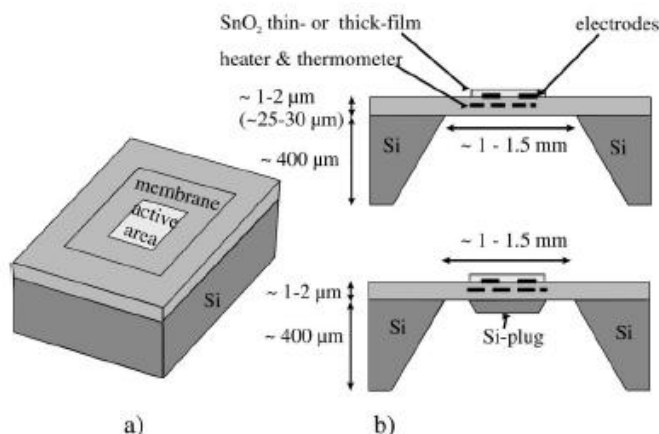


Figure I.4 Schematic of a suspended-membrane-type gas sensor: a) top view; b) side view[6]

The centre of the membrane is heated to 400 °C by a heater and the substrate itself stays nearly at ambient temperature. A disadvantage lies in the need of double-side alignment for the bulk silicon etch from the backside [7].

I.5.3. Membrane efficiency

In this chapter we will see the different parameters that influence in membrane efficiency. They are membrane material and shape and heater material and shape.

I.5.3.1. Membrane materials and shape

Essential membrane requirements can be summarized as follows:[8]

- ✓ Mechanical stability;
- ✓ Low stress material;
- ✓ Low thermal conductivity;
- ✓ High chemical inertness under the KOH etchant (the same film must work as etch-stop allowing the membrane to form or act as masking layer during the silicon bulk micromachining process);
- ✓ Film deposition process and material compatible with IC technology.

Typically a square shape membrane is used [7-11]. The materials more commonly used are silicon dioxide and silicon nitride [12, 13]. But other materials have been tested:

- Cardinali et al [8] modify the silicon nitride low pressure chemical vapour deposition (LPCVD) process to obtain a low stress membrane film. Experimental characterization of fabricated devices shows that a $1.5 \times 1.5 \text{ mm}^2$ membrane, 250 nm thick, breaks at a maximum overpressure of 100 kPa, while it deflects about 35 μm when a pressure of 40 kPa above the atmospheric pressure is applied.
- Astié et al [14] use an oxynitride membrane because compared to silicon membrane sensors reduce significantly losses by conduction, allowing a shrink of areas of membrane and the die size area. They also study the influence of the thickness of the membrane on power consumption for a sensor with a silicon oxynitride membrane.
- Briand et al [15, 16] investigate different thin films, geometry and dimensions regarding their power consumption, temperature distribution over the sensing area and robustness when annealed at high temperatures. The membranes sizes investigated were 1.0×1.0 and $1.5 \times 1.5 \text{ mm}^2$ every one with and without silicon plug.

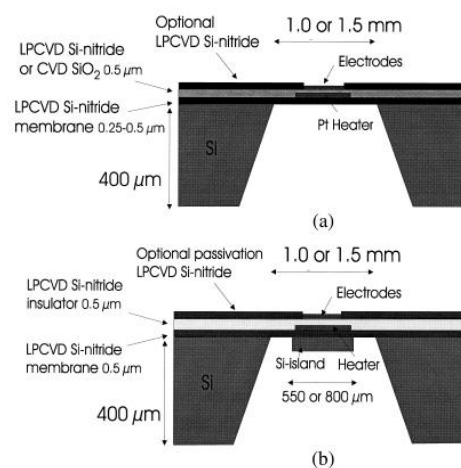


Figure 1.5: Schematic of micro-hotplates without (s) and with (b) Si island. [16]

- Dori et al [10] use a Si_3N_4 membrane for its lower intrinsic stress. Also Manginell et al [17] use a Si_3N_4 membrane. Last one has dimensions $2.2 \text{ mm} \times 2.2 \text{ mm}$ and thickness $0.5 \mu\text{m}$ and it is suspended over a cavity fabricated in Si substrate using Bosch deep-reactive ion etching (DRIE) technique. The heater is fabricated of platinum and achieves $200 \text{ }^\circ\text{C}$ in 4 ms with an electrical power of 100 mW.
- Sabaté et al [18] determine the mechanical properties of the films that usually compose a membrane. They use three different samples: A) 300 nm Si_3N_4 LPCVD; B) 300 nm Si_3N_4 LPCVD and 800 nm SiO_2 PECVD; C) 300 nm Si_3N_4 LPCVD and 350 nm Si_3N_4 PECVD. They also determine the thermal conductivity in multilayered membranes[19].

- Ducso et al [20] use a novel bulk-micromachining technique using laterally selective porous silicon formation by anodization. This requires no double-sided alignment.
- Gràcia et al [21] make a set of thermo-mechanical tests with different active area size and membrane size. Larger membranes was of $1500 \times 1500 \mu\text{m}^2$ show poorer fabrication yield. However, the unbroken membranes showed the same good behaviour against vibration and mechanical shocks than smaller ones. Structures that include a silicon plug under the active area could withstand more overpressure, possibly due to a better stress distribution.

I.5.3.2. Heater materials and shape

Platinum and doped polysilicon are the materials more used in heaters because they exhibit high stability in temperature cycles [7], a good thermal conduction, which ensures intrinsic temperature uniformity of the heater, and a constant and relatively high temperature coefficient, which provides a simple way to obtain a temperature measurement by monitoring resistance variations.[8, 9]

Creemer et al [22] compare platinum heater and Titanium nitride (TiN) as a heater material. TiN has two additional advantages. Its residual stress can be tuned over a wide range, increasing the strength of the hotplate. In addition, it has a very moderate heat conductivity (15W/mK for bulk material). This promises low conductive losses through the connecting wires. The TiN heater can emit 40% more power than the platinum heater, but TiN must be protected against oxidation during processing.

Simple meandered polysilicon microheater resistor on $2 \mu\text{m}$ thick SiO_2 and $100, 200 \text{ nm}$ thick Si_3N_4 have been used by Gotz et al [23], even when reaching a good temperature uniformity was not the main goal of the authors.

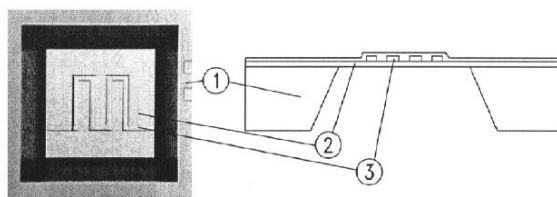


Figure I.6: Photograph (real view) and schematic cross section of simple meandered microheater resistor [23]

Barretino et al [24] use silicon plug in order to homogenize temperature distribution in the active area. They also developed monolithic controllers for the sensors [25, 26]

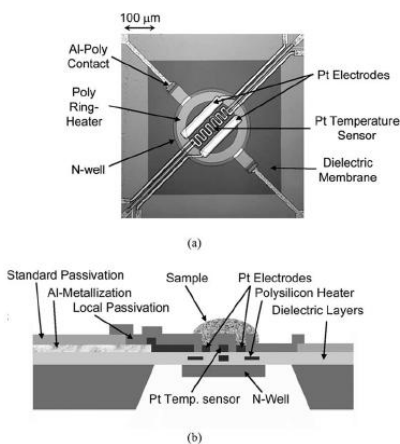


Figure I.7: Microhotplate with a silicon plug [24]

Voiculescu et al [27] use a metal heat distribution plate between the heater and the adsorbent layer.

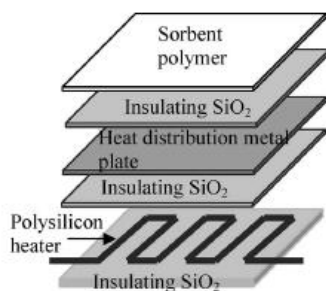


Figure I.8: Principal layers of a microhotplate that is fabricated in CMOS technology and used as a micropreconcentrator.[27]

Rossi et al [28, 29] used a polysilicon microheater resistor as well, defined on different types of membranes. They conclude that a good compromise between consumption and temperature homogeneity is obtained for values of S_r/S_m (ratio between heater and membrane area) between 0.05 and 0.1

A novel loop-shaped polysilicon meandered heater on a stacked membrane ($SiO_2/Si_3N_4/SiO_2$) has been proposed by Laconte et al [11]. This structure features a very good uniformity and very low power consumption (20mW at 400°C).

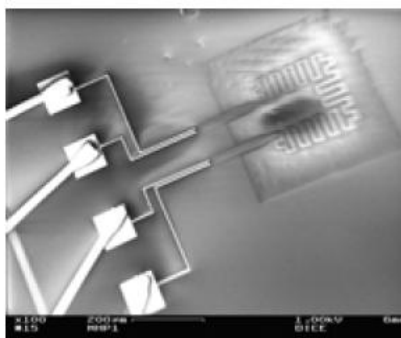


Figure I.9 Novel loop-shaped [11]

Astié et al. [30] propose a ‘S’ shape for the sensor and the polysilicon heater.

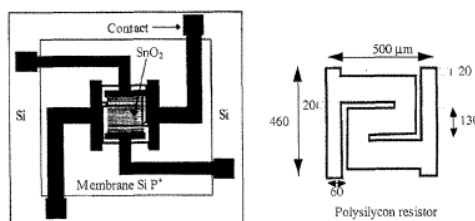


Figure I.10: Schematic drawing of the ‘S’ shaped sensor and polysilicon heater (top view) [30]

Optimum temperature uniformity said to be obtained with a Pt double spiral resistor [8-10, 31, 32]. Guidi et al [32] use a double spiral with variable width. They could achieve a reduction of the radial temperature gradient from about $5 \text{ K}\mu\text{m}^{-1}$ for a standard meander shape heater to $0.2 \text{ K}\mu\text{m}^{-1}$ for their double spiral shaped Pt heater. Aigner et al [33] varies the heater width with a factor 2.5 to obtain a uniform temperature distribution.

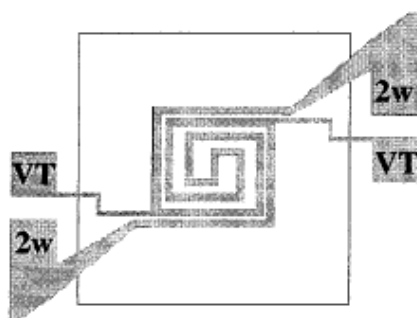


Figure I.11: Pt double spiral resistor [9]

The ratio between the membrane size and the active area of the device has been kept equal to 2 to reduce the thermal power conduction towards the Si substrate.[31] Lee et al [34] have selected a ratio of 3:1 for this sizes.

I.5.4. Electro thermal simulations

Astié et al [14] use electro-thermal simulation by finite element method (SESES) in order to optimise the sensors. The effect of the length of the polysilicon heater, the size of the hole in the polysilicon heater and the membrane area on the temperature distribution and power consumption have been evaluated. They use the following boundary conditions: “according to experimental observation, the temperature at the periphery of the die is constant and equal to 30°C ; on the upper and lower surfaces of the membrane, the heat is dissipated through convective exchange with the gaseous phase. The exchange coefficient is taken as $250 \text{ W/m}^2\text{K}$ for the upper surface and $125 \text{ W/m}^2\text{K}$ for the lower surface deduced from experimental measurement in vacuum; radiation losses have been considered negligible.”

	Simulation	Experimental
Power consumption (mW)	64.5	65
Average temperature (°C)	420	420
Contact temperature (°C)	250	280

Table I-2: Comparison of the experimental measurements with the simulations of the performance of the new sensor design for $T_{\max}=450^{\circ}\text{C}$ [14]

Cardinali et al and Baroncini et al [8, 35] use ISETCAD SOLIDIS in order to study temperature distribution of the heater.

Belmonte et al [36] use thermal and mechanical simulations with FEM analysis tool ANSYS. Temperature gradient simulations and mechanical stress simulations of the sensor micro-hotplate are required in order to establish the geometrical characteristics of the structure that they use.

Rossi et al [28] use a numerical simulation using finite elements ANSYS. The boundary conditions used are: free convection on the entire structure (convection coefficient, h , has been estimated at $100 \text{ W/m}^2\text{K}$ from IR observations), radiation can be neglected for temperatures lower than 400°C .

Bognar et al [37] use the SUNRED program to study the thermal behaviour of a microheater in order to compare unsupported and supported structures. Furjes et al [38] also use SUNRED and they compare the simulations with COSMOS.

Briand et al [15] study the temperature distribution over the sensing area and the power consumption depending on the silicon island thickness, which was optimised for both applications using the software MEMCAD from Microcosm Technologies.

Puigcorbe et al [39] analyse and quantify the thermal fatigue in micromachined gas sensors by combining experimental materials models with coupled thermo-mechanical FEM simulations.

Gotz et al[40] use FEM program ANSYS 5.1. They study the power consumption as a function of membrane size and the temperature distribution with and without silicon plug. By adding a silicon plug of about $10 \mu\text{m}$ thickness just beneath the active area a very uniform temperature distribution is obtained.

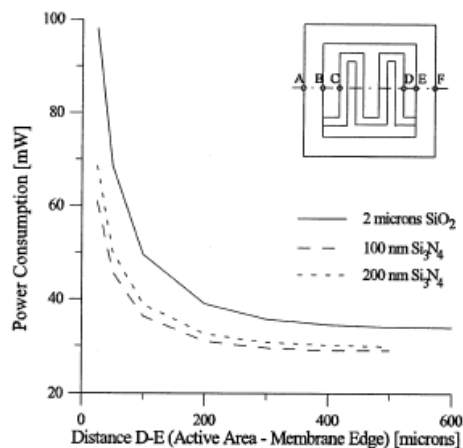


Figure I.12: Simulated power consumption for three different membranes versus the membrane size at 350 °C average temperature.[40]

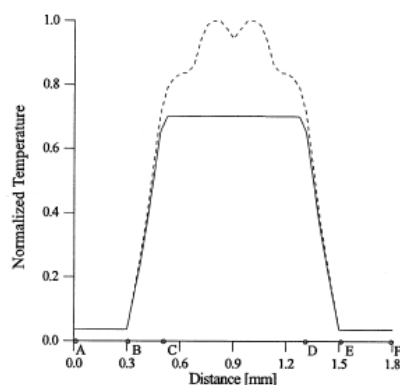


Figure I.13: Simulated temperature across the chip for membranes with (—) and without silicon plug. 0.0 corresponds to 0 °C and 1.0 to the maximum temperature in °C.[40]

Gotz et al [23] use FEM simulations (ANSYS 5.2). From simulations it can be observed that for a minimum distance between the heated central area and the edge of the membrane exceeding 200 μm , thermal isolation is practically not improved further.

Udrea et al [41] also use electro-thermal simulation with ISE-Solidis tool. They use the Dirichlet boundary condition: the temperature along the bottom of the silicon wafer is equivalent to an ideal heat reservoir of the ambient temperature.

Fung et al [42] use finite-element analysis programs PATRAN and ABAQUS for the thermal analysis.

I.5.5. Summary

Membranes have been much studied and materials, shape and technology used determine their performance.

Preconcentrators' membranes have requirements listed:

- ✓ Peak of temperature is lower than in sensors (desorption values).
- ✓ Homogenisation temperature is needed to obtain a narrow desorption peak which is necessary to has a big concentration.
- ✓ Homogenisation temperature is absolute needed when gases discrimination should be achieved.
- ✓ Larger area is needed in order to have more adsorbent material.

Membranes microfabricated in silicon are used because it is possible to heat the centre at high temperatures maintaining the substrate nearly at ambient temperature. Also it is possible to fabricated in the same substrate preconcentrators and sensors.

More common membrane materials are silicon dioxide and silicon nitride, because they have low thermal conductivity. We use this materials in our membrane.

Heater designs have been studied. Bibliography reports the use of a platinum double spiral resistor to obtain optimum temperature homogeneity. We will study temperature homogenisation running electrothermal simulations. We will simulate different heaters to see which are better.

More homogenisation is obtained using a silicon plug thermal diffuser under the heater or a metal heat distribution plate between the heater and the adsorbent layer, but this last one needs more fabrication steps due to the electrical conductivity of this layer. We will run simulations using a silicon plug in order to see if it increases homogenize temperature.

I.6. References

1. Voiculescu, I., M. Zaghloul, and N. Narasimhan," Microfabricated chemical preconcentrators for gas-phase microanalytical detection systems". Trends in Analytical Chemistry, 2008. pp. 327-343
2. Yeom, J., C. Field, B. Bae, R. Masel, and M. Shannon," The design, fabrication and characterization of a silicon microheater for an integrated MEMS gas preconcentrator". JOURNAL OF MICROMECHANICS AND MICROENGINEERING, 2008.
3. Voiculescu, I.," Design and Development of MEMS Devices for Trace Detection of Hazardous Materials". Dissertation, George Washington University, 2005.
4. Kim, M. and S. Mitra," A microfabricated microconcentrator for sensors and gas chromatography". JOURNAL OF CHROMATOGRAPHY A, 2003. pp. 1-11
5. Swart, N. and A. NATHAN," Design optimization of Integrated microhotplates". SENSORS AND ACTUATORS A-PHYSICAL, 1994. pp. 3-10
6. Simon, T., N. Barsan, M. Bauer, and U. Weimar," Micromachined metal oxide gas sensors: opportunities to improve sensor performance". SENSORS AND ACTUATORS B-CHEMICAL, 2001. pp. 1-26
7. Sberveglieri, G., W. Hellmich, and G. Muller," Silicon hotplates for metal oxide gas sensor elements". MICROSYSTEM TECHNOLOGIES, 1997. pp. 183-190
8. Cardinali, G., L. Dori, M. Fiorini, I. Sayago, G. Faglia, C. Perego, et al.," A smart sensor system for carbon monoxide detection". ANALOG INTEGRATED CIRCUITS AND SIGNAL PROCESSING, 1997. pp. 275-296
9. Baroncini, M., P. Placidi, G. Cardinali, and A. Scorzoni," Thermal characterization of a microheater for micromachined gas sensors". SENSORS AND ACTUATORS A-PHYSICAL, 2004. pp. 8-14
10. Dori, L., P. Maccagnani, G. Cardinali, M. Fiorini, I. Sayago, S. Guerri, et al. "New material and heater geometry for high performance micromachined thermally insulated structures in gas sensor applications". 1997. Warsaw, Poland.
11. Laconte, J., C. Dupont, A. Akheyar, J. Raskin, and P. Flandre. "Fully CMOS compatible low-power microheater". 2002. Cannes.
12. Vincenzi, D., M. Butturi, V. Guidi, M. Carotta, G. Martinelli, V. Guarnieri, et al.," Development of a low-power thick-film gas sensor deposited by screen-printing technique onto a micromachined hotplate". SENSORS AND ACTUATORS B-CHEMICAL, 2001. pp. 95-99
13. Demarne, V. and A. Grisel," An integrated low-power thin-film co gas sensor on silicon". Sensors and Actuators, 1988. pp. 301-313
14. Astie, S., A. Gue, E. Scheid, and J. Guillemet," Design of a low power SnO₂ gas sensor integrated on silicon oxynitride membrane". SENSORS AND ACTUATORS B-CHEMICAL, 2000. pp. 84-88
15. Briand, D., S. Heimgartner, M. Gretillat, B. van der Schoot, and N. de Rooij," Thermal optimization of micro-hotplates that have a silicon island". JOURNAL OF MICROMECHANICS AND MICROENGINEERING, 2002. pp. 971-978
16. Briand, D., A. Krauss, B. van der Schoot, U. Weimar, N. Barsan, W. Gopel, et al.," Design and fabrication of high-temperature micro-hotplates for drop-coated gas sensors". SENSORS AND ACTUATORS B-CHEMICAL, 2000. pp. 223-233

17. Manginell, R., P. Ronald, G. Frye-Mason, R. Kottenstette, P. Lewis, and C. Wong. "Microfabricated planar preconcentrator". 2000. Cleveland.
18. Sabate, N., I. Gracia, J. Santander, L. Fonseca, E. Figueras, C. Cane, et al.," Mechanical characterization of thermal flow sensors membranes". *SENSORS AND ACTUATORS A-PHYSICAL*, 2006. pp. 260-266
19. Sabate, N., J. Santander, I. Gracia, L. Fonseca, E. Figueras, E. Cabruja, et al.," Characterization of thermal conductivity in thin film multilayered membranes". *THIN SOLID FILMS*, 2005. pp. 328-333
20. Ducso, C., E. Vazsonyi, M. Adam, I. Szabo, I. Barsony, J. Gardeniers, et al.," Porous silicon bulk micromachining for thermally isolated membrane formation". *SENSORS AND ACTUATORS A-PHYSICAL*, 1997. pp. 235-239
21. Gracia, I., J. Santander, C. Cane, M. Horrillo, I. Sayago, and J. Gutierrez," Results on the reliability of silicon micromachined structures for semiconductor gas sensors". *SENSORS AND ACTUATORS B-CHEMICAL*, 2001. pp. 409-415
22. Creemer, J., W. van der Vlist, C. de Boer, H. Zandbergen, and P. Sarro. "MEMS Hotplates with TiN as a heater material". 2005.
23. Gotz, A., I. Gracia, C. Cane, and E. LoraTamayo," Thermal and mechanical aspects for designing micromachined low-power gas sensors". *JOURNAL OF MICROMECHANICS AND MICROENGINEERING*, 1997. pp. 247-249
24. Barrettino, D., M. Graf, W. Song, K. Kirstein, A. Hierlemann, and H. Baltes," Hotplate-based monolithic CMOS microsystems for gas detection and material characterization for operating temperatures up to 500(circle)C". *IEEE JOURNAL OF SOLID-STATE CIRCUITS*, 2004. pp. 1202-1207
25. Barrettino, D., M. Graf, S. Taschini, S. Hafizovic, C. Hagleitner, and A. Hierlemann," CMOS monolithic metal-oxide gas sensor microsystems". *IEEE SENSORS JOURNAL*, 2006. pp. 276-286
26. Barrettino, D., P. Malcovati, M. Graf, S. Hafizovic, and A. Hierlemann," CMOS-based monolithic controllers for smart sensors comprising micromembranes and microcantilevers". *IEEE TRANSACTIONS ON CIRCUITS AND SYSTEMS I-REGULAR PAPERS*, 2007. pp. 141-152
27. Voiculescu, I., R. McGill, M. Zaghloul, D. Mott, J. Stepnowski, S. Stepnowski, et al.," Micropreconcentrator for enhanced trace detection of explosives and chemical agents". *IEEE SENSORS JOURNAL*, 2006. pp. 1094-1104
28. Rossi, C., E. Scheid, and D. Esteve," Theoretical and experimental study of silicon micromachined microheater with dielectric stacked membranes". *SENSORS AND ACTUATORS A-PHYSICAL*, 1997. pp. 183-189
29. Rossi, C., P. Temple-Boyer, and D. Esteve," Realization and performance of thin SiO₂/SiN_x membrane for microheater applications". *SENSORS AND ACTUATORS A-PHYSICAL*, 1998. pp. 241-245
30. Astie, S., A. Gue, E. Scheid, L. Lescouzeres, and A. Cassagnes," Optimization of an integrated SnO₂ gas sensor using a FEM simulator". *SENSORS AND ACTUATORS A-PHYSICAL*, 1998. pp. 205-211
31. Faglia, G., E. Comini, M. Pardo, A. Taroni, G. Cardinali, S. Nicoletti, et al.," Micromachined gas sensors for environmental pollutants". *MICROSYSTEM TECHNOLOGIES*, 1999. pp. 54-59

32. Guidi, V., G. Cardinali, L. Dori, G. Faglia, M. Ferroni, G. Martinelli, et al.," Thin-film gas sensor implemented on a low-power-consumption micromachined silicon structure". *SENSORS AND ACTUATORS B-CHEMICAL*, 1998. pp. 88-92
33. Aigner, R., M. Dietl, R. Katterloher, and V. Klee," Si-planar-pellistor: Designs for temperature modulated operation". *SENSORS AND ACTUATORS B-CHEMICAL*, 1996. pp. 151-155
34. Lee, D.D., W.Y. Chung, M.S. Choi, and J.M. Baek," Low-power micro gas sensor". *Sensors And Actuators B-Chemical*, 1996. pp. 147-150
35. Baroncini, M., P. Placidi, A. Scorzoni, G. Cardinali, L. Dori, and S. Nicoletti. "Accurate extraction of the temperature of the heating element in micromachined gas sensor". 2001. Sydney, Australia.
36. Belmonte, J., J. Puigcorbe, J. Arbiol, A. Vila, J. Morante, N. Sabate, et al.," High-temperature low-power performing micromachined suspended micro-hotplate for gas sensing applications". *SENSORS AND ACTUATORS B-CHEMICAL*, 2006. pp. 826-835
37. Bogнар, G., P. Furjes, V. Szekely, and M. Rencz," Transient thermal characterisation of hot plates". *MICROSYSTEM TECHNOLOGIES-MICRO-AND NANOSYSTEMS-INFORMATION STORAGE AND PROCESSING SYSTEMS*, 2005. pp. 154-159
38. Furjes, P., G. Bogнар, and I. Barsony," Powerful tools for thermal characterisation of MEMS". *SENSORS AND ACTUATORS B-CHEMICAL*, 2006. pp. 270-277
39. Puigcorbe, J., A. Vila, and J. Morante," Thermal fatigue modeling of micromachined gas sensors". *SENSORS AND ACTUATORS B-CHEMICAL*, 2003. pp. 275-281
40. Gotz, A., I. Gracia, C. Cane, E. Lora-Tamayo, M. Horrillo, J. Getino, et al.," A micromachined solid state integrated gas sensor for the detection of aromatic hydrocarbons". *SENSORS AND ACTUATORS B-CHEMICAL*, 1997. pp. 483-487
41. Udrea, F., J. Gardner, D. Setiadi, J. Covington, T. Dogaru, C. Lua, et al.," Design and simulations of SOICMOS micro-hotplate gas sensors". *SENSORS AND ACTUATORS B-CHEMICAL*, 2001. pp. 180-190
42. Fung, S., Z. Tang, P. Chan, J. Sin, and P. Cheung," Thermal analysis and design of a micro-hotplate for integrated gas-sensor applications". *Sensors and Actuators A*, 1996. pp. 482-487

II. ELECTRO-THERMAL SIMULATIONS

II.1. Introduction

Our first objective is to design a silicon micro-hotplate membrane as large as possible to be used as a pre-concentrator. It will have an adsorbing layer that, at ambient temperature, will capture volatiles during some time. After that, It will be heated to desorb these volatiles in much less time, in order to be detected by a sensor. Volatiles concentration will be higher. Large membranes are necessary to have more area for the adsorbing layer. Also, a temperature homogeneity in this area is important to have a narrow desorption peak.

In this chapter we will see simulations developed in order to study membranes behaviour and improve this to be used as a preconcentrator. Firstly, we will define initial design and simulations parameters. Secondly, we will study the way to simplify in order to decrease simulation time. Then, we will study initial design heater behaviour and with these results we will design new heaters to improve temperature homogeneity. Finally, we include a silicon plug improving more.

II.1.1. Initial preconcentrator design

A first membrane was designed and fabricated in the CNM (Centre Nacional de Microelectrònica) of Barcelona. Membrane area has a size of $3000 \times 1000 \mu\text{m}^2$ and heater area has a size of $2500 \times 500 \mu\text{m}^2$.

The membrane is composed by:

- ✓ A mechanical support: Silicon substrate $300 \mu\text{m}$ thick, anisotropically completely etched from the backside to reduce heat losses.
- ✓ A dielectric block: Three layers of low thermal conductivity $\text{SiO}_2/\text{Si}_3\text{N}_4/\text{SiO}_2$ to ensure the thermal insulation of the structure ($1.2 \mu\text{m}$ thick) resulting in a very low thermal mass. They are fabricated as follows:
 - Thermal oxidation at $950 \text{ }^\circ\text{C}$ in order to grow 1000 \AA of a SiO_2 layer.
 - A LPCVD deposition of 3000 \AA of Si_3N_4 layer.
 - A PECVD deposition of 8000 \AA of SiO_2
- ✓ A heater: A platinum layer is deposited by sputtering and shaped by lift off. It has a double spiral shape to improve the uniformity of the temperature distribution under the adsorbing layer. The heater has a thickness of 2500 \AA . The heater is designed to have a separation of $50 \mu\text{m}$ between sticks and its width $50 \mu\text{m}$ in the side sticks, $80 \mu\text{m}$ in the central stick and $120 \mu\text{m}$ in the electrical contacts. A layer of titanium is deposited prior to platinum to promote the heater adhesion to the substrate.

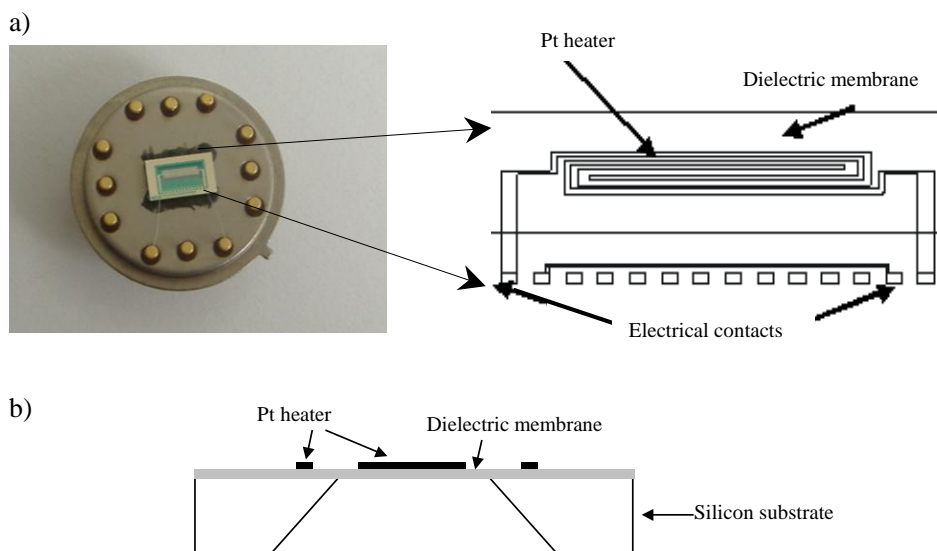


Figure II-1: Initial design: a) A view from the top of the membrane b) A cross sectional view of the membrane

II.1.2. Subdomain and boundary conditions

Most part of simulations shown in this chapter are run using the same parameters. We define here usual values. If there is no other definition this values are applied.

Subdomain parameters are applied to each constructed part of the entire device. They are related to material and depend on the simulation model. Values used in our simulation are listed in Table II-1.

		Silicon	Silicon dioxide	Silicon nitride	Platinum
Conductive media DC	Resistivity at reference temperature ($\Omega \cdot m$)	$1 \cdot 10^{13}$	$1 \cdot 10^{13}$	$1 \cdot 10^{12}$	$2.095 \cdot 10^{-7}$
	Temperature coefficient (1/K)	0	0	0	$2.349 \cdot 10^{-3}$
Heat transfer	Thermal conductivity ($W/(m \cdot K)$)	130	1.4	20	71.6
	Density (kg/m^3)	2329	2200	3100	21450
	Heat capacity at constant pressure ($J/(kg \cdot K)$)	700	730	700	133

Table II-1: Subdomain parameters

Boundary conditions are applied to each outer surface. Boundary conditions must be defined for each model. In the ‘Conductive media DC’ model a electric contact where the voltage is applied and an electric ground are needed. In the ‘Heat transfer’ model we use the constant temperature in the contact between the membrane and the bulk, that will be explained by our simplification hypothesis in next Chapter II.2. The rest of the surfaces has a heat flux boundary condition which emulate the heat transferred to the air around the membrane. Values used are listed in Table II-2.

		Boundary condition	Value
Conductive media DC	Electric contact	Voltage	V_{in}
	Electric ground	Ground	
	All the rest	Electric insulation	
Heat transfer	Base contact	$T_{amb} + \text{constant}$	$300 + 0.6$
	All the rest	Heat flux	90

Table II-2: Boundary conditions

V_{in} is the voltage applied. This is different for each heater and it is the necessary to reach a maximum temperature of $500 \text{ K} \pm 3 \text{ K}$.

In our model we replaced the air above the membrane by a generic heat flux boundary condition with an imposed constant heat transfer coefficient. When it is used to simulate a natural convection it could take values between 30 and $120 \text{ W/m}^2\text{K}$. This value will influence in power consumption and in maximum temperature, but it does not have a big influence in the thermal homogenisation distribution. We have used an intermediate value of $90 \text{ W/m}^2\text{K}$. Bibliography reports similar values: $100 \text{ W/m}^2\text{K}$ estimated from IR observations [1], $125 \text{ W/m}^2\text{K}$ for the front side and 60 for the back side of the membrane [2]. Using experimental results it will be adjusted in Chapter IV.2.

II.2. Simplification hypothesis

Silicon bulk has a thickness of 300 μm , this is really big compared to the membrane thickness (1.2 μm) and the heater thickness (2500 \AA). Due to this and the ratio between thickness (μm) and width (mm) this structure is difficult to mesh.

In order to reduce simulation time and computing resources we will try to avoid simulate the silicon bulk and the air surrounding. In this chapter we will study if it is possible to find an equivalent thermal boundary condition which let us avoid simulate the silicon bulk.

We have the heater element in contact with the membrane and this with the silicon bulk. We study which way is distributed the heat. First of all, we will see the resistance to distribute the heat of each element. (See Figure II-2)

The heater element lose temperature in three ways:

- ✓ Radiation to the air: this is said to be negligible until 700 K [1-6]

Heat loses by radiation is calculated with:

$$q'' = \sigma(T_h^4 - T_{amb}^4)$$

where σ is the radiation constant $5.7 \cdot 10^{-8} \text{W}/(\text{m}^2 \text{K}^4)$

T_h is the heated temperature and T_{amb} is the ambient temperature in Kelvin

$$q'' = 5.7 \cdot 10^{-8} (500^4 - 300^4) = 3100 \text{ W}/\text{m}^2$$

- ✓ Natural convection: this is a heat flux to the air in values from 1 to 200 $\text{W}/\text{m}^2 \text{K}$.

Taking a value of $h = 90 \text{ W}/\text{m}^2 \text{K}$ the air resistance is:

$$\frac{1}{h} = \frac{1}{90} = 1.1 \cdot 10^{-2} \frac{\text{m}^2 \text{K}}{\text{W}} = 1.1 \cdot 10^{-2} \frac{\text{m}^2 \text{K}}{\text{W}} \cdot \frac{1}{3000 \mu\text{m} \cdot 1000 \mu\text{m}} = 3666.67 \frac{\text{K}}{\text{W}}$$

Heat loses by convection is calculated with:

$$q'' = h(T_h - T_{amb})$$

$$q'' = 90(500 - 300) = 18000 \text{ W}/\text{m}^2$$

- ✓ Conduction to the air: If we calculate the air resistance in a zone of 3 mm x 1 mm:

$$\frac{\delta}{k} = \frac{5 \text{ mm}}{0.0025 \frac{\text{W}}{\text{mK}}} = 0.2 \frac{\text{m}^2 \text{K}}{\text{W}} \frac{1}{3 \text{ mm} \cdot 1 \text{ mm}} = 66666.67 \frac{\text{K}}{\text{W}}$$

- ✓ Conduction to the membrane and bulk: due to the low thermal conductivity of the materials of the membrane its resistance is higher than the air. For the calculation of resistance we consider the silicon nitride due to the higher thermal conductivity (20 W/mK in front of the thermal conductivity of the silicon dioxide 1.4 W/mK)

$$\frac{\delta}{k} = \frac{250 \mu\text{m}}{20 \frac{\text{W}}{\text{mK}}} = 1.25 \cdot 10^{-5} \frac{\text{m}^2 \text{K}}{\text{W}} \frac{1}{8000 \mu\text{m} \cdot 3000 \text{ \AA}} = 5208.3 \frac{\text{K}}{\text{W}}$$

So the most influence is the air on the top of the heater because it presents the smallest resistance. Radiation represents a 16 % of the heat lose respect natural convection. For the moment we have neglected it, in Chapter IV.2 we will study if it is quite accurate.

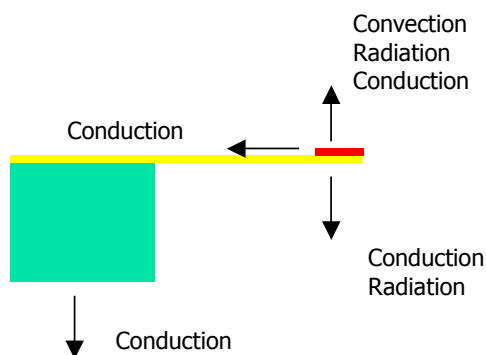


Figure II-2: Heat evacuation

To see if it is equivalent to substitute the silicon bulk by a boundary condition we will simulate only a piece of silicon with a bit of membrane and heater with air in the bottom in order to see the temperature in the end of bulk.

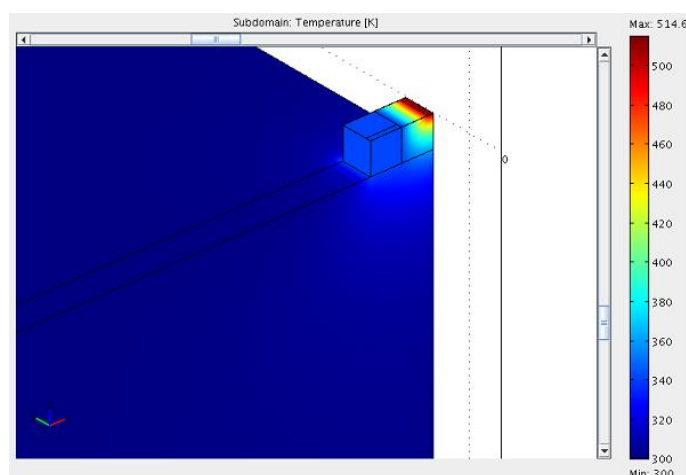


Figure II-3: Piece of silicon with air in the bottom.

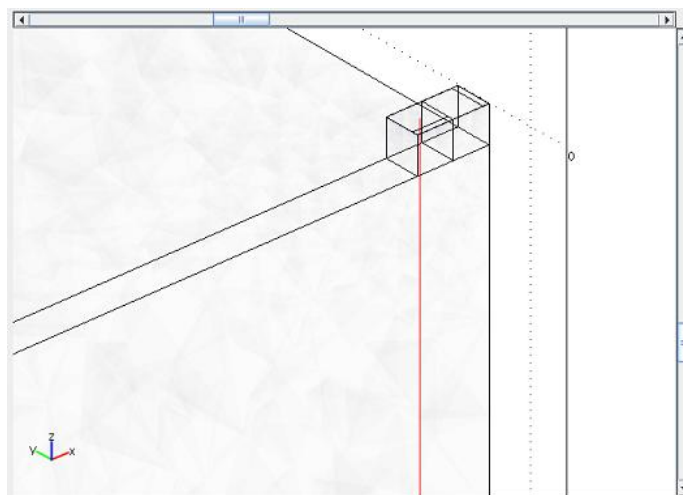


Figure II-4: Piece of silicon with air in the bottom. Red line defines next temperature profile

Figure II-5 shows the temperature profile with two different heat flux $200 \text{ W/m}^2\text{K}$ and $90 \text{ W/m}^2\text{K}$. We can see that the temperature inside the silicon is constant at a value in the Tamb-Theater range. This depends on the heat loosed by the top. For this we will use: $T_{amb} + \text{constant}$.

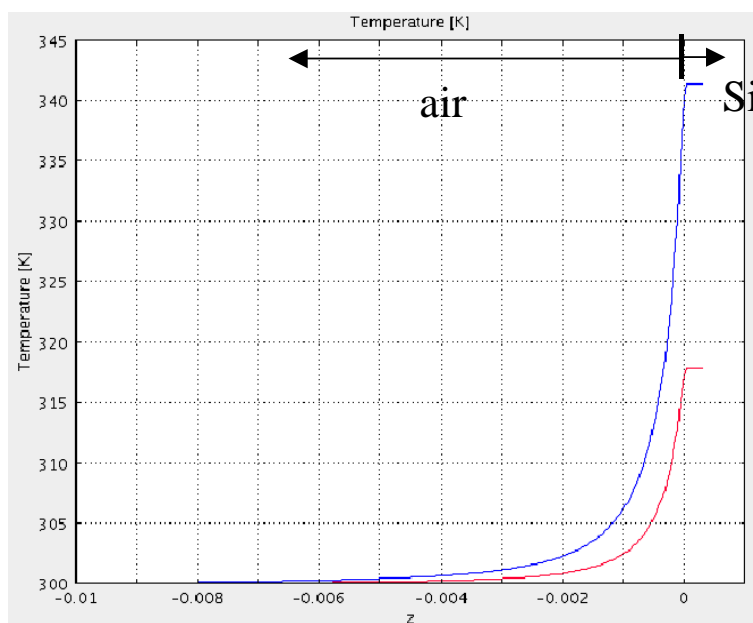


Figure II-5: Temperature profile with two different heat flux (red line is $200 \text{ W/m}^2\text{K}$ and blue line $90 \text{ W/m}^2\text{K}$)

We look for equivalent conditions. For this, we simulate the entire system with the next boundary conditions:

- ✓ $h=90 \text{ W/mK}$ heat flux in top and bottom membrane surfaces and $T_{amb}=300 \text{ K}$. (The air is simplified by this condition),
- ✓ 300 K at the bulk back plane,
- ✓ We will apply 6 V to reach 500 K and 10 V to reach almost 700 K

Figure II-6 shows temperature distribution for 6 V applied.

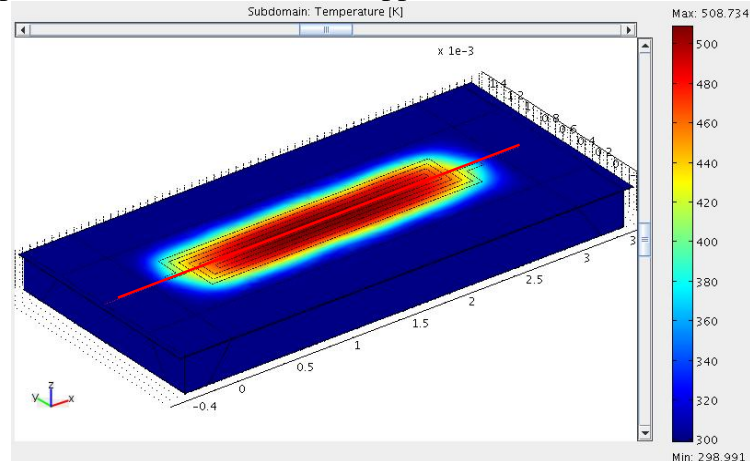


Figure II-6: Temperature distribution of the whole system

Figure II-7 shows temperature distribution on plane x-y. In both images (Figures Figure II-6 and Figure II-7) red line defines the cuts made in the 2D temperature profile represented in Figures Figure II-8 and Figure II-9.

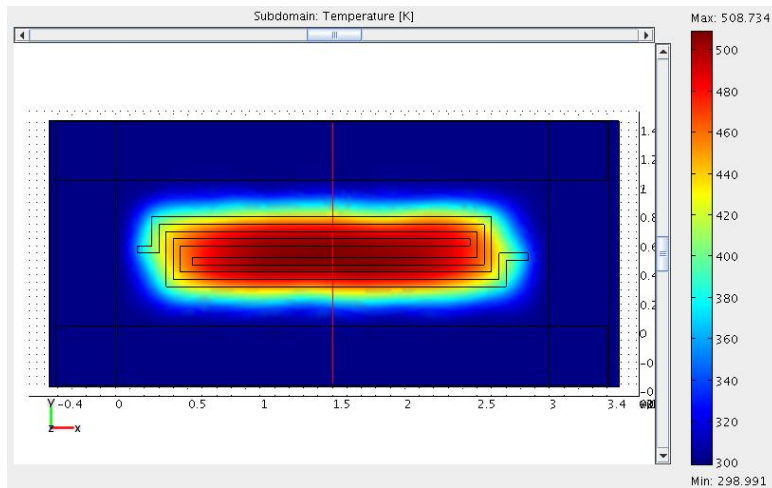


Figure II-7: Temperature distribution on plane x-y

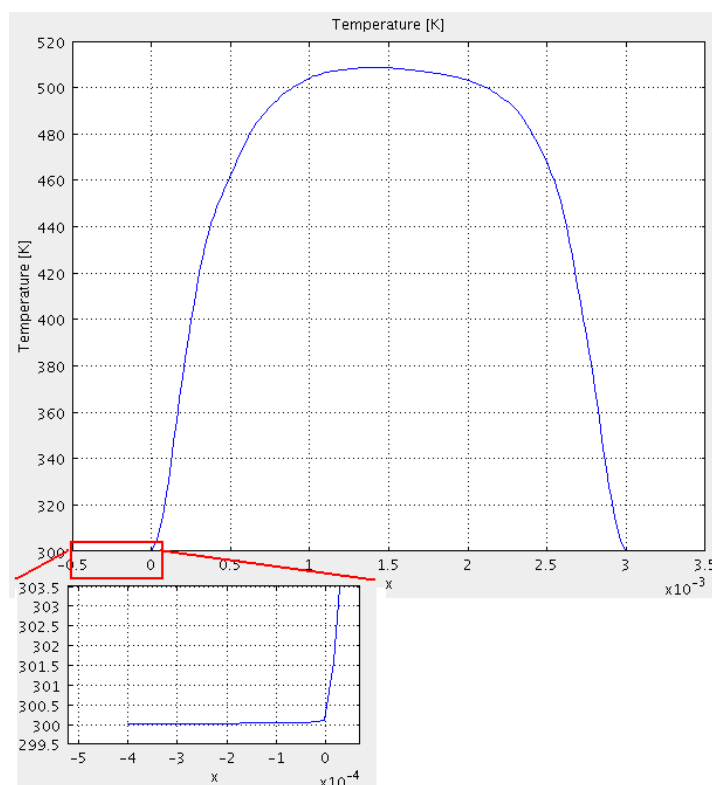


Figure II-8: Temperature profile in the x axis (red line in **Figure II-6**)

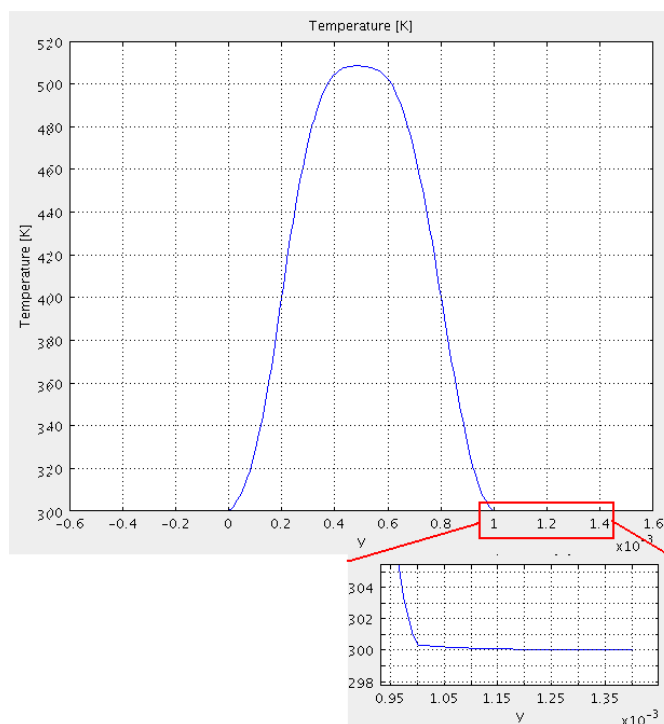


Figure II-9: Temperature profile in the y axis (red line in **Figure II-7**)

So, due to low thermal resistivity of the silicon bulk, the temperature in the back of the silicon bulk is the same that in the membrane/bulk contact points.

We repeat simulations applying a higher voltage (10 V) in order to see if we can use this simplification with a higher temperature in the centre of the membrane.

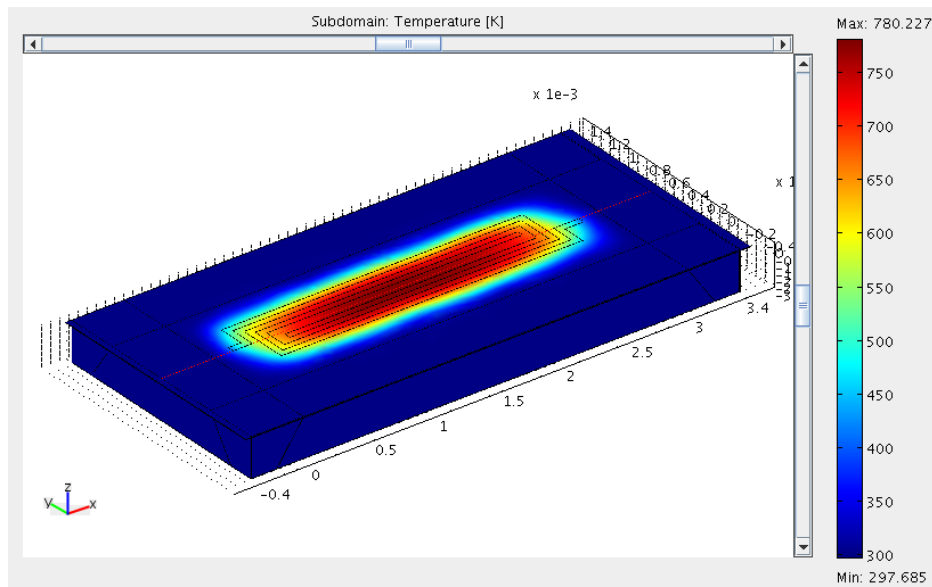


Figure II-10: Temperature distribution of the whole system (10 V)

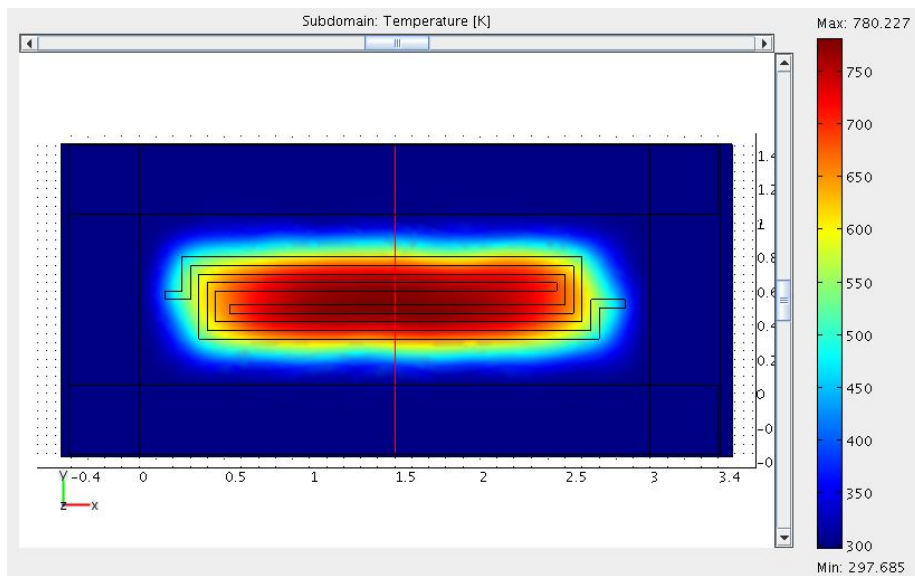


Figure II-11: Temperature distribution on plane x-y (10 V)

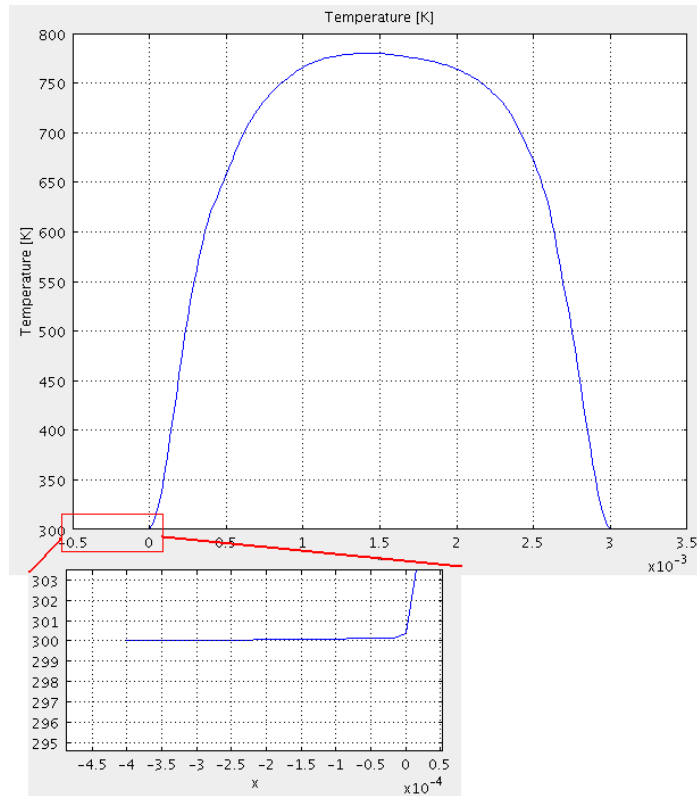


Figure II-12: Temperature profile in the x axis (10 V) (red line in Figure II-10)

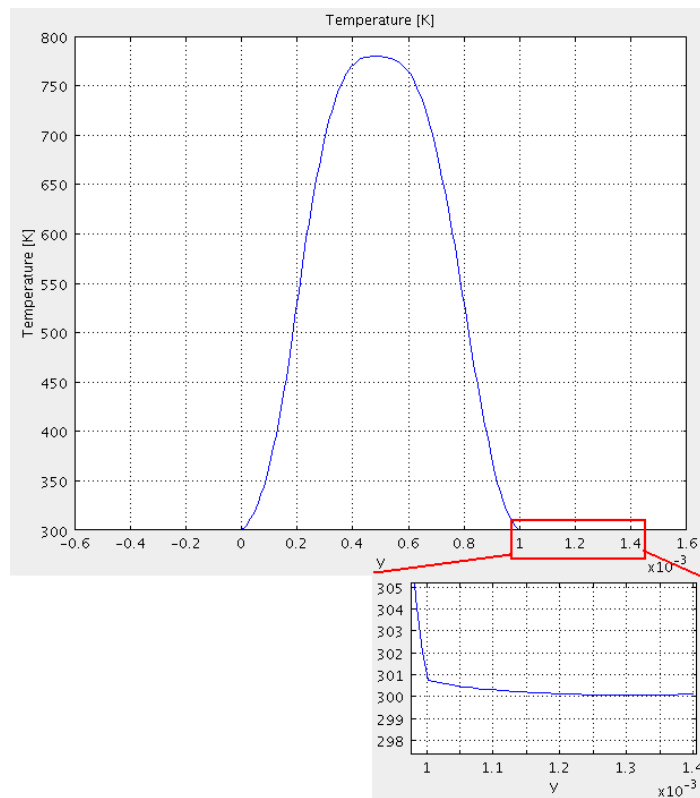


Figure II-13: Temperature profile in the y axis (10 V) (red line in Figure II-11)

We obtain the bottom bulk temperature in the contact with the membrane even if temperature in heater is higher.

So we will use only membrane for simulation with a temperature forced in the contact between membrane and silicon bulk ($T_{amb} + \text{constant} = 300 + 0.6 \text{ K}$).

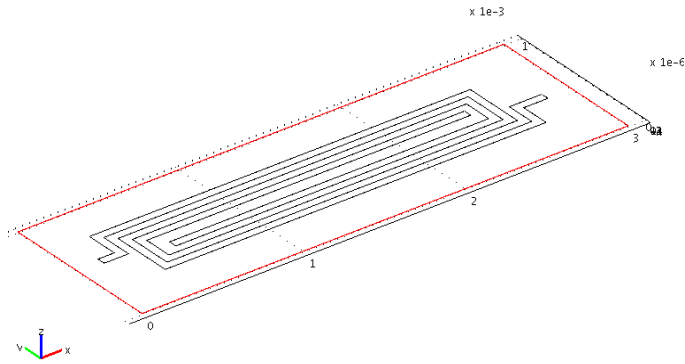


Figure II-14: Contact between membrane and silicon bulk

II.3. Initial heater design simulations

In this chapter we will see simulations developed on first heater design. We will simulate dynamic behaviour in order to obtain the system time response. Then, we will study temperature homogeneity. Both are determinant factors to obtain a narrow desorption peak.

Initial heater design has a double spiral shape. It is designed with a separation of $50\ \mu\text{m}$ between sticks, $50\ \mu\text{m}$ width in the side sticks and $80\ \mu\text{m}$ in the central stick. Its thickness is $2500\ \text{\AA}$.

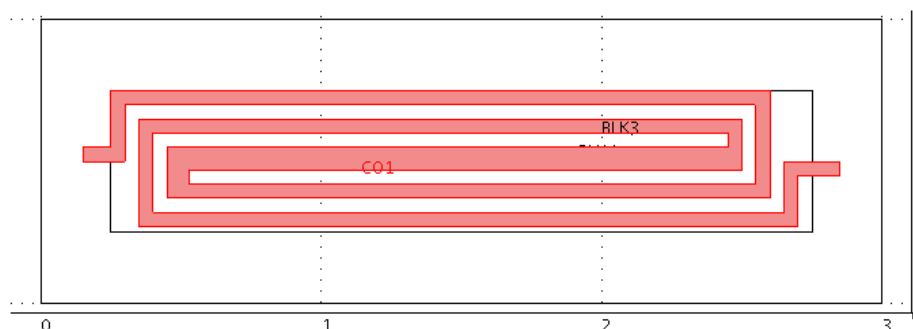


Figure II-15: Initial design

II.3.1. Rising time

We study the rising time at two points, one in the centre and the other one in a corner. This two points are chosen because they are the best and worst cases. In the centre point, we obtain the maximum temperature and it is the quickest time. In the corner we have the minimum temperature and it is the slower one. So, tacking this two points we can see both extremes. Intermediate points will have continuity between them tacking intermediate values.

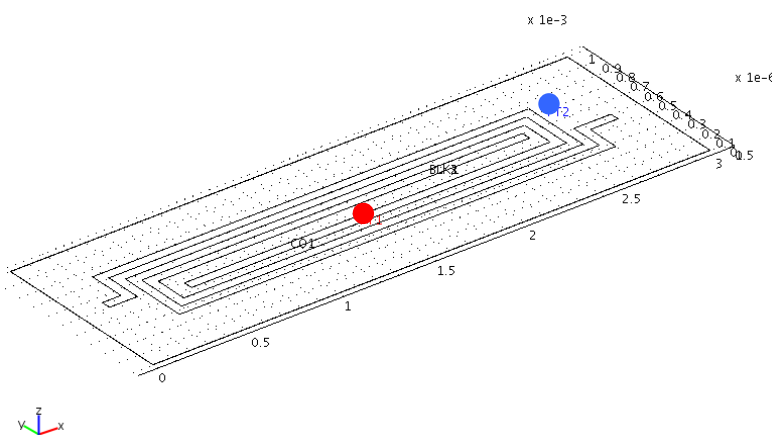


Figure II-16: Localization points

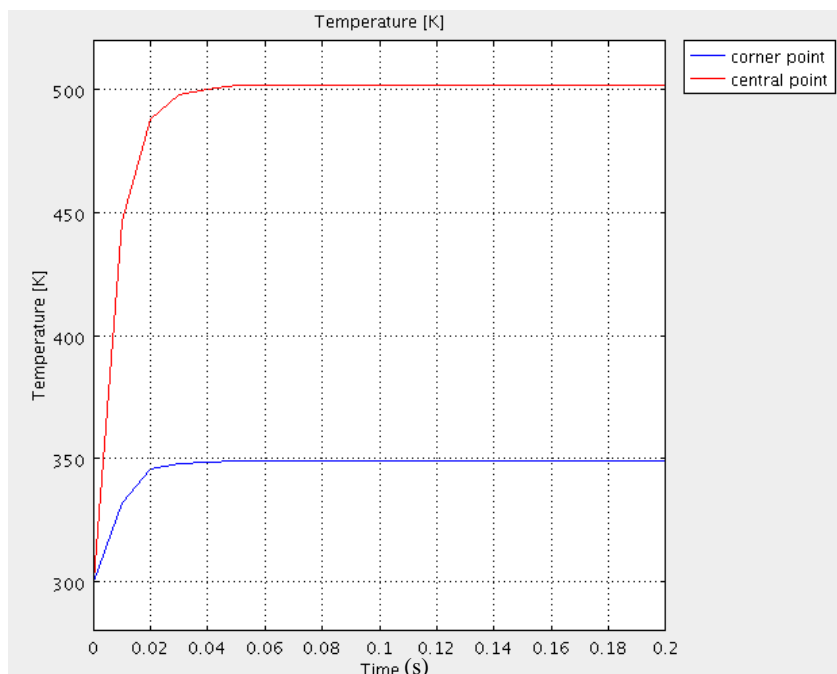


Figure II-17: Dynamic response initial design

Raising time is in the order of tens of milliseconds, so it's acceptable to be used in systems with sensors with a time response of seconds. [7-9]

II.3.2. Temperature homogeneity

Evaluating the temperature distribution in our device, for a 500 K steady peak temperature, the maximum temperature difference around membrane was more than 100 K.

In this chapter, graphics named as diagonal temperature profiles in this chapter are in fact the projection of the diagonal on the x axis.

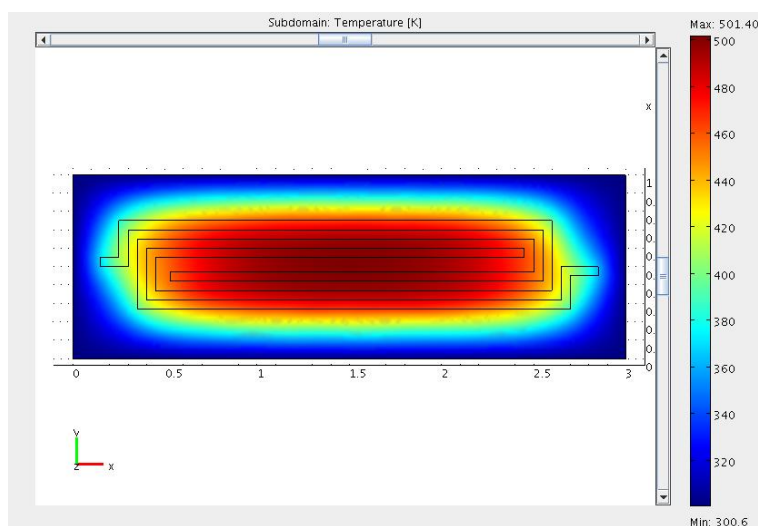


Figure II-18: x-y temperature distribution for initial design

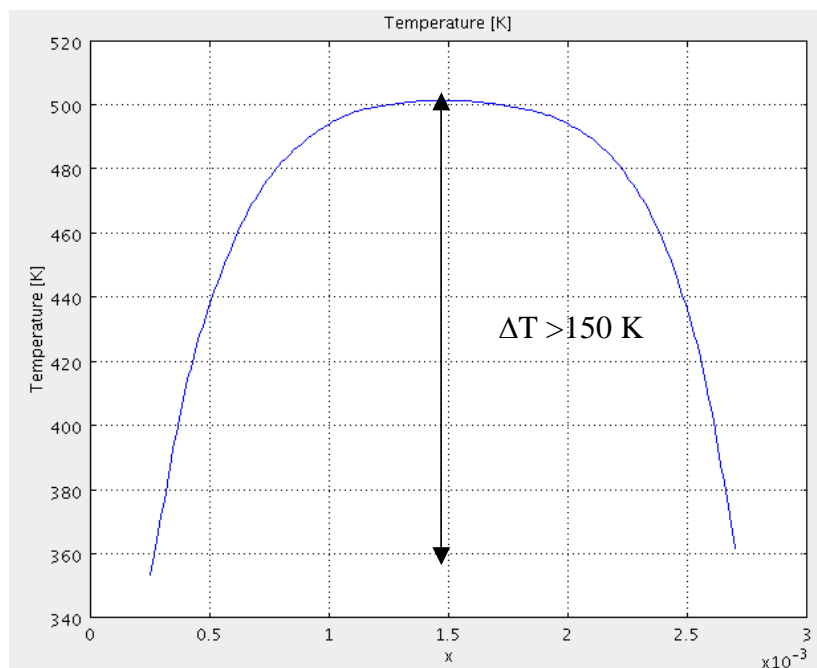


Figure II-19: Temperature profile along diagonal for initial design

Temperature homogeneity in the active area is necessary in order to have a narrow desorption peak and to discriminate different volatiles. It is possible to heat the corner at 500 K applying 220 mW (three times more) but the centre is heated at more of 700 K so it is inefficient. In order to discriminate we need heat the adsorbent material at the desorption temperature for the first volatile, then it will be heated at the second desorption temperature. In Figure II-19 we can see there is more than 150 K of different between the centre and the corner of the heater area, using this we could have the desorption of two volatiles at the same time or some area without desorbing.

Desorption temperatures depends on the adsorbent material and volatiles species to be concentrated. As worst case scenario, a temperature homogeneity in steady state better than 15 K is set as design target.

If we only use area heated with a difference of temperature of 15 K as active area (we only have adsorbent material on this), we can see in Figure II-20 that this area is really small compared to membrane area, so we are losing a lot of area. Figure II-21 shows a comparison of areas.

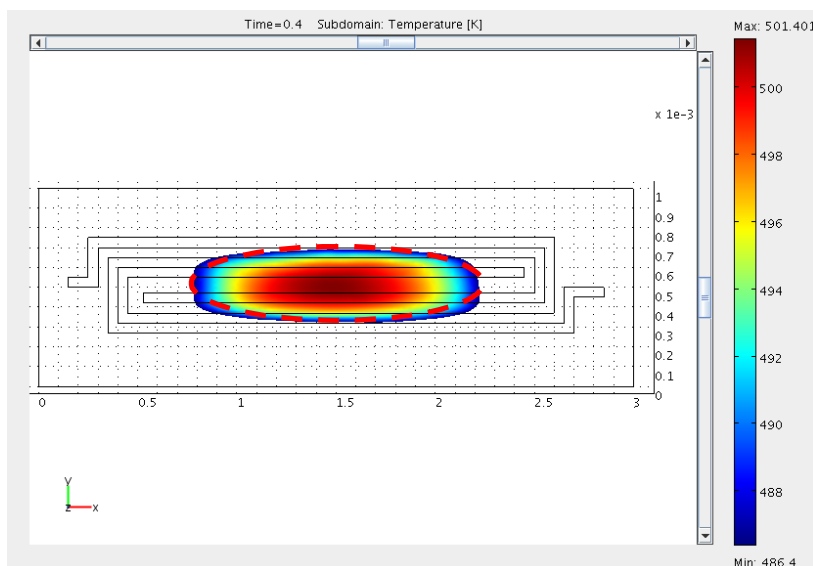


Figure II-20: Area where $\Delta T < 15$ K. (Red line will be used to compare this area)

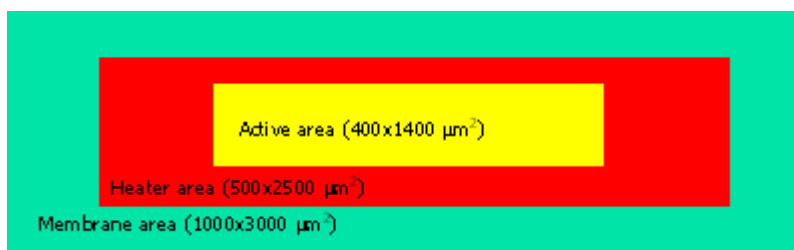


Figure II-21: Area comparison

Heater area / Membrane area = 0.4166
 Active area / Membrane area = 0.186

We are able to use just a 18 % of the membrane. So we need some changes in order to reach the biggest possible active area. Firstly, we will see if the distance between membrane and heater area is optimised or we could use a lower distance in order to increase heater area. Secondly, we will optimise the heater shape in order to homogenize temperature in more heater area. Finally, we will study the use of a diffuser.

II.3.3. Power consumption as a function of distance from the heater to the membrane edge

The idea of this simulations is to study if we could use more area without increasing membrane area in order to use more membrane. We will keep constant the heater area ($1250000 \mu\text{m}^2$) and we will modify the membrane in order to study the power consumption as a function of distance from the heater to the edge of the membrane.

d (μm)	Membrane area (μm^2)	Heater area Membrane area	Power consumption (mW)	Power consumption per unit of area (mW/mm ²)	T max (K)	delta T	Power consumption
							Heater area * Kelvin (mW/mm ² *K)
50	1560000	0,80	116,43	93,14	502,71	205,71	0,45
100	1890000	0,66	93,42	74,74	500,65	203,65	0,37
150	2240000	0,56	83,31	66,65	500,91	203,91	0,33
200	2610000	0,48	77,75	62,20	498,20	201,20	0,31
250	3000000	0,42	75,60	60,48	499,98	202,98	0,30
300	3410000	0,37	73,99	59,19	500,72	203,72	0,29
350	3840000	0,33	73,63	58,90	501,82	204,82	0,29
400	4290000	0,29	73,43	58,75	502,71	205,71	0,29
450	4760000	0,26	72,86	58,29	501,31	204,31	0,29

Table II-3: Distance from the heater to the edge membrane study

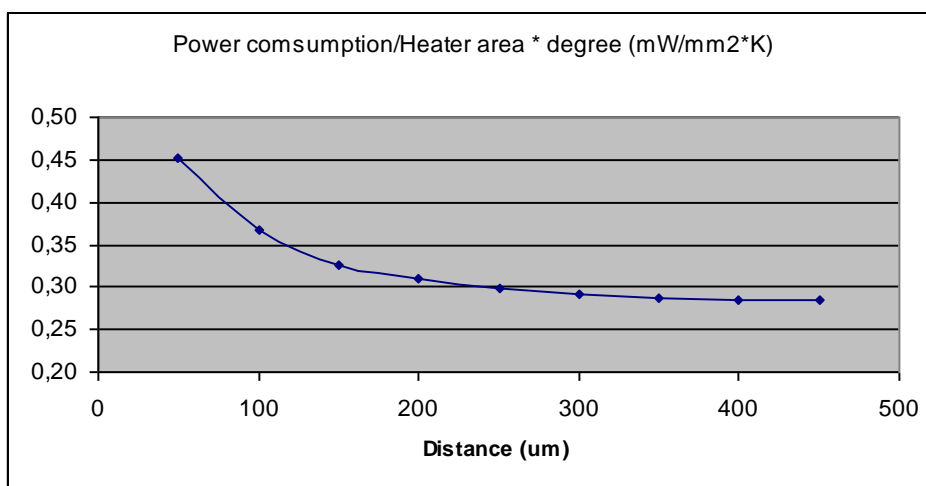


Figure II-22: Power consumption as a function of distance from the heater to the edge membrane

Figure II-22 shows the influence of the distance between the heater and the edge membrane on the power consumption. We can see that the power consumption decreases with increasing distance but for a distance exceeding $250 \mu\text{m}$ the thermal isolation is practically not improved further. So, we will use this distance because smaller one needs higher power consumption and thermal isolation is worst. Thus, we could not obtain more area by reducing distance between heater and silicon plug without increase a lot the power consumption. If we want increment area, we will need larger membranes.

II.4. Heater design

In order to obtain better temperature homogeneity in the active area we have designed some heaters with different shape. The idea is to solve the problem that the central part of the heater is at temperature higher and external parts are at lower temperature. So, we will design heaters in order to heat corners of the area at the same temperature than the centre.

II.4.1. Design 1: 4 heaters

Our objective will be heat the corners. For this reason, in this design we try to make four heaters, every one in a quarter of the active area. Also tracks in the middle are wider than the exteriors ones because this receive the heat around them. This design will be called: 4 heaters.

Every one of the four heaters has the next dimensions:

Width of each track: beginning in the top 15 μm , 15 μm , 30 μm , 30 μm , 60 μm

Distance between tracks: 15-15-30-30-20 μm

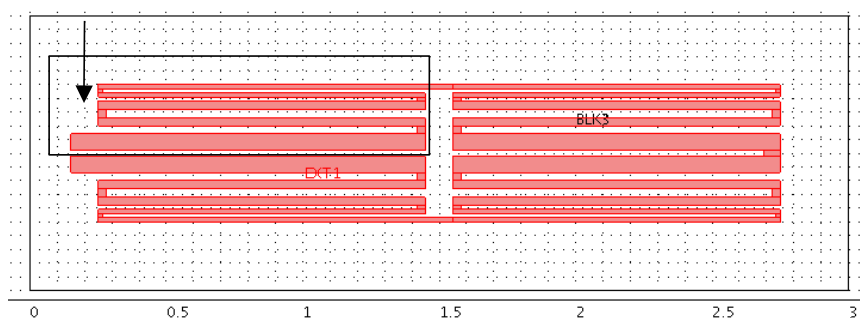


Figure II-23: Design "4 heaters"

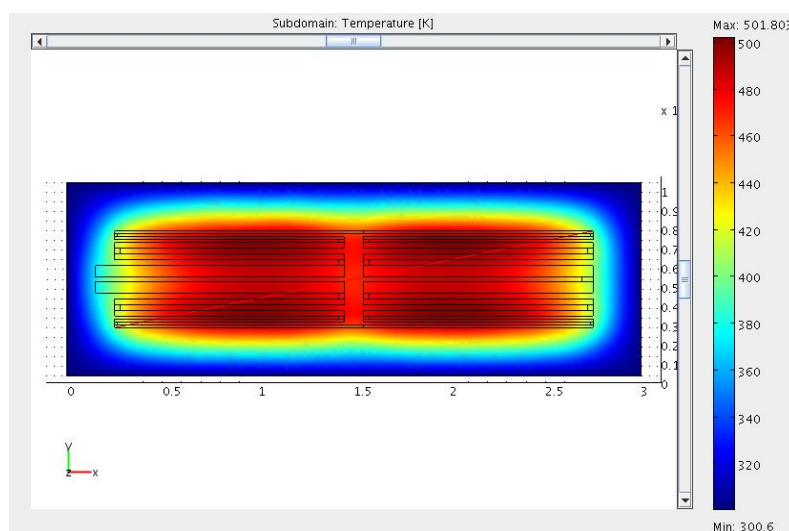


Figure II-24: x-y temperature distribution "4 heaters"

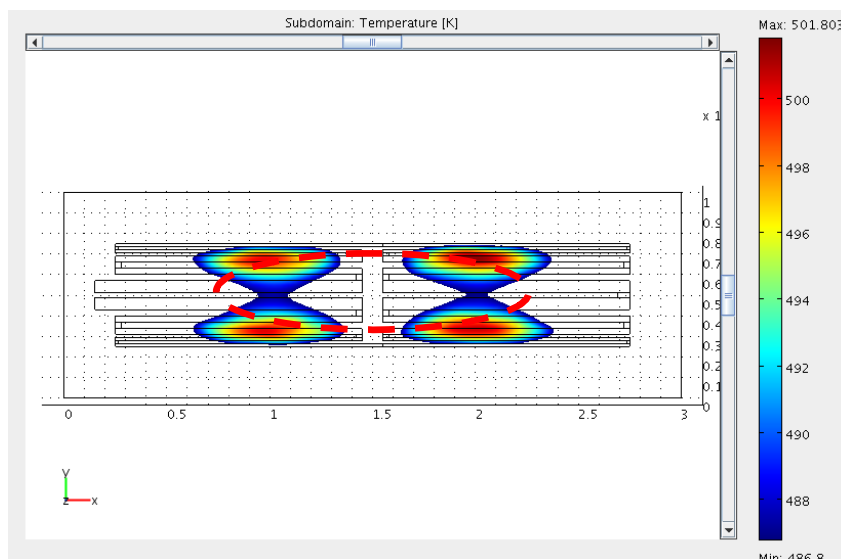


Figure II-25: Area where $\Delta T < 15$ K (4 heaters)

Figure II-25 shows area where temperature difference is smaller than 15 K we have not improved. Figure II-26 shows area heated with a difference smaller than 25 K. This is a 22 % of the membrane, which improves the 20 % of the initial design. In order to improve more, we must take 30 K (Figure II-27), where we have an active area about 36 % of the membrane in front of the initial design with 25 % of the membrane for $\Delta T < 30$ K.

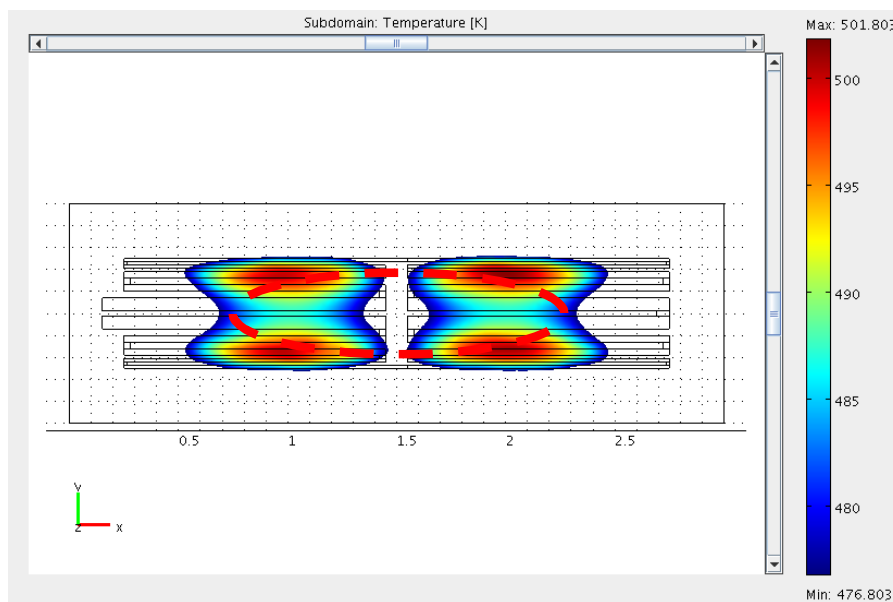


Figure II-26: Area where $\Delta T < 25$ K (4 heaters)

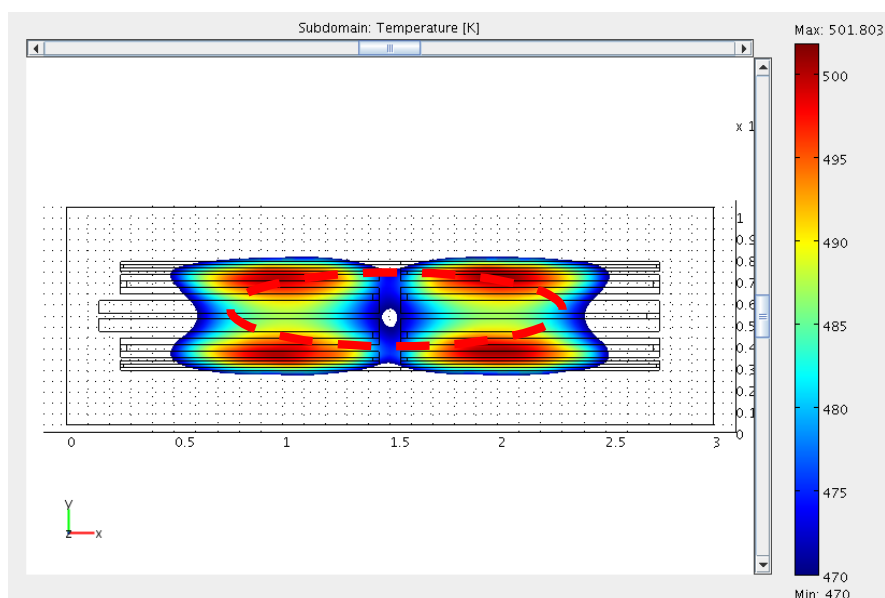


Figure II-27: Area where $\Delta T < 30$ K (4 heaters)

II.4.2. Design 2: Around the oval

In this case the idea was to heat only the external parts and reach temperature in the centre by a distribution plate of platinum (without electric connexion).

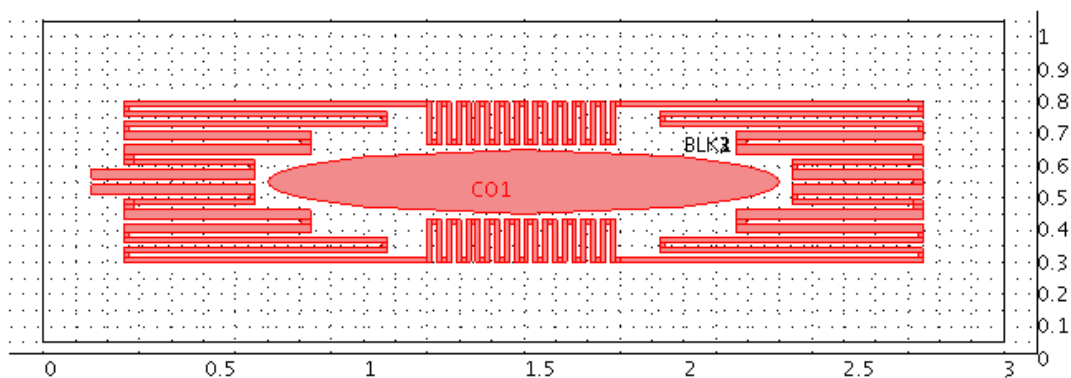


Figure II-28: Design "around the oval"

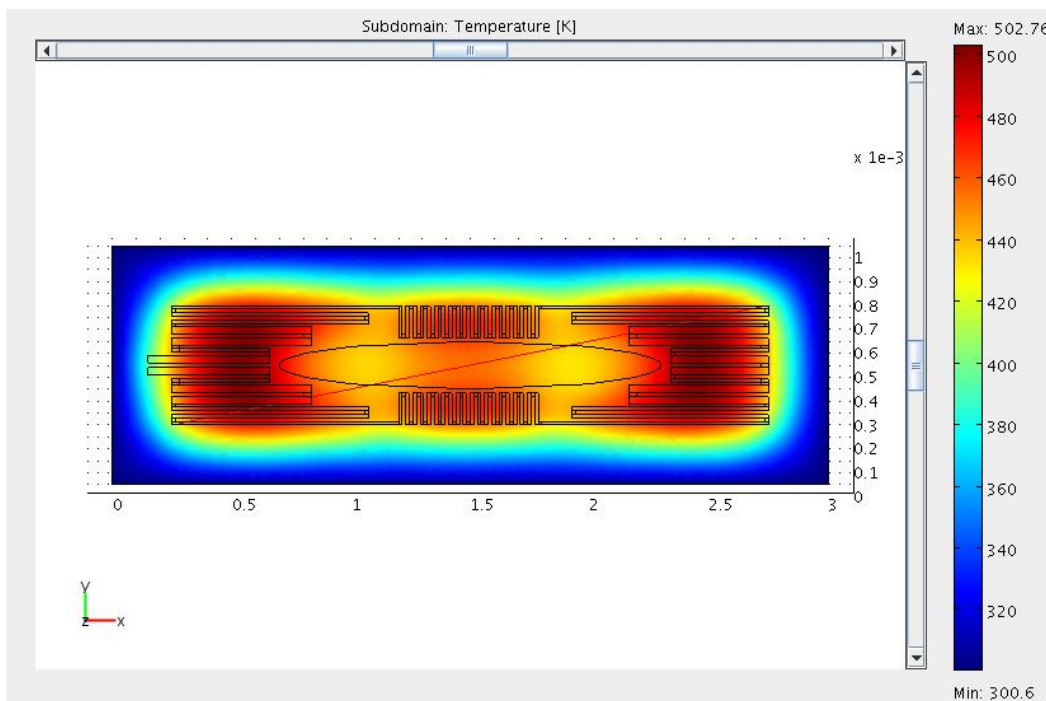


Figure II-29: x-y temperature distribution “around the oval”

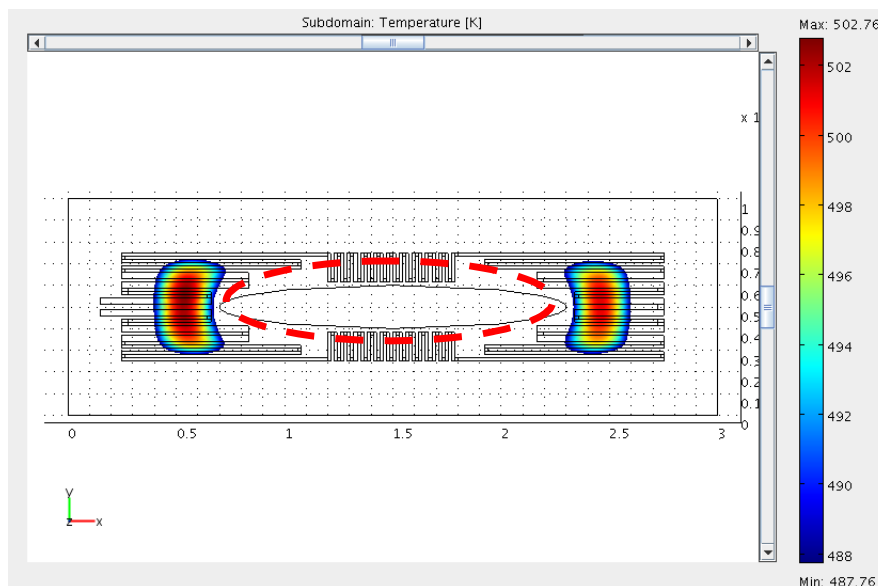


Figure II-30: Area where $\Delta T < 15$ K (Around the oval)

Taking area where difference temperature is smaller than 15 K we have not improved. Figure II-31 shows area where difference temperature is smaller than 25 K this design is not improving until we take a difference temperature is smaller than 60 K (Figure II-32) which is too high difference.

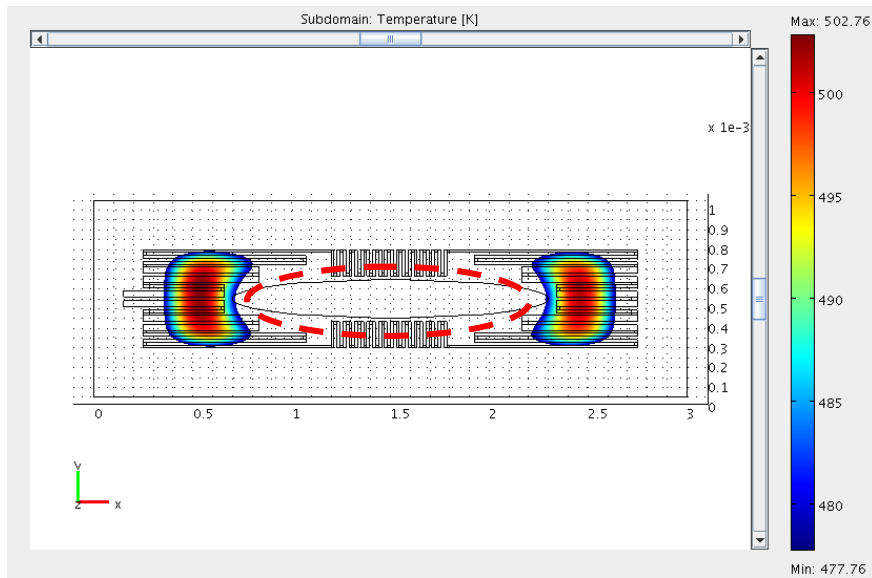


Figure II-31: Area where $\Delta T < 25$ K (Around the oval)

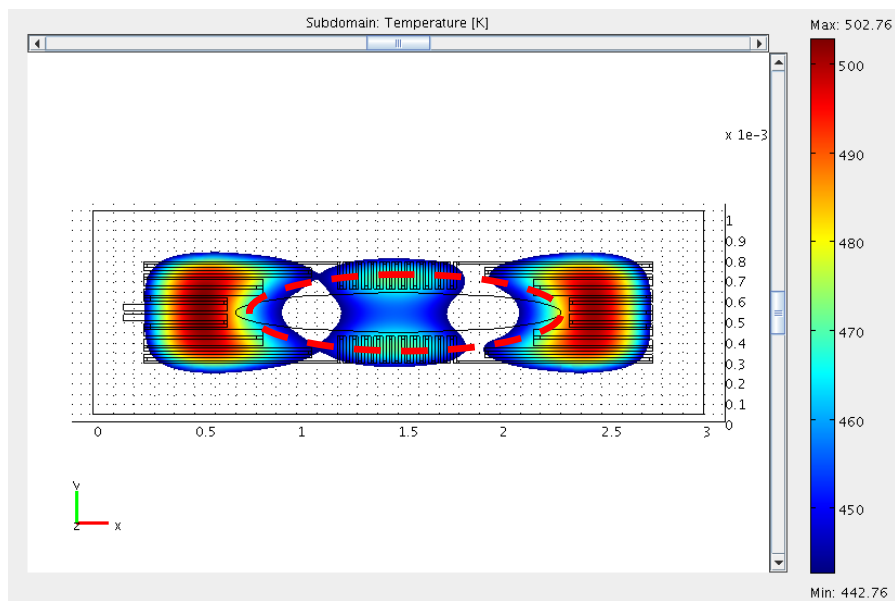


Figure II-32: Area where $\Delta T < 60$ K (Around the oval)

II.4.3. Design 3: 15-30-60-80

In this case we use the idea to make every track the double of its external one and vary the distance between them. [10]

Width of each track: 15-30-60-80-60-30-15 μm

Distance between tracks: 25-40-40-40-40-25 μm

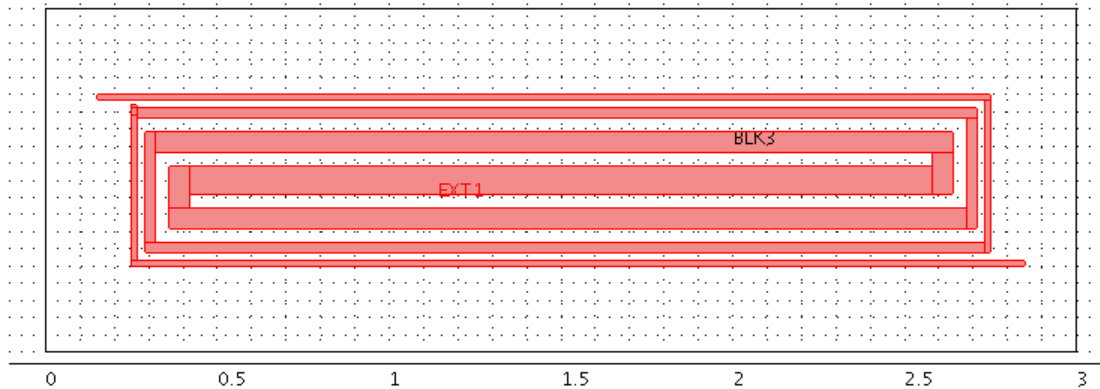


Figure II-33: Design "15-30-60-80"

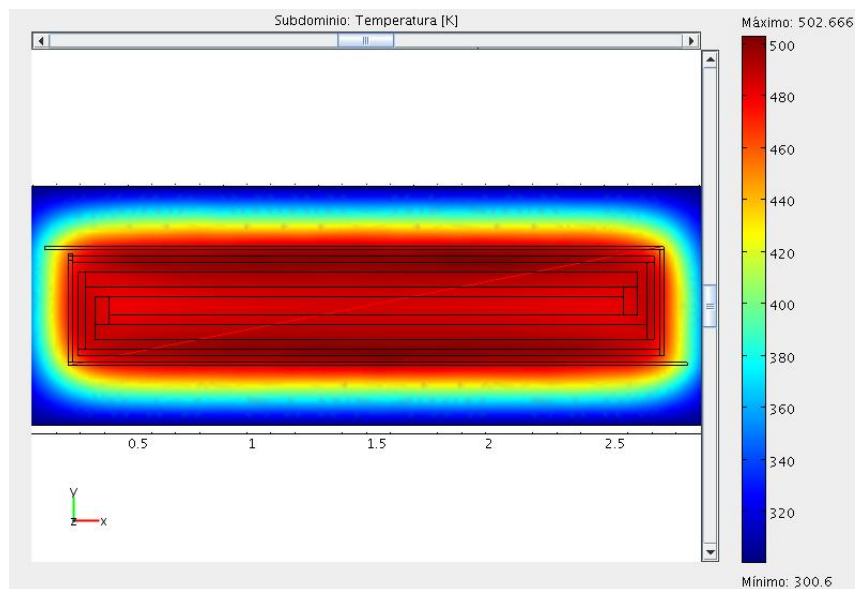


Figure II-34: x-y temperature distribution "15-30-60-80"

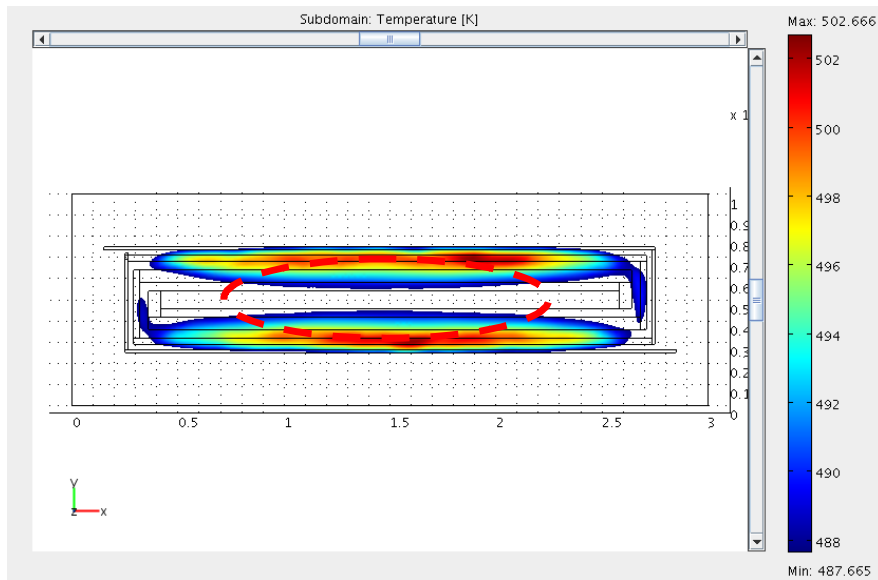


Figure II-35: Area where $\Delta T < 15$ K (15-30-60-80)

This has been improved. With this design we have a 29 % of the membrane heated at the desired temperature, but it can improved much more if we accept a difference of temperature of 25 K (See Figure II-36).

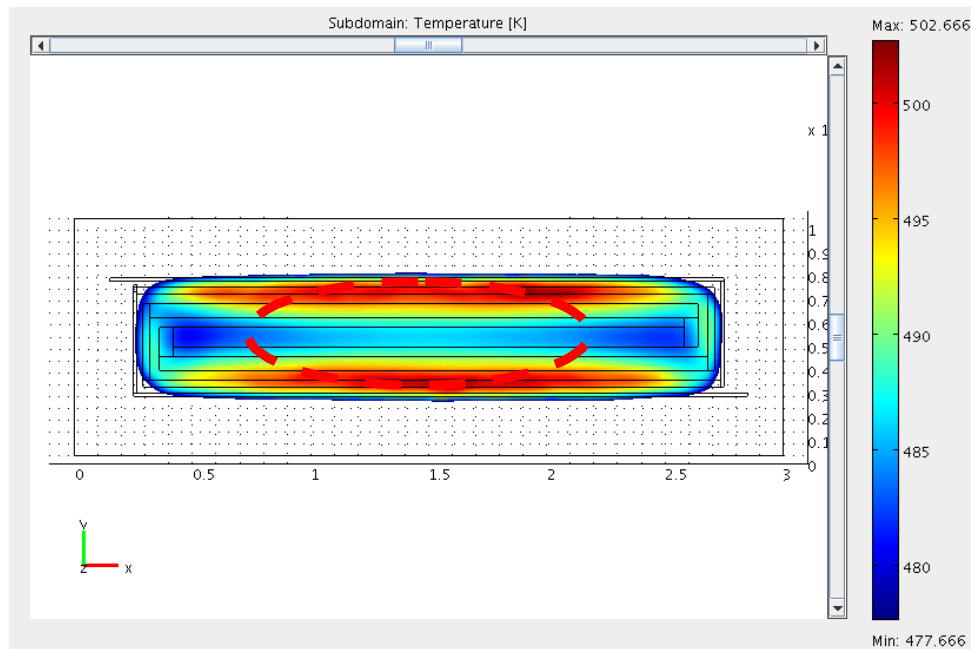


Figure II-36: Area where $\Delta T < 25$ K (15-30-60-80)

II.4.4. Comparison

Next table shows a summary of all designs:

$$\left. \begin{array}{l} \text{Membrane area : } 3 \text{ mm}^2 \\ \text{Heater area : } 1.25 \text{ mm}^2 \end{array} \right\} \frac{\text{Heater area}}{\text{Membrane area}} = 41.67 \%$$

Heater represents a 41.67 % of the membrane, in order to compare designs between them, we will use the percentage related to the heater area.

Design	Power consumption (mW)	Active area [mm ²] ($\Delta T < 15$ K)	$\frac{\text{Active area}}{\text{Heater area}}$ ($\Delta T < 15$ K)	Active area [mm ²] ($\Delta T < 25$ K)	$\frac{\text{Active area}}{\text{Heater area}}$ ($\Delta T < 25$ K)
Initial design	76.884	0.56	44.8 %	0.6	48 %
4 heaters	86.516	0.32	25.6 %	0.7	56 %
Around the oval	80.901	0.24	19.2 %	0.32	25.6 %
15-30-60-80	98.056	0.88	70.4 %	1.21	96.8 %

Table II-4: Summary of new design related to the heater area

Figure II-37 shows the temperature profile along the diagonal for new heater designs. We can see that the best improvement is reached with the 15-30-60-80 design . We have improved the difference temperature corner-centre from more than 150 K (See Figure II-19) to approximately 60 K.

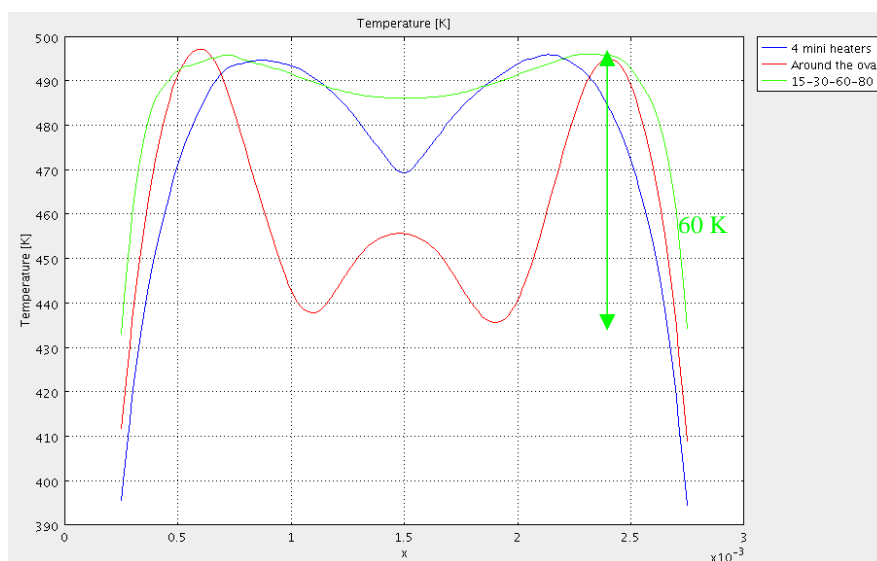


Figure II-37: Temperature profile along the diagonal for new designs

We discard the design around the oval because in this case there is big difference of temperature in the centre.

Bibliography [11-14] reports that to obtain an optimum temperature uniformity a Pt double spiral resistor is used. Guidi et al. [10] propose that a double spiral shape with variable width exhibits better temperature uniformity than a double spiral shape with constant width. Using a large aspect ratio membrane variable width is more important than double spiral shape. The double spiral shape influences more in square heaters.

To obtain further improvement in homogenisation we will need to use a silicon plug as a diffuser. We will see this in next chapter.

II.5. Silicon plug diffuser

In this chapter we will use a silicon plug as a diffuser in order to improve temperature homogeneity [15-17]. We will study how this plug influences on power consumption and rising time.

II.5.1. Initial design with silicon plug

We simulate the initial design with an added silicon plug. We use two different thickness of silicon plug: $5\ \mu\text{m}$ and $10\ \mu\text{m}$. We evaluate different thickness in order to see the thermal influence and to study which is better to fabricate taking into account that it introduces a costly step. Fabrication time of this silicon plug is exponential to its thickness. Then we study temperature distribution, response time in two points (See Figure II-16) and power consumption.

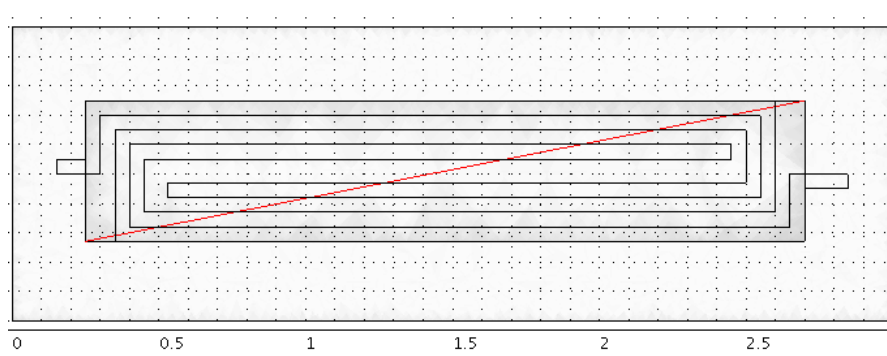


Figure II-38: Red line defines the diagonal profile

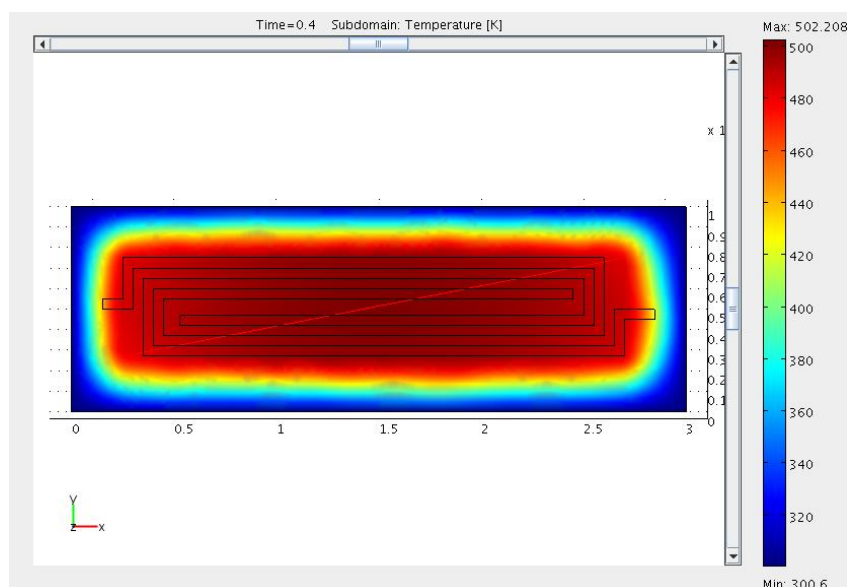


Figure II-39: Initial design with a silicon plug thickness $5\ \mu\text{m}$

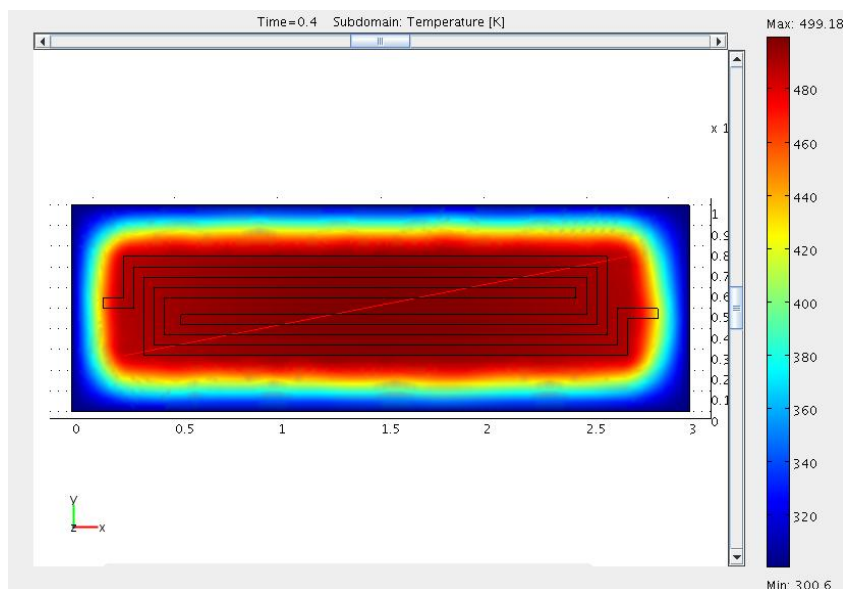


Figure II-40: Initial design with a silicon plug thickness 10 μm

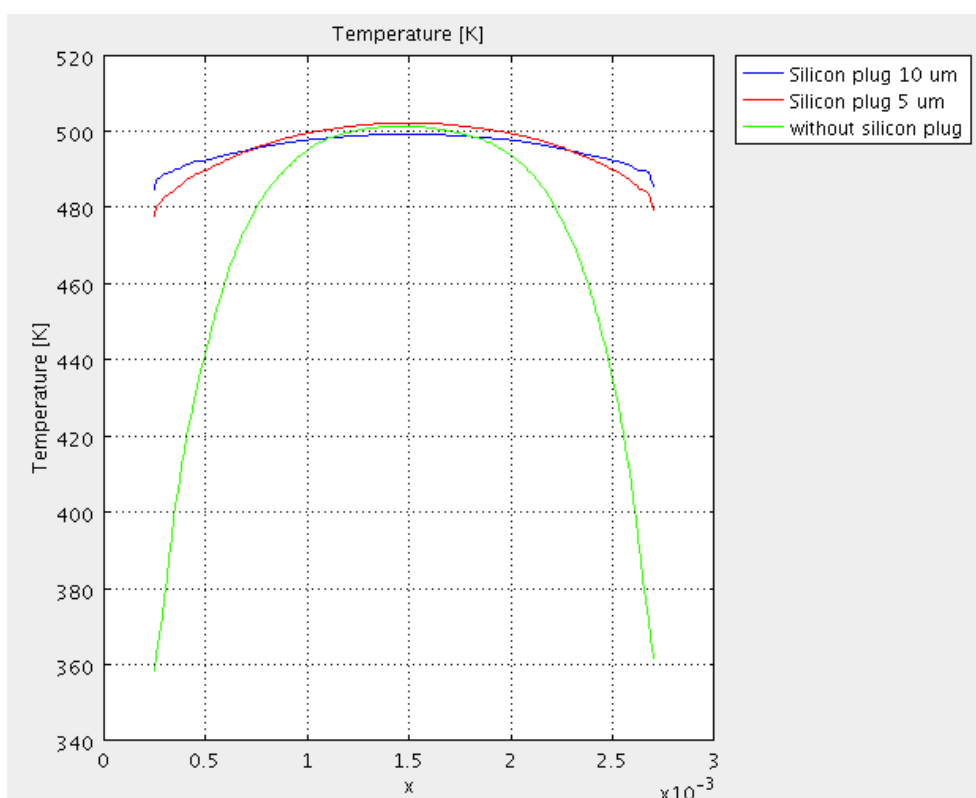


Figure II-41: Temperature profile along the diagonal initial design with silicon plug

Figure II-41 shows the diagonal profile in three cases: without silicon plug (green line), with a silicon plug of 5 μm (red line) and with a silicon plug of 10 μm (blue line). Without a silicon plug we have a differences of temperatures around 150 K. Using a silicon of 5 μm differences of temperature is around 20 K and using a silicon plug of 10 μm is less than 20 K. Now we will see the raising time in each case.

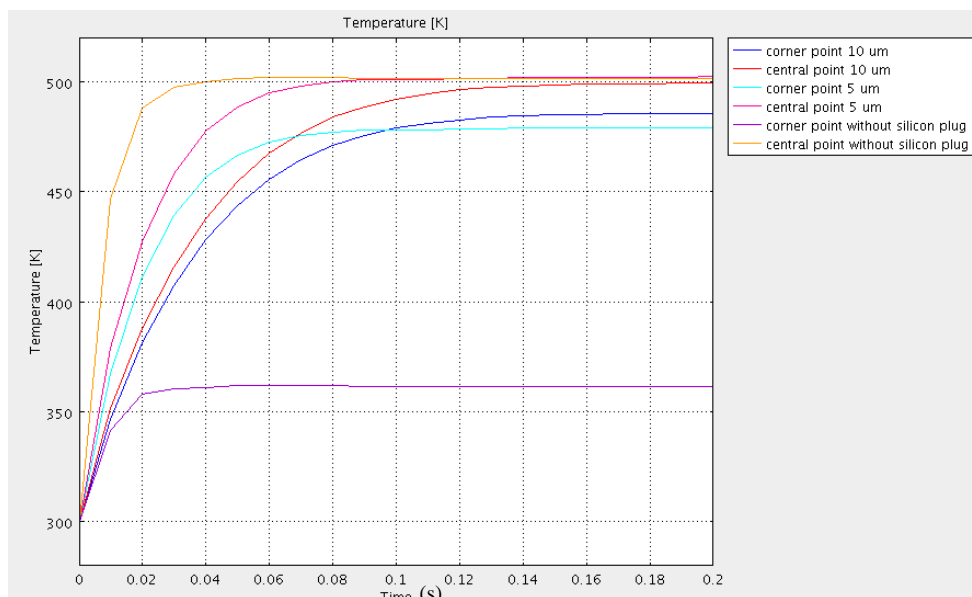


Figure II-42: Dynamic response initial design with different silicon plugs

Figure II-42 shows rising times for the centre and corner points, in the three cases studied. As thicker is the silicon plug longer is the rising time, but, as we have said before, this is not determinant because sensor has a response time of seconds.

Design	Power consumption (mW)	ΔT (K)	Rising time (ms)
Initial Design	76.884	>150	50 ms
Initial Design + 5 μm Silicon plug	112.591	>20	100 ms
Initial Design+ 10 μm Silicon plug	114.297	<20	150 ms

Table II-5: Silicon plug influences on initial design

Conclusions:

- ✓ With a silicon plug we improve temperature homogeneity, so the difference of temperature between centre and corner is smaller: from 150 K to less than 20 K.
- ✓ Rising time in membrane centre with silicon plug is three times bigger (50 – 150 ms) but it's not determinant for us tacking into account that the sensor has response time in order of seconds.
- ✓ Difference of rising time at corners is not comparable because they are reaching really different temperatures
- ✓ Power consumption with a silicon plug doubles respect one without it, because we are heating much more area at high temperature which increases heat losses

10 μm depth silicon plug homogenise temperature better than 5 μm depth. But as thicker is more complex is the fabrication. We have decided a silicon plug 5 μm depth will be used, because it homogenizes enough and it is less costly.

II.5.2. 15-30-60-80 design with silicon plug

Now, we will study the behaviour with a silicon plug beneath the 15-30-60-80 heater. In this case we have simulated the same heater with different silicon plug thickness. In Table II-6 we can see the difference of temperature between centre and corner of the heater area as a function of the silicon plug thickness.

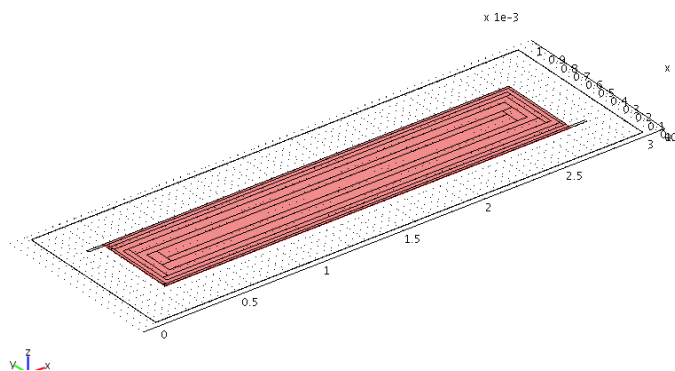


Figure II-43: Silicon plug beneath the 15-30-60-80 heater

Silicon plug thick (μm)	Difference temperature (K)
1	35
2.5	16
5	11
7.5	9
10	7

Table II-6: Comparison difference of temperature with different thick silicon plug. Heater 15-30-60-80

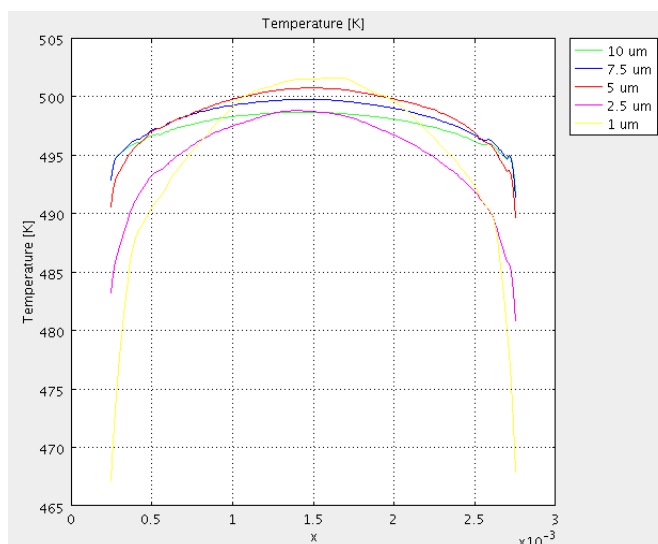


Figure II-44: Temperature profile along the diagonal 15-30-60-80 design with different thickness of silicon plug

With this design we need a less thick plug compared to the initial design in order to obtain the same temperature homogenisation. So, despite homogenisation carried out by the silicon plug, best heater design should be used.

II.5.3. Power consumption as a function of distance from the silicon plug to the membrane edge

We have studied the power consumption as a function of distance from the silicon plug to the edge membrane. The silicon plug has a thickness of 10 μm .

The membrane has a dimension of 1000 μm * 3000 μm , so the area is 3000000 μm^2 .

d (μm)	Heater area (μm^2)	$\frac{\text{Heater area}}{\text{Membrane area}}$	Power consumption (mW)
0	3000000	1,000	10266,804
50	2610000	0,870	3919,429
100	2240000	0,747	1770,700
200	1890000	0,630	685,693
250	1560000	0,520	337,031
300	1250000	0,417	229,334
350	960000	0,320	155,485

Table II-7: Distance from the silicon plug to the edge membrane study

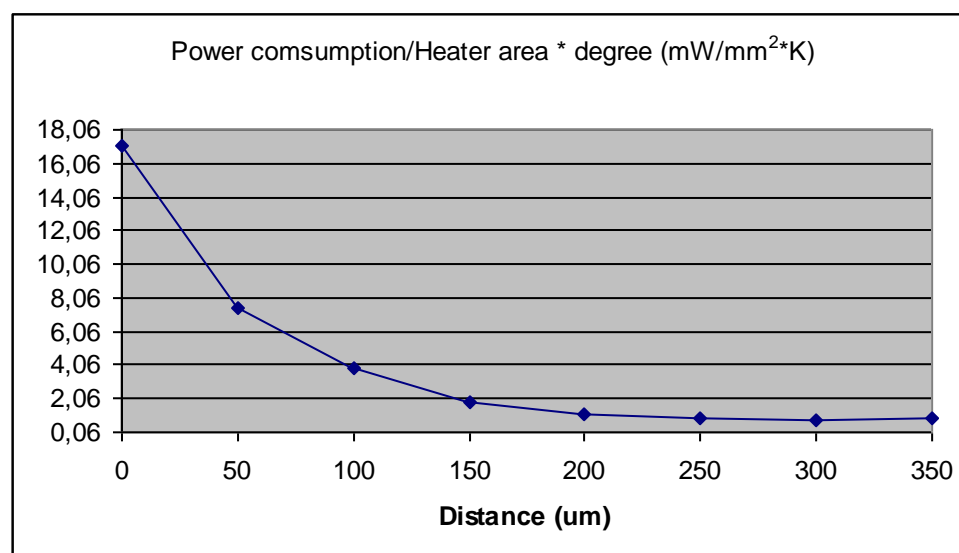


Figure II-45: Power consumption as a function of distance from the silicon plug to the edge membrane

Figure II-45 shows the influence of the size of the membrane on the power consumption. We can see that the power consumption decreases with increasing distance but for a distance exceeding 250 μm the thermal isolation is practically not improved further.

II. 6. Conclusions

In our initial design there is more than 150 K of difference between the centre and the corner of the heater area. Using this design, if we use area with a temperature difference smaller than 15 K, we are able to use just a 18 % of the membrane.

We have studied the distance between the heater and the edge membrane. We will use a distance of 250 μm , because a smaller one needs higher power consumption.

We have designed two heaters (4 heaters and 15-30-60-80 designs) which improve temperature homogenisation. We have seen that a platinum double spiral resistor is not an optimum heater design. A double spiral shape with variable width exhibits better temperature uniformity than constant width.

A silicon plug introduced under the heater area improves temperature homogeneity. Rising time is also increased but it's not determinant for us, tacking into account that the sensor has response time in order of seconds. Power consumption with a silicon plug doubles respect one without it, because we are heating much more area at high temperature which increases heat losses. A 5 μm depth silicon plug will be used, because it homogenizes enough to our application and it is less costly than one deeper. Despite homogenisation carried out by the silicon plug, best heater design should be used.

II.7. References

1. Rossi, C., E. Scheid, and D. Esteve," Theoretical and experimental study of silicon micromachined microheater with dielectric stacked membranes". *SENSORS AND ACTUATORS A-PHYSICAL*, 1997. pp. 183-189
2. Astie, S., A. Gue, E. Scheid, L. Lescouzeres, and A. Cassagnes," Optimization of an integrated SnO₂ gas sensor using a FEM simulator". *SENSORS AND ACTUATORS A-PHYSICAL*, 1998. pp. 205-211
3. Sberveglieri, G., W. Hellmich, and G. Muller," Silicon hotplates for metal oxide gas sensor elements". *MICROSYSTEM TECHNOLOGIES*, 1997. pp. 183-190
4. Plaza, J., M. Lopez-Bosque, I. Gracia, C. Cane, J. Wollenstein, G. Kuhner, et al.," A glass/silicon technology for low-power robust gas sensors". *IEEE SENSORS JOURNAL*, 2004. pp. 195-206
5. Solzbacher, F., C. Imawan, H. Steffes, E. Obermeier, and H. Moller," A modular system of SiC-based microhotplates for the application in metal oxide gas sensors". *SENSORS AND ACTUATORS B-CHEMICAL*, 2000. pp. 95-101
6. Triantafyllopoulou, R., S. Chatzandroulis, C. Tsamis, and A. Tserepi," Alternative micro-hotplate design for low power sensor arrays". *MICROELECTRONIC ENGINEERING*, 2006. pp. 1189-1191
7. Kunt, T., T. McAvoy, R. Cavicchi, and S. Semancik," Optimization of temperature programmed sensing for gas identification using micro-hotplate sensors". *SENSORS AND ACTUATORS B-CHEMICAL*, 1998. pp. 24-43
8. Stankova, M., X. Vilanova, J. Calderer, E. Llobet, J. Brezmes, I. Gràcia, et al.," Sensitivity and selectivity improvement of rf sputtered WO₃ microhotplate gas sensors". *SENSORS AND ACTUATORS B-CHEMICAL*, 2005. pp. 241-248
9. Blanco, F.; *DISEÑO Y CARACTERIZACIÓN DE PRECONCENTRADORES PARA MICROSISTEMAS INTEGRADOS: APLICACIÓN A LA DETECCIÓN DE BENCENO*; Ingeniería Electrónica, Eléctrica i Automática; URV; 2009
10. Guidi, V., G. Cardinali, L. Dori, G. Faglia, M. Ferroni, G. Martinelli, et al.," Thin-film gas sensor implemented on a low-power-consumption micromachined silicon structure". *SENSORS AND ACTUATORS B-CHEMICAL*, 1998. pp. 88-92
11. Cardinali, G., L. Dori, M. Fiorini, I. Sayago, G. Faglia, C. Perego, et al.," A smart sensor system for carbon monoxide detection". *ANALOG INTEGRATED CIRCUITS AND SIGNAL PROCESSING*, 1997. pp. 275-296
12. Baroncini, M., P. Placidi, G. Cardinali, and A. Scorzoni," Thermal characterization of a microheater for micromachined gas sensors". *SENSORS AND ACTUATORS A-PHYSICAL*, 2004. pp. 8-14
13. Dori, L., P. Maccagnani, G. Cardinali, M. Fiorini, I. Sayago, S. Guerri, et al. "New material and heater geometry for high performance micromachined thermally insulated structures in gas sensor applications". 1997. Warsaw, Poland.
14. Faglia, G., E. Comini, M. Pardo, A. Taroni, G. Cardinali, S. Nicoletti, et al.," Micromachined gas sensors for environmental pollutants". *MICROSYSTEM TECHNOLOGIES*, 1999. pp. 54-59
15. Gotz, A., I. Gracia, C. Cane, and E. LoraTamayo," Thermal and mechanical aspects for designing micromachined low-power gas sensors". *JOURNAL OF MICROMECHANICS AND MICROENGINEERING*, 1997. pp. 247-249

16. Briand, D., A. Krauss, B. van der Schoot, U. Weimar, N. Barsan, W. Gopel, et al.," Design and fabrication of high-temperature micro-hotplates for drop-coated gas sensors". *SENSORS AND ACTUATORS B-CHEMICAL*, 2000. pp. 223-233
17. Barrettino, D., M. Graf, W. Song, K. Kirstein, A. Hierlemann, and H. Baltes," Hotplate-based monolithic CMOS microsystems for gas detection and material characterization for operating temperatures up to 500(circle)C". *IEEE JOURNAL OF SOLID-STATE CIRCUITS*, 2004. pp. 1202-1207

III. NEW MEMBRANES DESIGN

III.1. Introduction

In order to have a larger area we have designed three new membranes: 1.5 mm x 5 mm, 2 mm x 4.5 mm and 3 mm x 3 mm.

In this chapter we study if it's better to use a big membrane or some small ones. We compare areas used to fabricate the membrane and areas usable to deposit adsorbent material. Then, we will design different heaters for this areas and finally we will compare all of them tacking into account power consumption, silicon area needed, active area obtained and thermal distribution.

III.2. Membrane shape and sizes

Table III-1 shows membranes sizes. We can see that for a given piece of silicon using a big membrane we have more heater area than using some small membranes. Comparing the same membrane area, a square membrane has more heater area than a rectangular one.

Membrane	x (mm)	y (mm)	Silicon area (mm ²)	Membrane area (mm ²)	Heater area (mm ²)
1 x 3	1	3	4,8564	3	1,25
1,5 x 5	1,5	5	10,4064	7,5	4,5
2 x 4,5	2	4,5	11,9064	9	6
3 x 3	3	3	11,6964	9	6,25

Table III-1: New membranes design

III.3. Heater design

For rectangular membranes we have designed two heaters. First one is a heater made joining as 15-30-60-80 heaters as necessary to fill the membrane area. Second heater design is a double spiral one.

III.3.1. Membrane area: 1.5 mm x 5 mm. Heater area: 1 mm x 4.5 mm A

In this case we have two 15-30-60-80 heaters together:

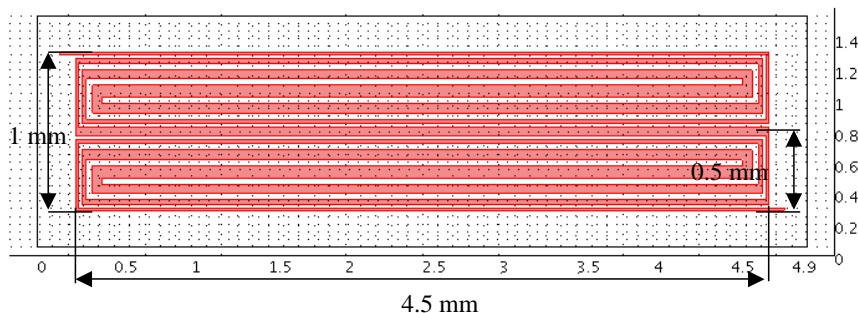


Figure III-1: Heater design for membrane 1.5 mm x 5 mm

Each one has dimensions specified in next figures. Figure III-2 shows track thickness and Figure III-3 shows separation between tracks.

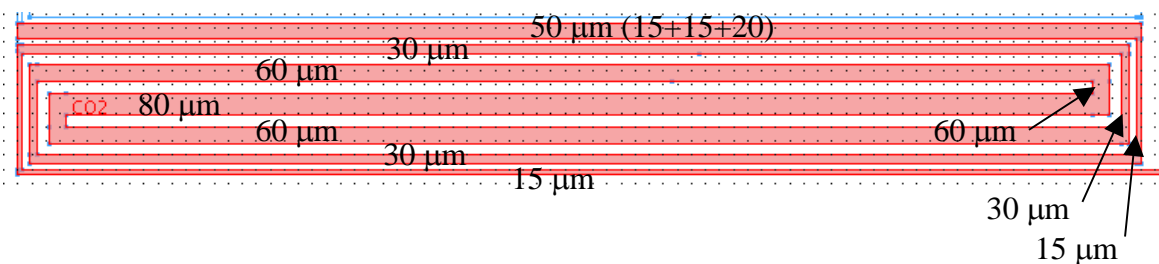


Figure III-2: Track thickness for design A for membrane 1.5 mm x 5 mm

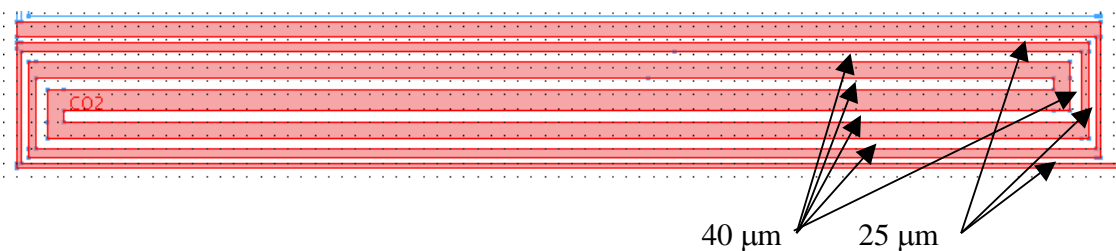


Figure III-3: Separation between tracks in design A for membrane 1.5 mm x 5 mm

Temperature distribution when a voltage of 23.5 V is applied is shown in Figure III-4. The current that is crossing the heater is 10.618 mA, so the power consumption is 249.523 mW.

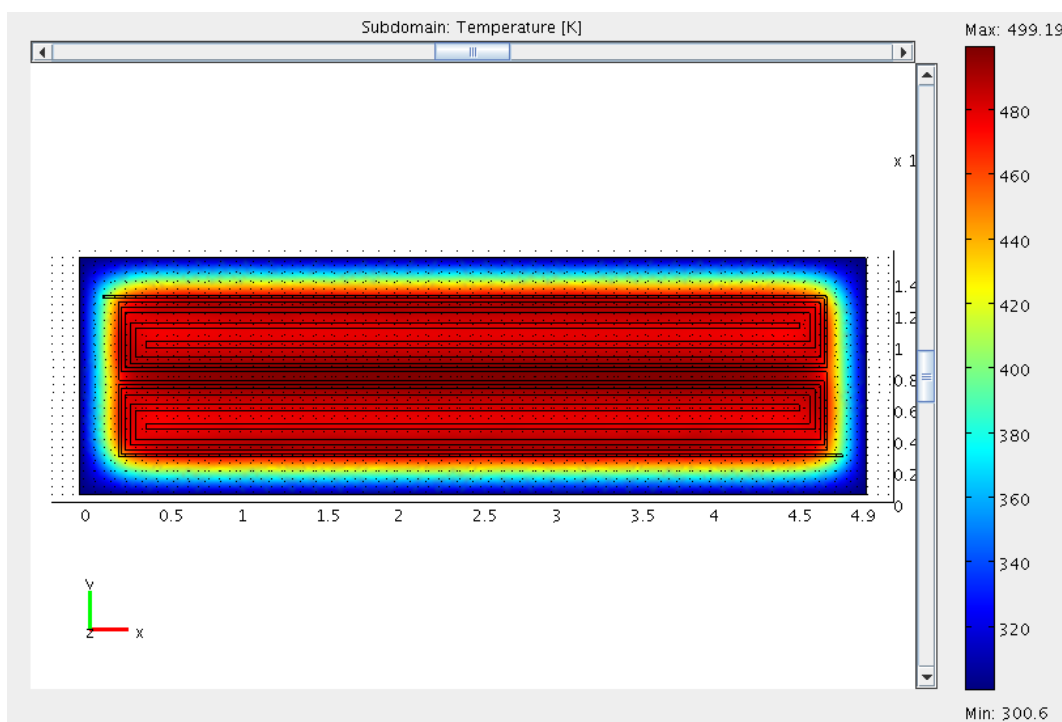


Figure III-4: Temperature distribution at heater design A, membrane 1.5 mm x 5 mm

We have a heated area with a difference of 25 K almost the heater area:

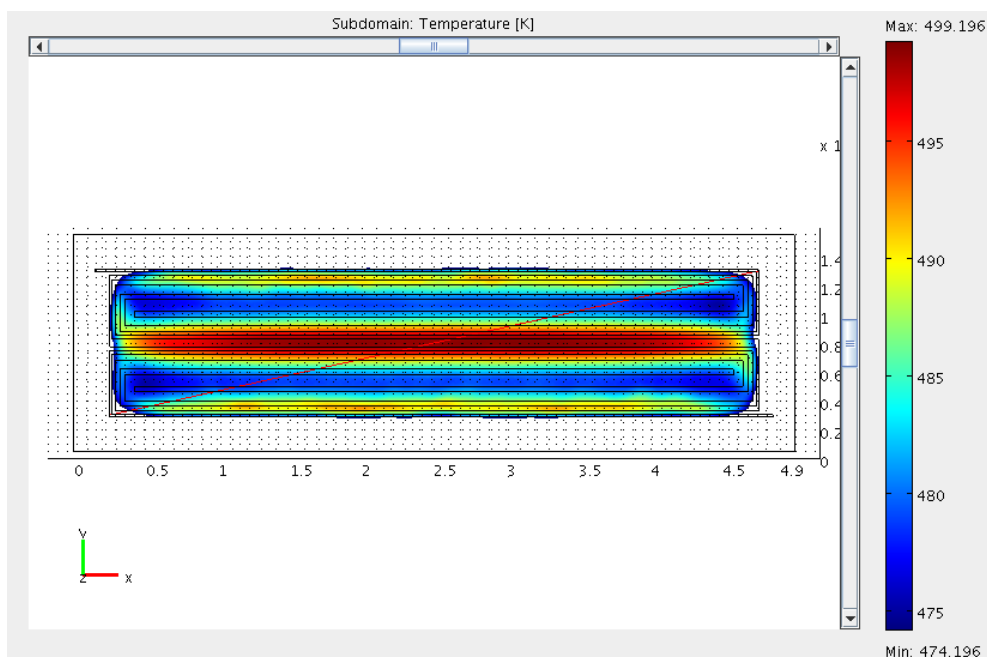


Figure III-5: Heated area within a difference of 25 K at heater design A, membrane 1.5 mm x 5 mm

In Figure III-5 we can see a red line crossing the diagonal of the heater which is used to see the 2D profile in next figure. $(x=250e-6; y=250e-6), (x=4750e-6; y=1250e-6)$

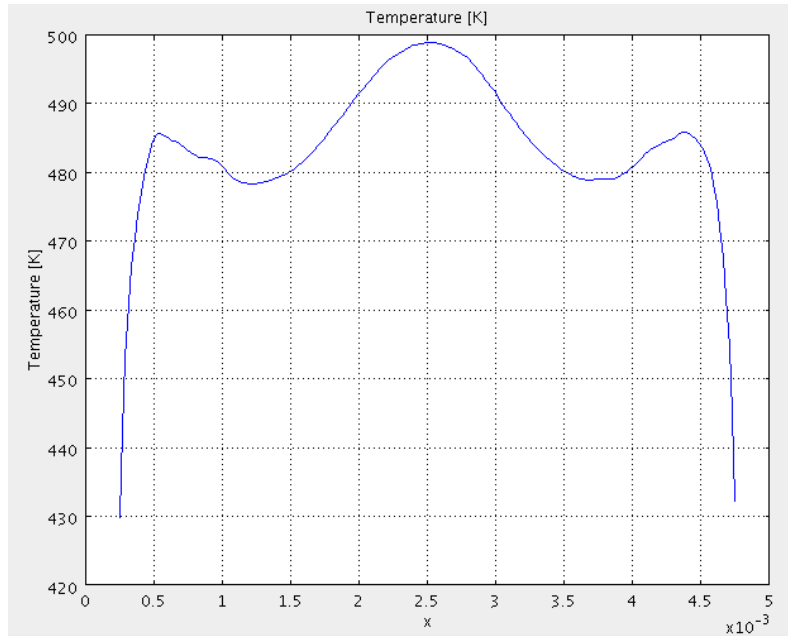


Figure III-6: Diagonal profile along the diagonal heater design A membrane 1.5 mm x 5 mm

III.3.2. Membrane area: 1.5 mm x 5 mm. Heater area: 1 mm x 4.5 mm B

In this case we design a double spiral:

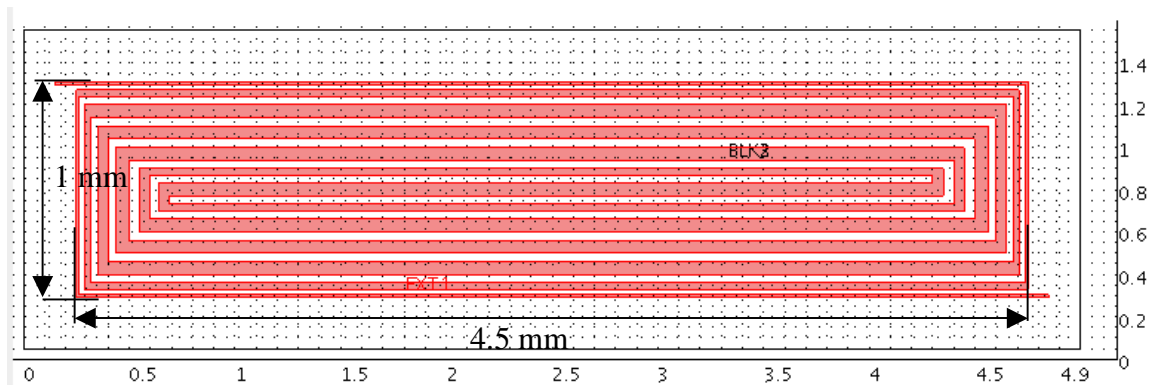


Figure III-7: Second heater design for membrane 1.5 mm x 5 mm

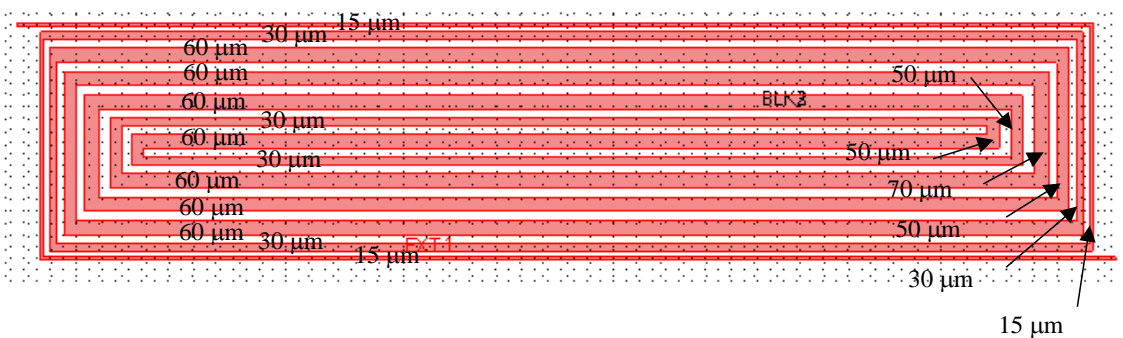


Figure III-8: Track thickness for design B for membrane 1.5 mm x 5 mm

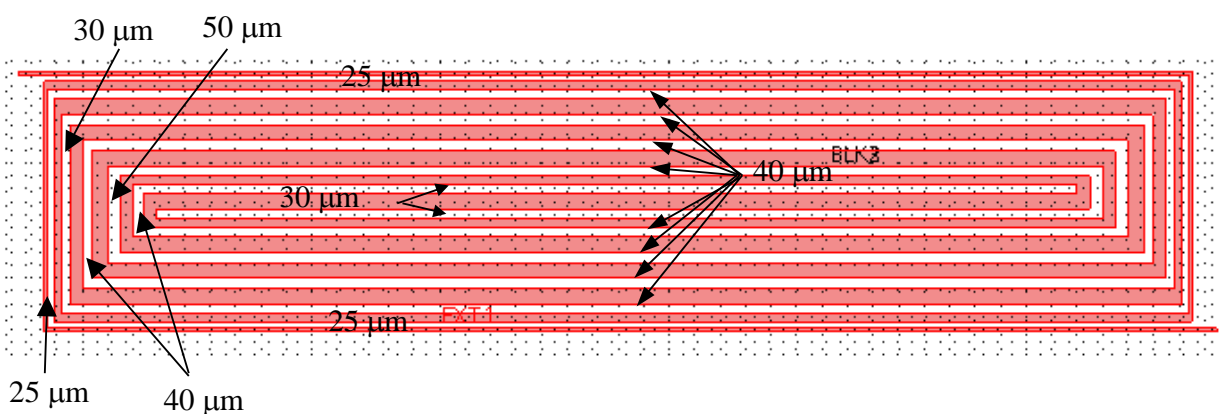


Figure III-9: Separation between tracks in design B for membrane 1.5 mm x 5 mm

Figure III-10 shows temperature distribution when a voltage of 24 V is applied. The current that is crossing the heater is 10.671 mA so, the power consumption is 256.104 mW.

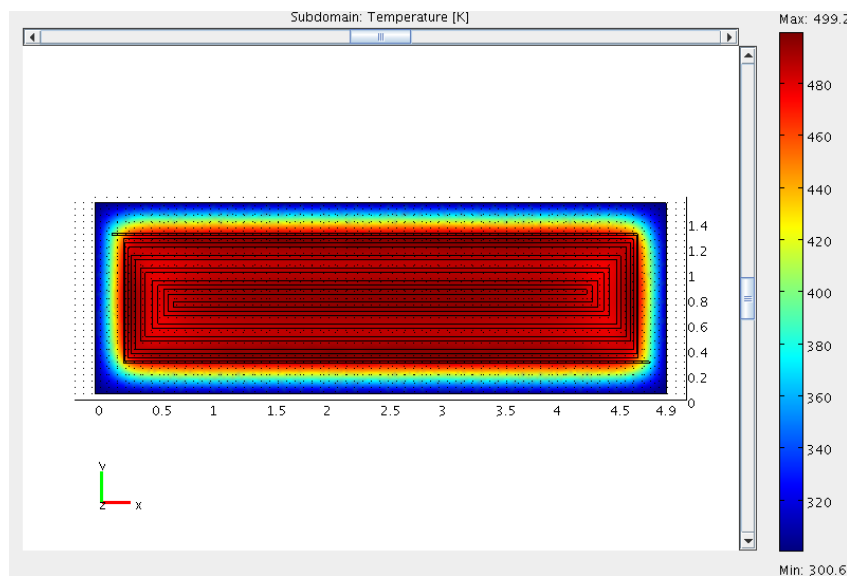


Figure III-10: Temperature distribution at heater design B, membrane 1.5 mm x 5 mm

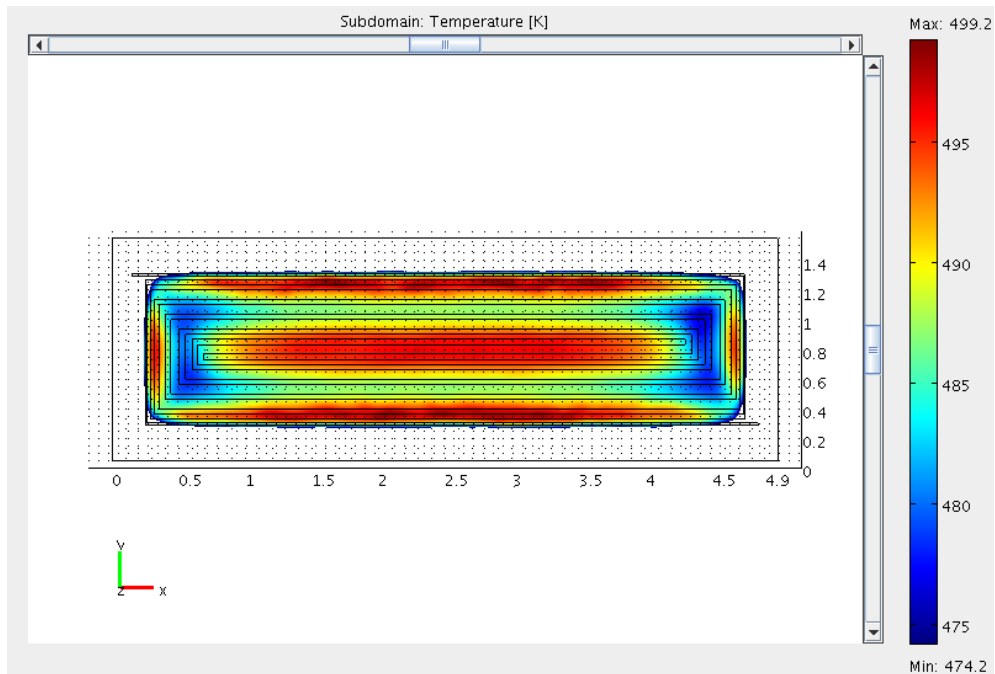


Figure III-11: Heated area within a difference of 25 K at heater design B, membrane 1.5 mm x 5 mm

2D profile ($x=250e-6; y=250e-6$), ($x=4750e-6; y=1250e-6$)

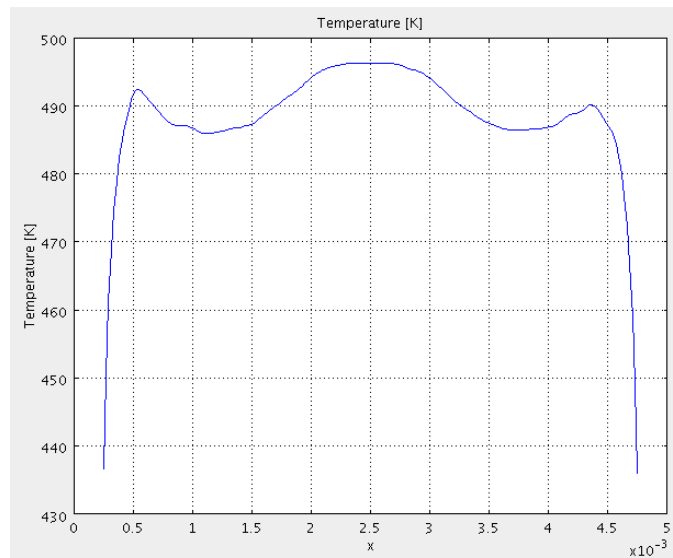


Figure III-12: Diagonal profile along the diagonal heater design B, membrane 1.5 mm x 5 mm

Figure III-13 shows both diagonal profiles together.

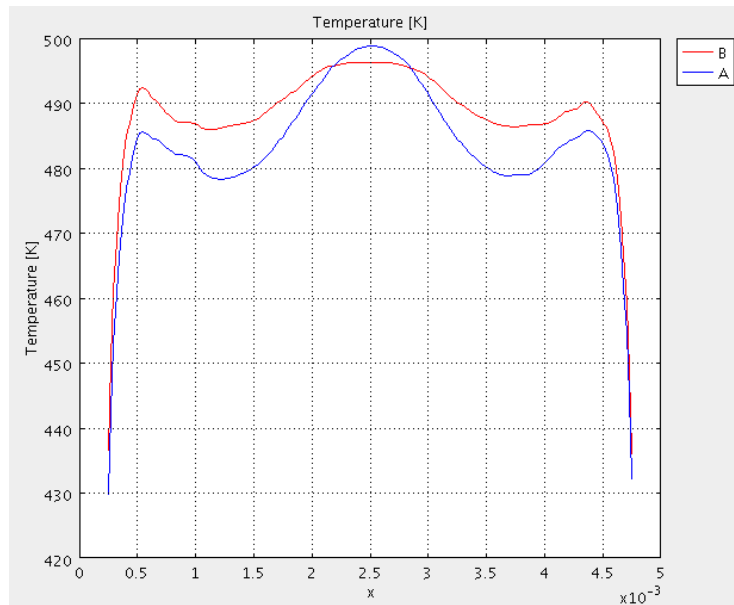


Figure III-13: Comparison between two heaters designed for membrane 1.5 mm x 5 mm

So we have two heater design which both of them have a difference of temperature less than 25 K. The heater design using an spiral is better tacking into account the temperature distribution (difference of temperature around 10 K).

III.3.3. Membrane area: 2 mm x 4.5 mm. Heater area: 1.5 mm x 4 mm A

In this case we have three spirals together:

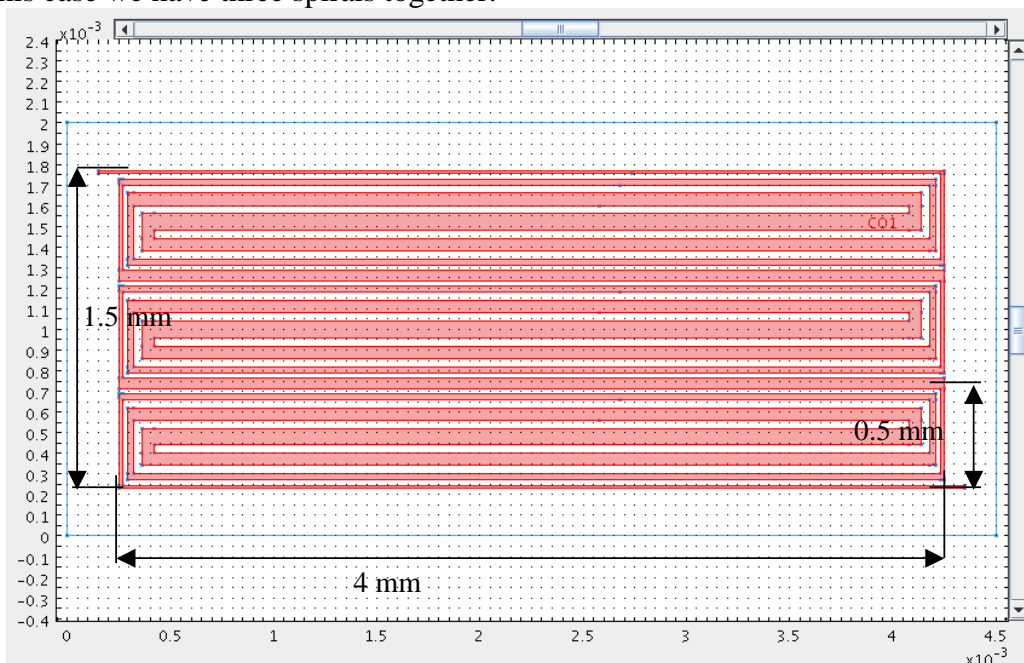


Figure III-14: Heater design for membrane 2 mm x 4.5 mm

Any one of this spirals have dimensions specified in next figures. In Figure III-15 we can see the track thickness and in Figure III-16 we can see the separation between tracks.

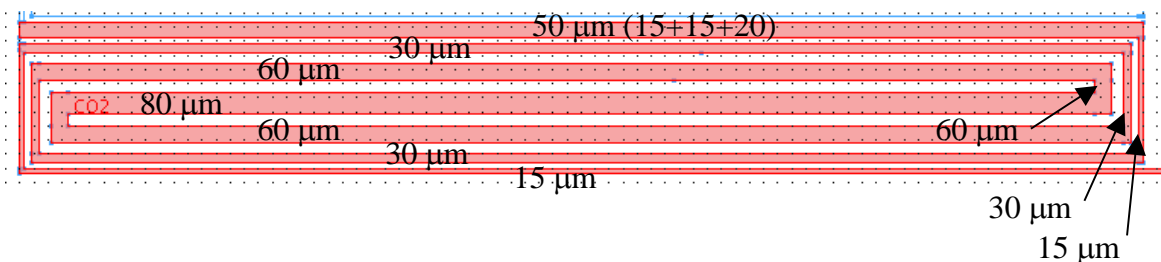


Figure III-15: Track thickness for design A for membrane 2 mm x 4.5 mm

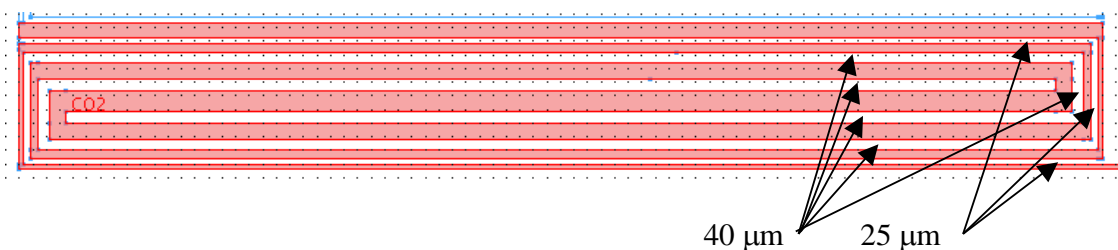


Figure III-16: Separation between tracks in design A for membrane 2 mm x 4.5 mm

Figure III-17 shows temperature distribution when a voltage of 28.5 V is applied. The current crossing the heater is 10.574 mA, so the power consumption is 301.359 mW.

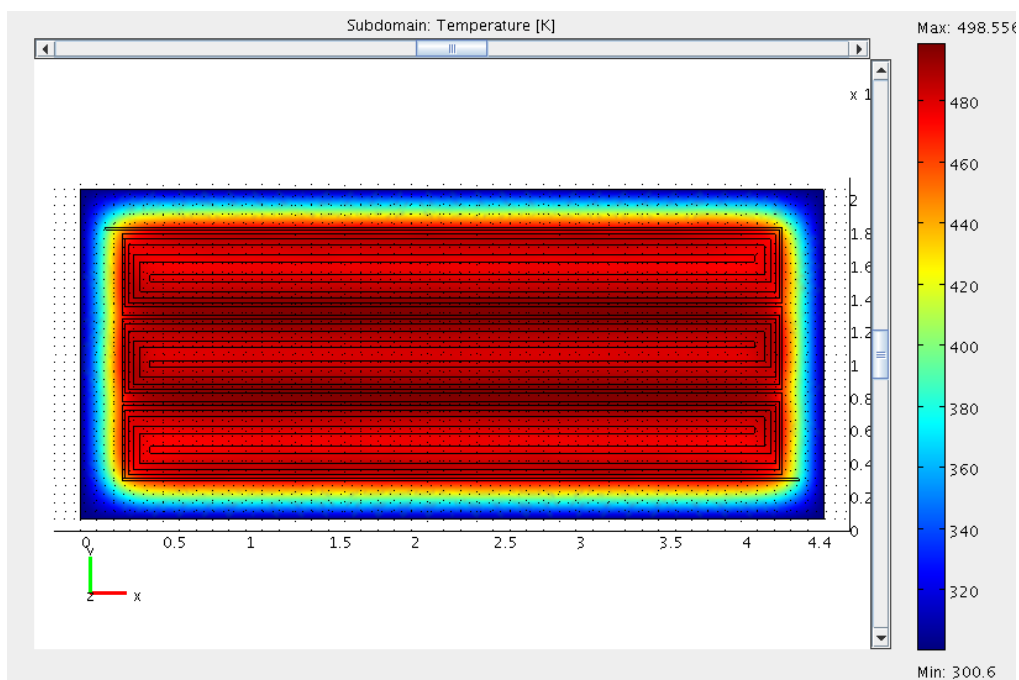


Figure III-17: Temperature distribution at heater design A, membrane 2 mm x 4.5 mm

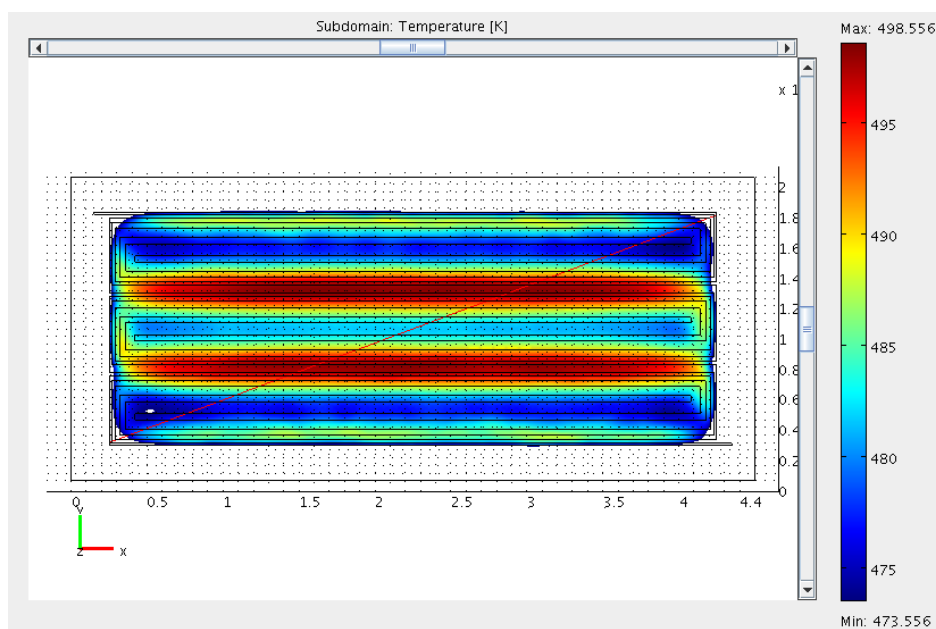


Figure III-18: Heated area within a difference of 25 K at heater design A, membrane 2 mm x 4.5 mm

In Figure III-19 we can see a red line crossing the diagonal of the heater which is used to see the 2D profile in next figure. $(x=250e-6; y=250e-6), (x=4250e-6; y=1750e-6)$

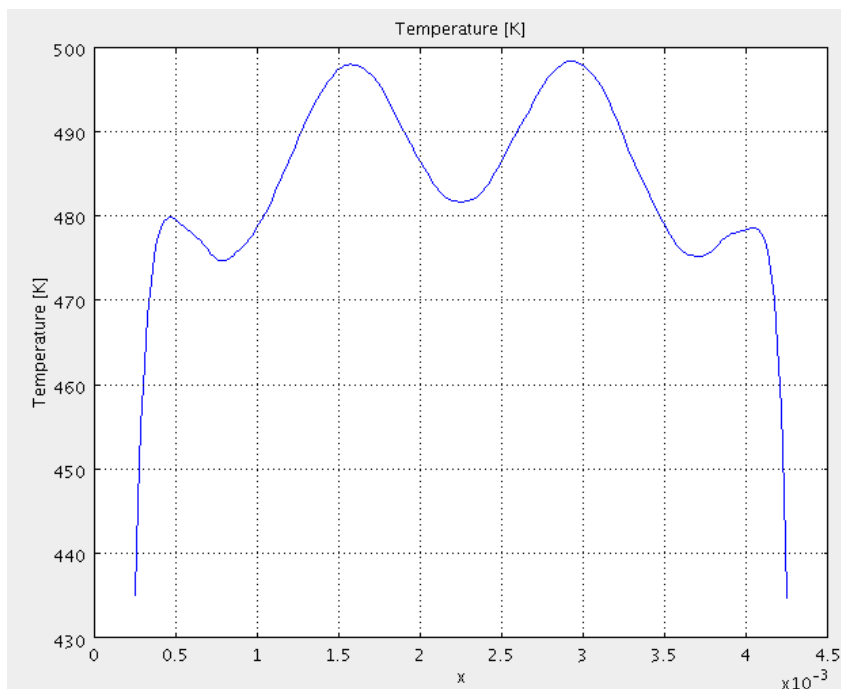


Figure III-19: Diagonal profile along the diagonal heater design A, membrane 2 mm x 4.5 mm

III.3.4. Membrane area: 2 mm x 4.5 mm. Heater area: 1.5 mm x 4 mm B

In this case we design an spiral:

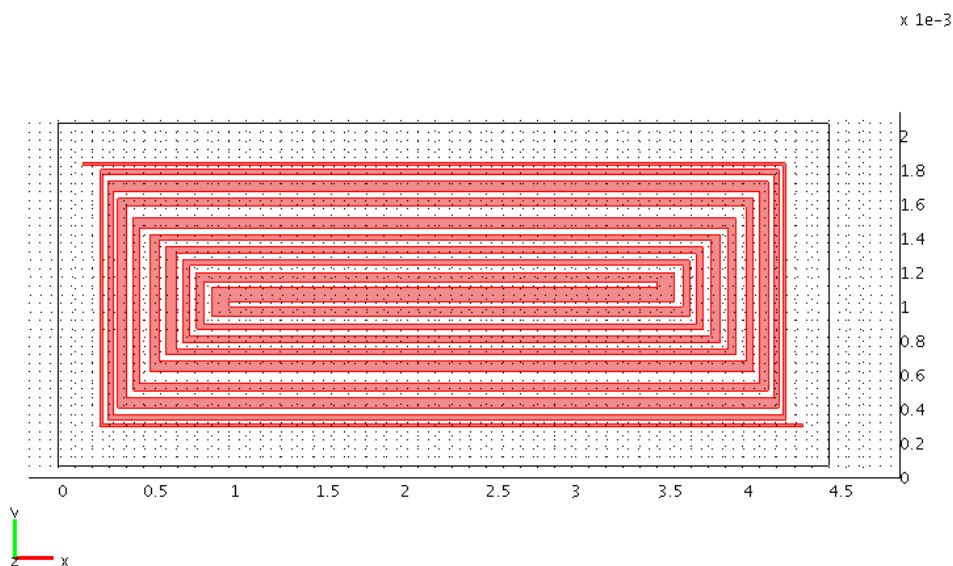


Figure III-20: Second heater design for membrane 2 mm x 4.5 mm

Track deep (from top to bottom): 15-30-60-40-60-30-40-30-60-60-60-30-40-30-60-40-60-30-15

Separation between tracks: 25 μm the first one, 50 μm the last one and 40 μm the rest.

Now we will see the temperature distribution when a voltage of 29.5 V is applied. The current that is crossing the heater is 10.336 mA so, the power consumption is 304.912 mW.

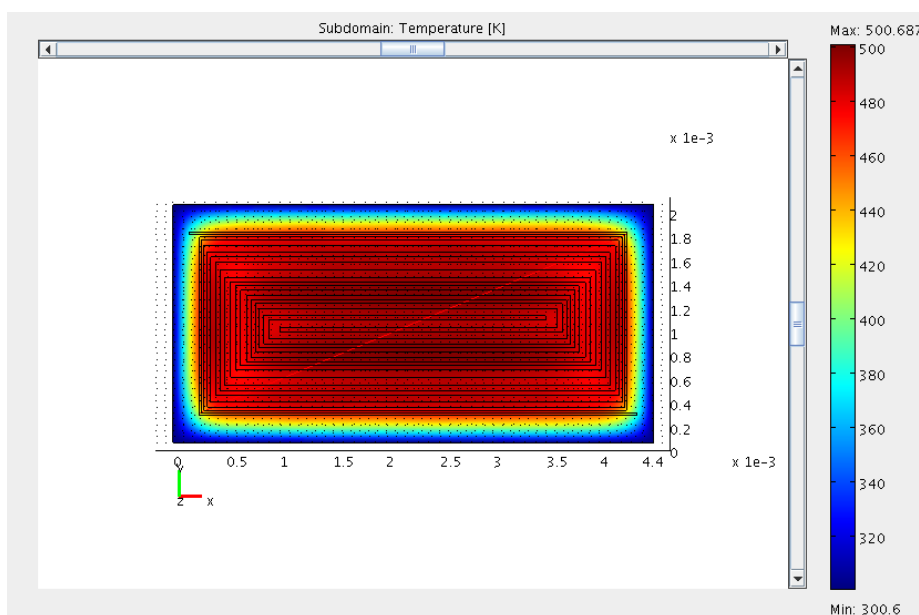


Figure III-21: Temperature distribution at heater design B, membrane 2 mm x 4.5 mm

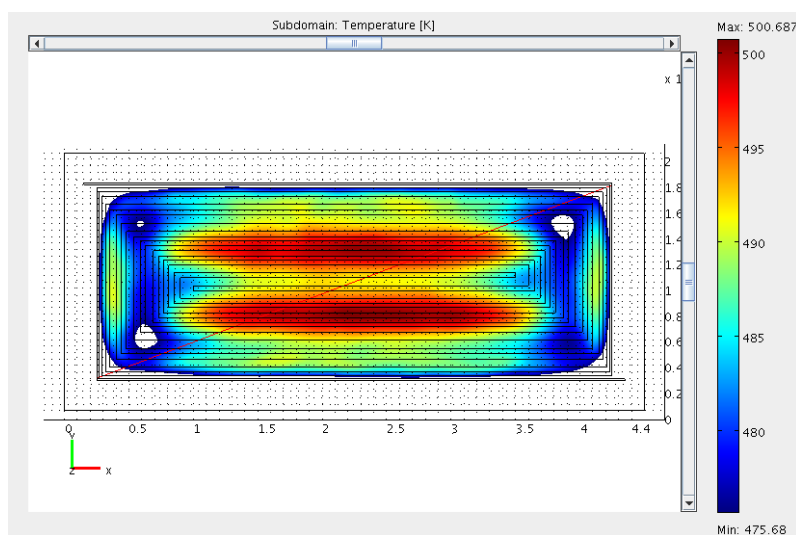


Figure III-22: Heated area within a difference of 25 K at heater design B, membrane 2 mm x 4.5 mm

2D diagonal profile $(x=250e-6; y=250e-6), (x=4250e-6; y=1750e-6)$

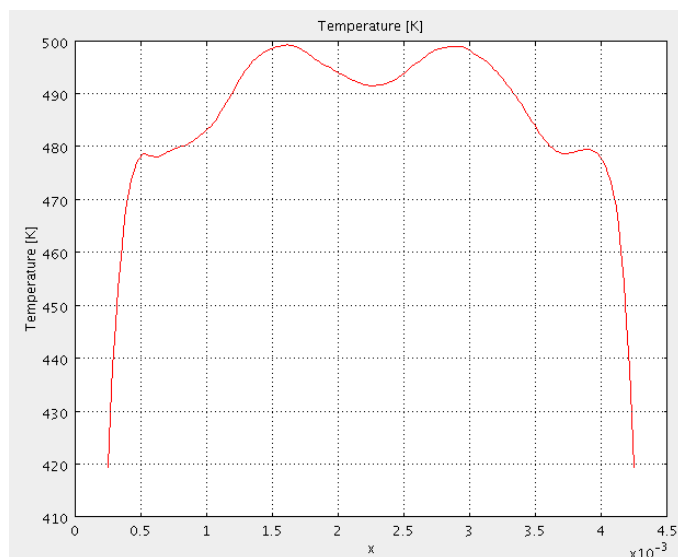


Figure III-23: Diagonal profile along the diagonal heater design B, membrane 2 mm x 4.5 mm

Figure III-24 shows both diagonal profiles together:

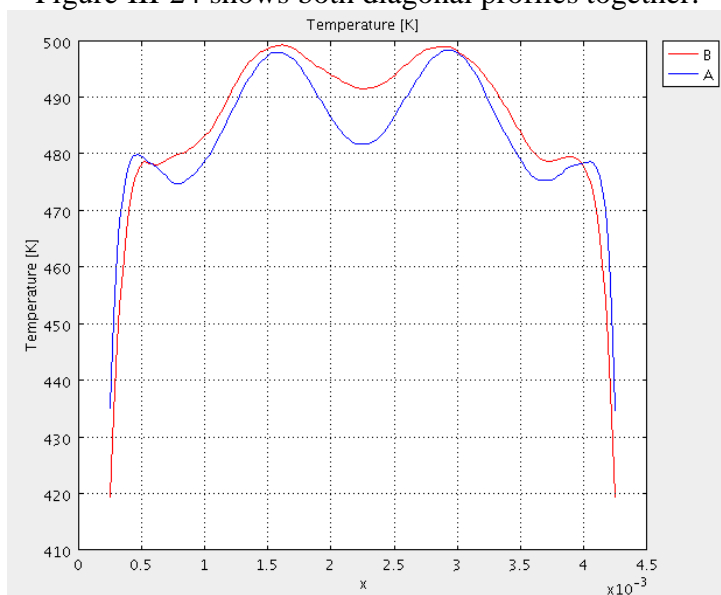


Figure III-24: Comparison between two heaters designed for membrane 2 mm x 4.5 mm

We have two heater design for a membrane of 2 mm x 4.5 mm which both of them have a difference of temperature less than 25 K. Once again, design with an spiral is more temperature homogeneous but in this case is no as big difference as in membranes of 1.5 mm x 5 mm.

III.3.5. Membrane area: 3 mm x 3 mm. Heater area: 2.5 mm x 2.5 mm

Again we use a double spiral heater design:

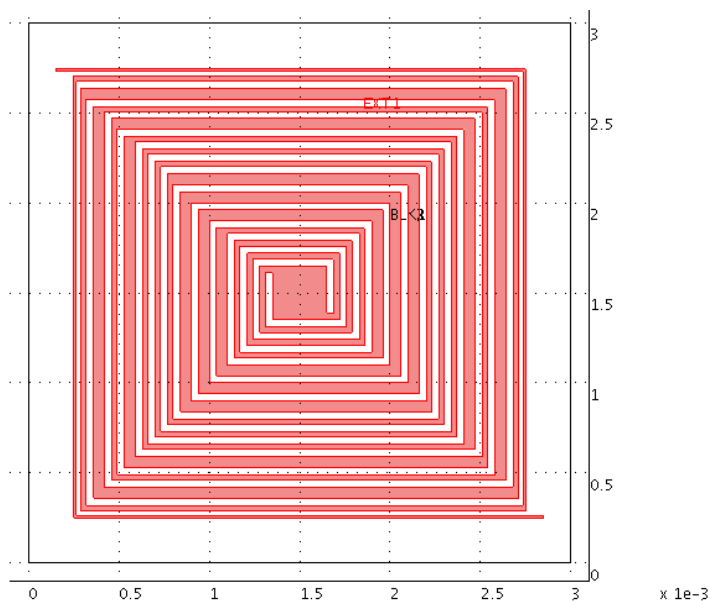


Figure III-25: Heater design for membrane 3 mm x 3 mm

Track thickness (from top to center): 15-30-60-30-60-30-30-60-60-60-30-30-30-40x40-300x300 μm
 Separation between tracks: 25 μm first one, 40 μm all others

Now we will see the temperature distribution when a voltage of 29.75 V is applied. The current crossing the heater is 9.714 mA, so the power consumption is 288.99 mW.

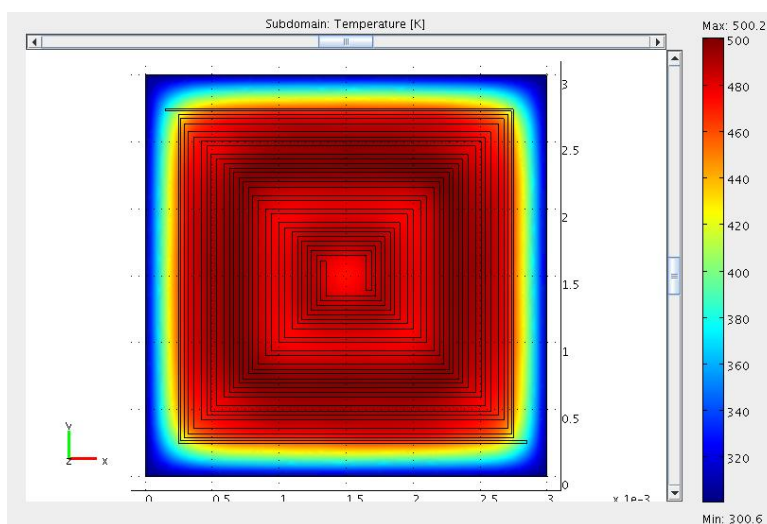


Figure III-26: Temperature distribution at heater design, membrane 3 mm x 3 mm

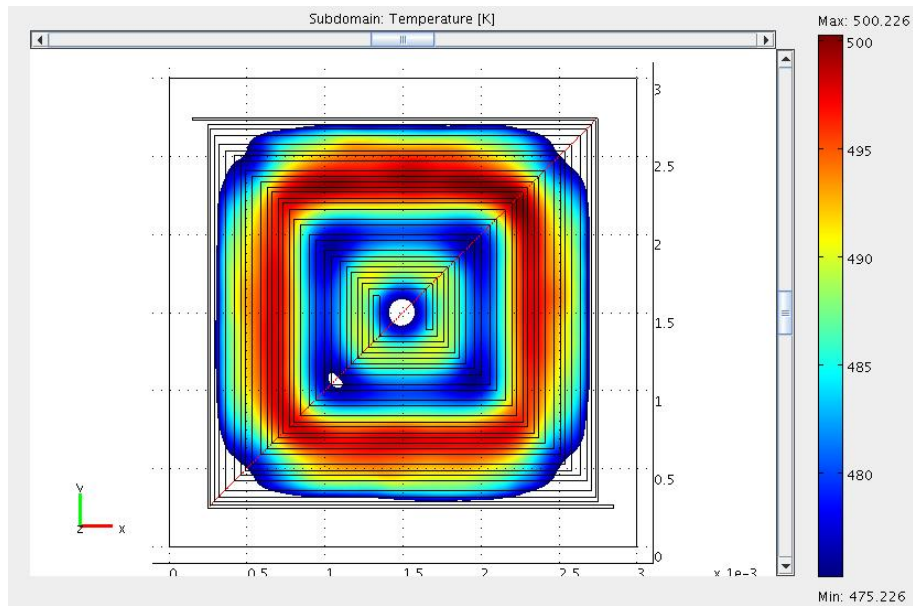


Figure III-27: Heated area within a difference of 25 K at heater design, membrane 3 mm x 3 mm

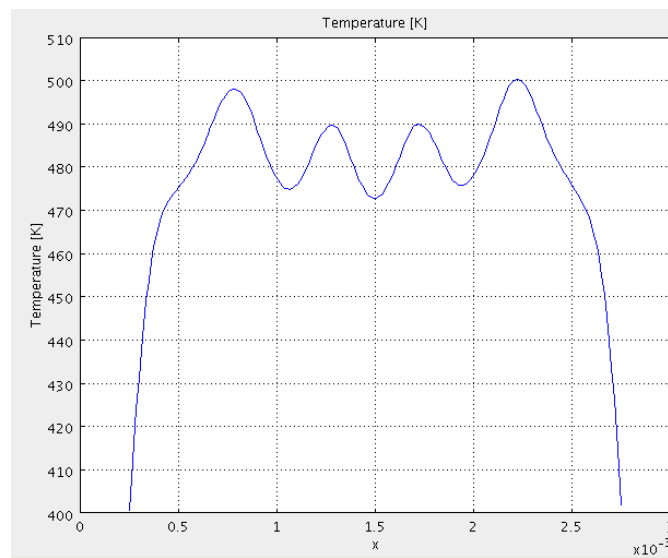


Figure III-28: Diagonal profile along the diagonal heater design, membrane 3 mm x 3 mm

III.4. Comparison

In this chapter we will study the difference between membranes. We use colours to differentiate membranes sizes: yellow is used for 1 mm x 3 mm, green for 1.5 mm x 5 mm, blue for 2 mm x 4.5 mm and purple for 3 mm x 3 mm.

Membrane (mm x mm)	x (mm)	y (mm)	Silicon area (mm ²)	Membrane area (mm ²)	Heater area (mm ²)	Membrane area/Silicon area (%)	Heater area / membrane area (%)	Heater area / Silicon area (%)
1x3	1	3	4,856	3	1,25	61,774	41,667	25,739
1,5x5	1,5	5	10,406	7,5	4,5	72,071	60,000	43,243
2x4,5	2	4,5	11,906	9	6	75,590	66,667	50,393
3x3	3	3	11,696	9	6,25	76,947	69,444	53,435

Table III-2: Comparison of different membranes respect membrane, heater and silicon areas

Big membranes are more effectives in terms of silicon area used.

Next step, we compare different heater designs:

Heater	Power consumption (mW)	Active area ($\Delta T < 25$ K)	Active area /membrane area (%)	Active area /silicon area (%)	Power consumption/Active area (mW/mm ²)
Initial design	76,884	0,64	21,33	13,18	120,13
4 heaters	86,516	0,70	23,33	14,41	123,59
15-30-60-80	98,056	1,22	40,67	25,12	80,37
1,5x5 A	249,523	4,41	58,80	42,38	56,58
1,5x5 B	256,104	4,46	59,47	42,86	57,42
2x4,5 A	301,359	5,84	64,89	49,05	51,60
2x4,5 B	304,912	5,28	58,67	44,35	57,75
3x3	288,990	5,55	61,68	47,46	52,06

Table III-3: Heater design comparison.

We observe that big membranes are more effective tacking into account power consumption by unit of area.

Then, we will study if it is better to use a big membrane or some small ones. In this way we will compare three small membranes of 1 x 3 mm² with one of 2 x 4.5 mm² and other one of 3 x 3 mm². In small membranes we have taken into account than when construct some membranes together it is necessary to have space between them to be sure membranes remain separated (400 μ m).

Heater	number of membranes	silicon area (mm ²)	membrane area (mm ²)	active area (mm ²)	Power consumption/Active area (mW/mm ²)
Initial design	3	15,7692	9	1,92	120,13
4 heaters	3	15,7692	9	2,10	123,59
15-30-60-80	3	15,7692	9	3,66	80,37
2x4,5 A	1	11,9064	9	5,84	51,60
2x4,5 B	1	11,9064	9	5,28	57,75
3x3	1	11,6964	9	5,55	52,06

Table III-4: Comparison of one big membrane with some small ones.

To obtain the same membrane area using small membranes, we need more silicon area. Also, with the small ones we obtain less active area. Studying the power consumption per unit of active area we observe that energetic efficiency is better in big membranes. So, it is more effective to construct a big membrane than some small ones.

Finally, we compare two big membranes: 2x4.5 mm² y 3x3 mm². In both cases membrane area is the same (9 mm²). We study differences to have a square or a rectangle shape:

Square membrane has more heater area and it needs less silicon area (See Table III-2) than rectangular membrane.

Tacking into account the active area (Table III-3) it depends on the heater design. Using design A in 2x4.5 mm² membrane we obtain a larger active area and a smaller power consumption per unit of area.

III.5. Silicon plug in new membranes

In this chapter we will study the effect of using a silicon plug of 5 μm depth in big membranes (See Chapter II.5). We will see the power consumption and thermal distribution of each one of them.

III.5.1. Membrane area: 1.5 mm x 5 mm

Heater	Membrane area [mm ²]	Heater area [mm ²]	Voltage [V]	Density current [A/m ²]	m ²	Current [A]	Power consumption [mW]
1,5x5 A	7,5	4,5	28	9,99E+08	1,25E-11	0,01249	349,64
1,5x5 B	7,5	4,5	28	8,25E+08	1,5E-11	0,01237	346,35

Table III-5: Power consumption membranes 1.5 mm x 5 mm using silicon plug

Thermal distribution:

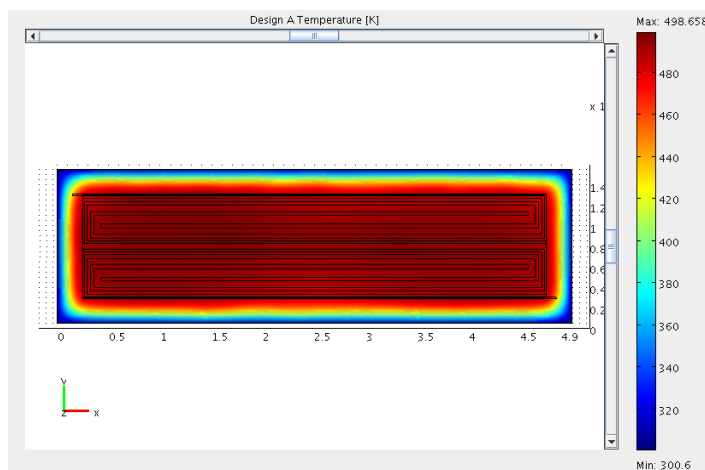


Figure III-29: Temperature distribution heater design A membrane 1.5 mm x 5 mm with a silicon plug

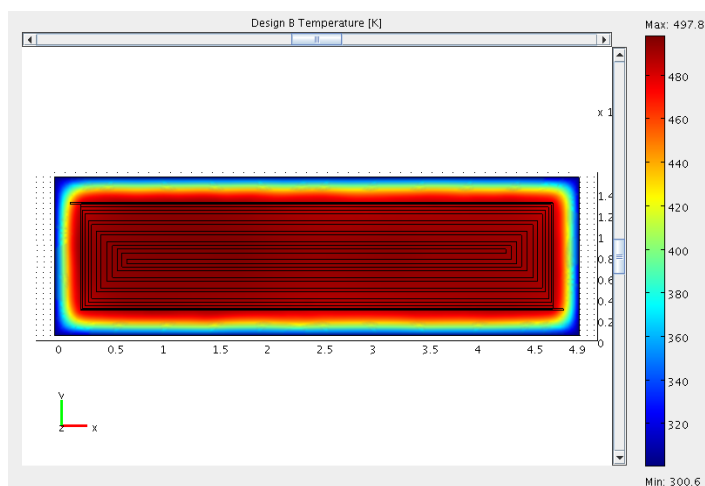


Figure III-30: Temperature distribution heater design B membrane 1.5 mm x 5 mm with a silicon plug

Heated area with a difference of 25 K:

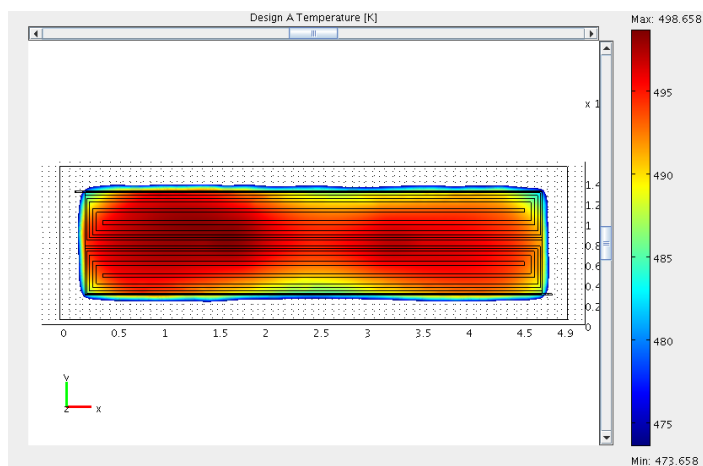


Figure III-31: Heated area with a difference of 25 K heater design A membrane 1.5 mm x 5 mm

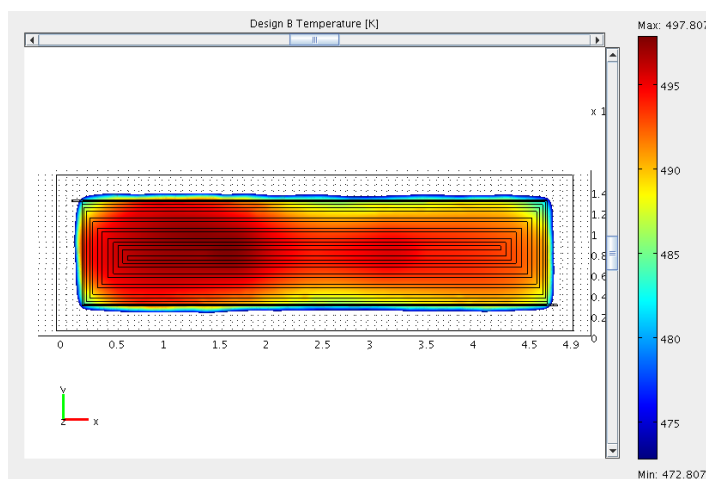


Figure III-32: Heated area with a difference of 25 K heater design B membrane 1.5 mm x 5 mm

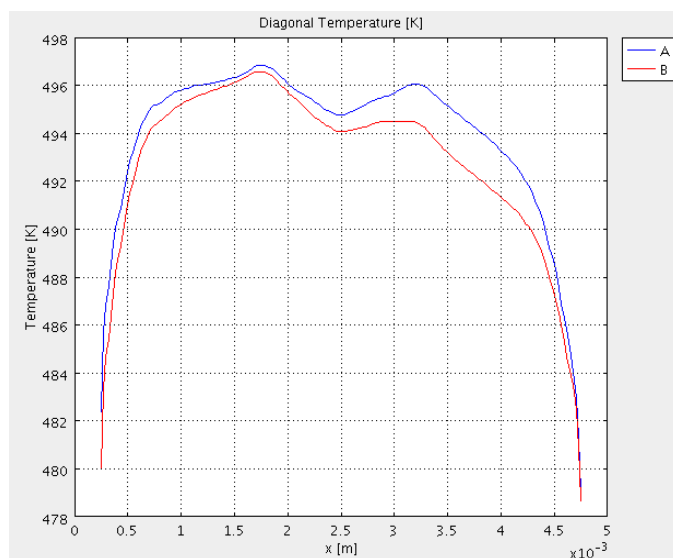


Figure III-33: Diagonal temperature profiles both heaters design membrane 1.5 mm x 5 mm with a silicon plug

III.5.2. Membrane area: 2 mm x 4.5 mm

Heater	Membrane area [mm ²]	Heater area [mm ²]	Volate [V]	Density current [A/m ²]	m ²	Current [A]	Power consumption [mW]
2*4,5A	9	6	33,3	6,06E+08	1,5E-11	0,00910	302,87
2*4,5B	9	6	34,5	7,85E+08	1,5E-11	0,01177	406,18

Table III-6: Power consumption membranes 2 mm x 4.5 mm using silicon plug

Thermal distribution:

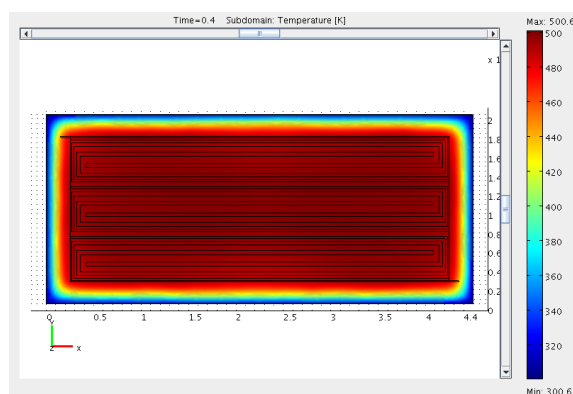


Figure III-34: Temperature distribution heater design A membrane 2 mm x 4.5 mm with a silicon plug

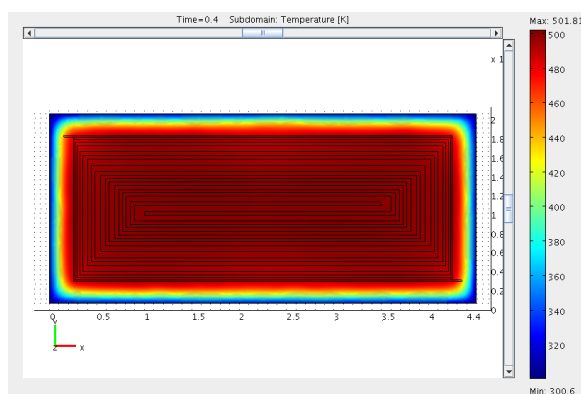


Figure III-35: Temperature distribution heater design B membrane 2 mm x 4.5 mm with a silicon plug

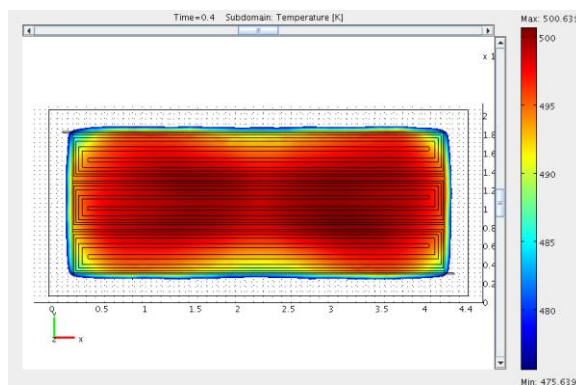


Figure III-36: Heated area with a difference of 25 K heater design A membrane 2 mm x 4.5 mm

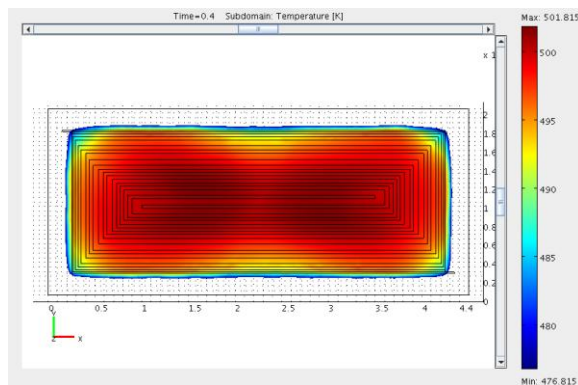


Figure III-37: Heated area with a difference of 25 K heater design B membrane 2 mm x 4.5 mm

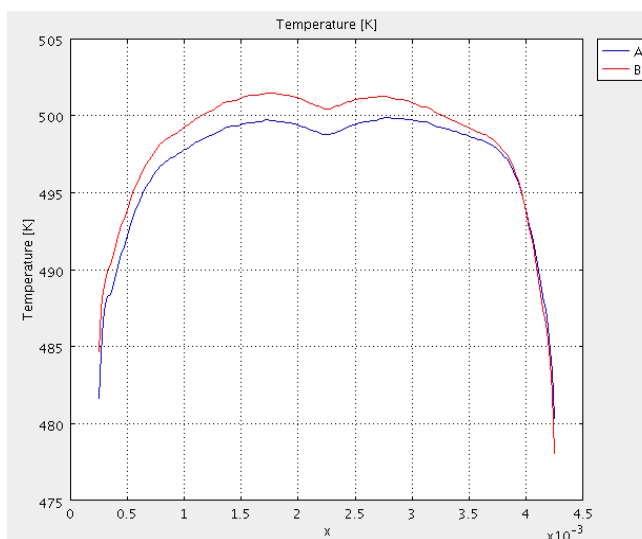


Figure III-38: Diagonal temperature profiles both heaters design membrane 2 mm x 4.5 mm with a silicon plug

III.5.3. Membrane area: 3 mm x 3 mm

Heater	Membrane area [mm ²]	Heater area [mm ²]	Volate [V]	Current [A]	Power consumption [mW]
3*3	9	6,25	35	0,00971	339,94

Table III-7: Power consumption membrane 3 mm x 3 mm using silicon plug

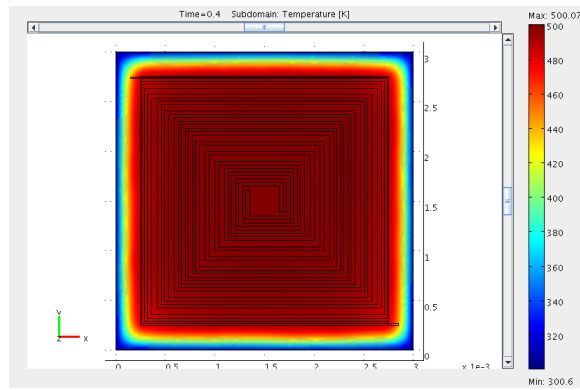


Figure III-39: Temperature distribution membrane 3 mm x 3 mm with a silicon plug

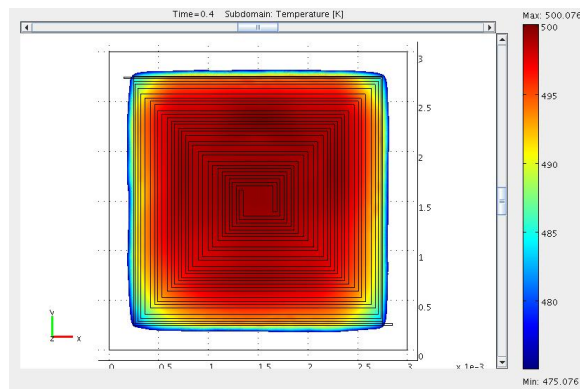


Figure III-40: Heated area with a difference of 25K membrane 3 mm x 3 mm

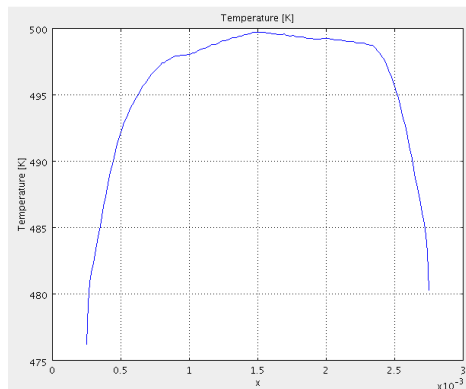


Figure III-41: Diagonal temperature profiles membrane 3 mm x 3 mm with a silicon plug

Using a silicon plug we are able to have all the heater area with a difference of temperature less than 15 K.

III.6. Conclusions

- ✓ Big membranes are more effective in terms of silicon area used.
- ✓ Big membranes are more effective taking into account active area.
- ✓ Big membranes are more effective taking into account power consumption by unit.
- ✓ To obtain the same active area is better to use a big membrane than some small ones.

- ✓ Square membranes are more effective in terms of silicon area used than rectangular ones.
- ✓ In terms of active area and power consumption by unit efficiency depends on the heater design.

- ✓ Using a silicon plug 5 μm depth in big membranes homogenisation temperature is increased reaching a difference of temperature inside the heater area less than 15 K.
- ✓ Power consumption is increased respect to membranes without silicon plug.

UNIVERSITAT ROVIRA I VIRGLI
MODELIZATION, SIMULATION AND DESIGN OF MICRO-ELECTRO-MECHANICAZED SYSTEMS (MEMS) PRECONCENTRATORS
FOR GAS SENSING
Roser Inglés Bort
ISBN:978-84-694-0327-3/DL:T-198-2011

IV. ELECTRO-THERMAL CHARACTERIZATION: EXPERIMENTAL RESULTS.

IV.1. Introduction

In this chapter we show fabricated membranes. We explain characterization devices and parameters. Finally, we show results, adjust simulations using measured parameters and compare both.

We have run a wafer process with new designed membranes (See Chapters II.5 and III.5). Every chip is 7 mm x 7 mm. The wafer is 10 cm diameter with a usable diameter of 8 cm. In one wafer there are 94 chips:

- 18 chips with a 3 mm x 3 mm membrane (Chip 1)
- 36 chips with a 2 mm x 4.5 mm membrane (18 with heater design A and 18 with heater design B), (Chips 2 and 2B)
- 34 chips with a 1.5 mm x 5 mm membrane (18 with heater design A and 16 with heater design B), (Chips 3 and 3B)
- 4 chips with three 1 mm x 3 mm membranes (Chip 4)
- 2 chips are used for mask alignment

All membranes have a silicon plug 5 μm depth under the membrane on the area delimited by the heater.

In chips with 1 mm x 3 mm membranes we pack three membranes in each single chip (See Figure IV-1 right). Each one has a heater design (Initial design, 4 heaters and 15-30-60-80). In 1.5 mm x 5 mm and 2 mm x 4.5 mm membranes we have implemented two different heater designs. In 3 mm x 3 mm membrane we have just one heater design (In this case there was a mask design error and heater was not completely connected. For this reason, we don't have experimental measurements of this membrane).

Some membranes have been encapsulated in a T8. Membranes are stick using glue. Contacts are done using thin wires of aluminum. We can see one encapsulated membrane in Figure IV-2.

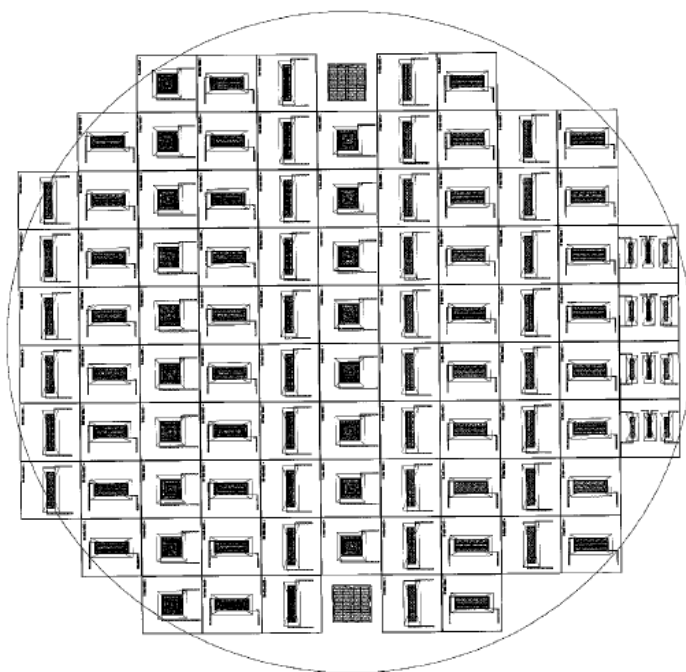


Figure IV-1: Mask wafer design

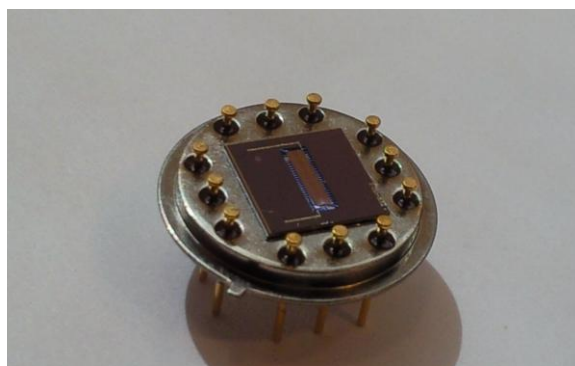


Figure IV-2: Encapsulated membrane

The aim of this fabrication and next characterization is to validate our simulations. We will compare resistance and maximum temperature reached on the membrane applying different voltages in order to see similarities and differences between experimental results and simulations.

For the characterization we have used a Kiethly 2430 multimeter for the electric parameters and a CEDIP Jade III MW infrared camera for the thermal ones. We have used the multimeter to apply a voltage at the heater and measure the current in order to obtain the resistance. In next chapter we will explain parameters used to adjust the infrared camera in order to measure temperatures reached in the membrane.

IV.1.1. Infra red camera parameters

Parameters adjustable in the infra red camera are: emissivity, background temperature, windows size and integration time. Each one of them will be explained:

- Emissivity for the entire device: there are materials with very different emissivity coefficient (metals have a very low emissivity coefficient, silicon materials have medium emissivity coefficient and glue has a very high emissivity coefficient). We use a emissivity of 0.9 that we must adjust lately. We use this value because the emissivity of silicon materials, more common on the surface device, is around this value.
- Background temperature: the camera is working at 93 K but we must adjust the background temperature in degrees and we can't use negatives values, so we introduce a temperature of 0 °C, for this reason we obtain in some images negatives temperatures.
- Windows size: in the infra red camera there are three windows sizes available. We use the biggest one because others are too small for our heaters. This is 320 pixel x 240 pixel with a frequency of 50 Hz, so it gives us a good temporal resolution.
- Integration time: we could work at different temperature ranges adjusting the integration time. An integration time of 375 μ s is needed for range 5-95 °C, 80 μ s for 80-175 °C and 25 μ s for 125-250 °C.

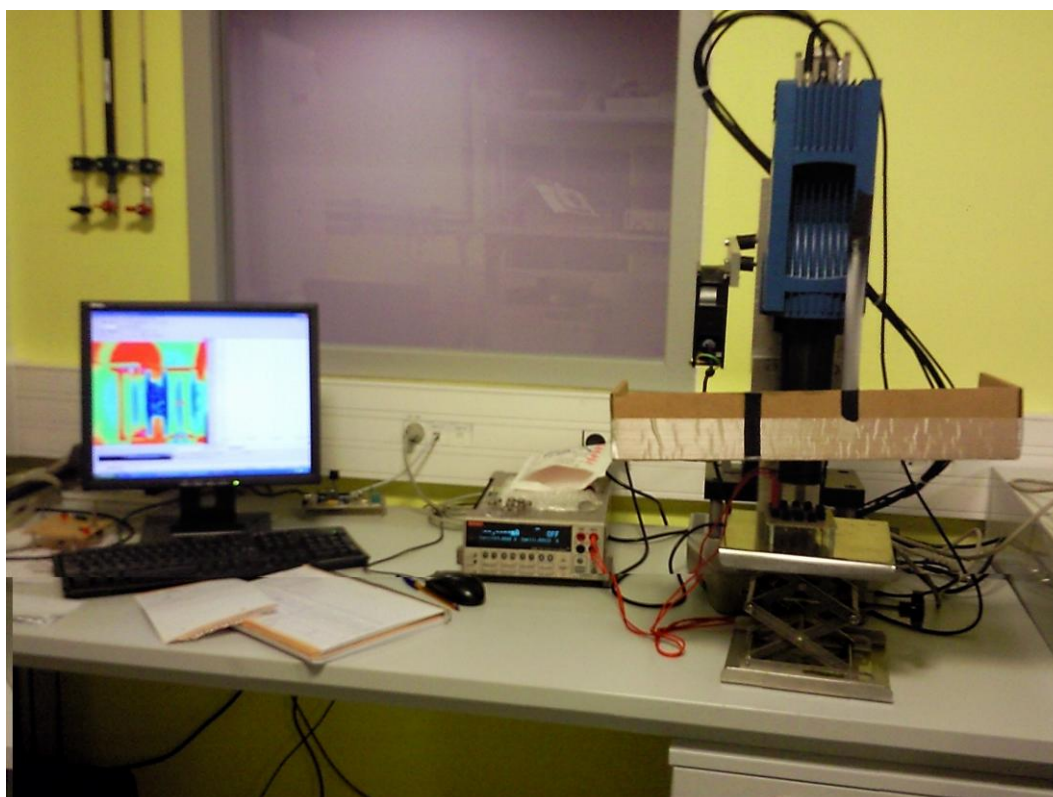


Figure IV-3: Infra red camera with multimeter and computer control

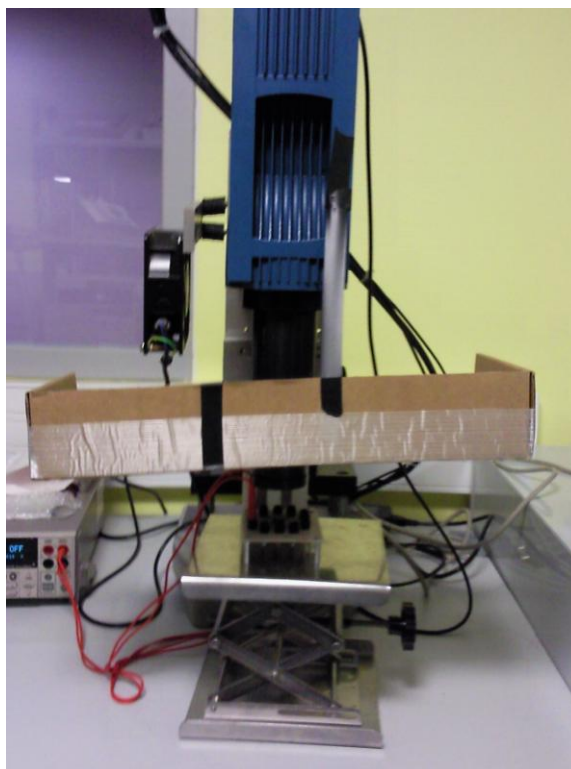


Figure IV-4: Infra red camera

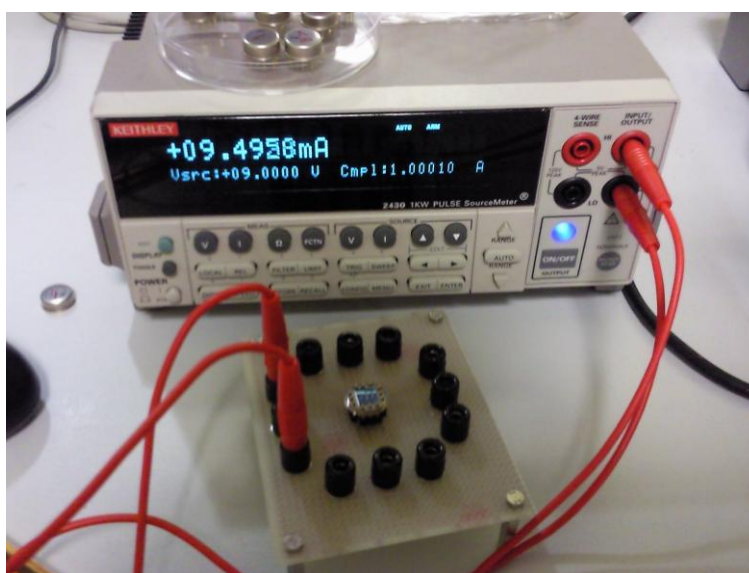


Figure IV-5: Multimeter and circuit for T8 encapsulated devices

In Figure IV-6 we can see an infra red image of a chip at ambient temperature. Temperature shown by the camera is between 260 and 295 K when ambient temperature is around 293 K. So, we are not seeing ambient temperature, we are seeing an emissivity map.

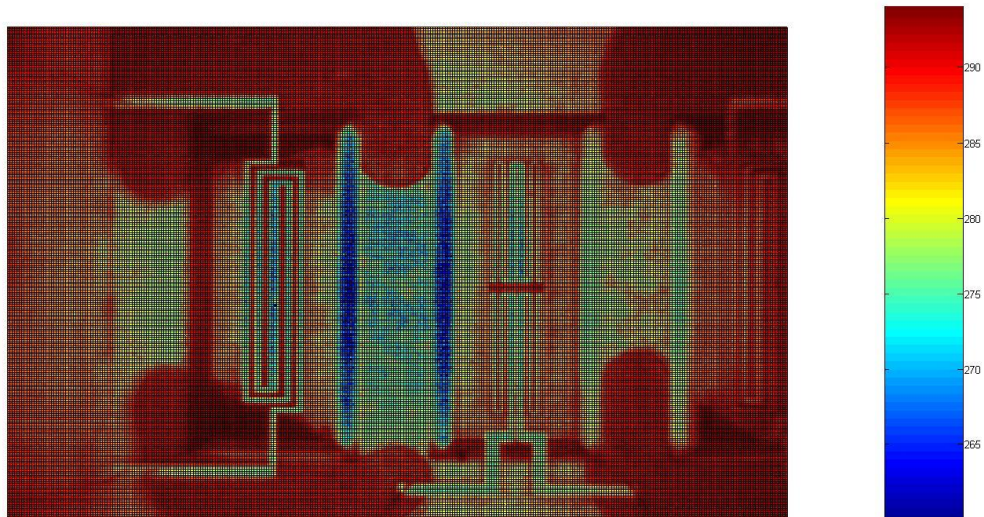


Figure IV-6: Initial design. Infra red camera image at ambient temperature

In next chapter we will try to solve this problem. First idea is painting in black the device in order to avoid different emissivity but we will see in next chapter that this don't solve the problem and the paint layer change our device thermal behavior. Next idea is to adjust emissivity pixel by pixel using a Matlab program, we will show this in chapter IV.1.2.2.

IV.1.2. Emissivity adjustment

IV.1.2.1. Physical solution

In order to solve the emissivity problem we have painted the device chip 1 with black paint (spray “Pinture noir HT” Laboratoires CEETAL, contain xylene). We have measured before and after applying the paint and we have seen that this paint layer is modifying the thermal behaviour of our device so we couldn't use this.

INITIAL DESIGN

V	I	R	# raising frames	Raising time (ms)
0.1	3.91E-004	256.08		
3	1.08E-002	278.55	9	180
4	1.35E-002	296.52	8	160
5	1.59E-002	314.66	6	120

INITIAL DESIGN Painted

V	I	R	ΔR	# raising frames	Raising time (ms)
0.1	3.99E-004	250.44	-5.64		
3	1.10E-002	273.5	-5.05	10	200
4	1.39E-002	286.94	-9.57	13	260
5	1.65E-002	303.77	-10.9	14	280

15-30-60-80

V	I	R	# raising frames	Raising time (ms)
0.1	1.37E-004	728.33		
3	4.02E-003	746.08		
5	6.25E-003	800.13	7	140
6	7.19E-003	834.49		
8	8.86E-003	902.93	6	120
9	9.59E-003	938.48	5	100

15-30-60-80 Painted

V	I	R	ΔR	# raising frames	Raising time (ms)
0.1	1.40E-004	711.79	-16.54		
3	4.07E-003	737.1	-8.98		
5	6.43E-003	777.73	-22.4	14	280
6	7.45E-003	805.48	-29.02		
8	9.30E-003	860.31	-42.63	13	260

Table IV-1: Electric parameters before and after painting the device

Resistance have changed and also the rising time, so the layer of paint is changing the conditions of our device.

IV.1.2.2. Post-processing solution

Then, we use a Matlab program for adjust the temperature of every pixel. We use the idea that the emitted heat is:

$$Q = E * k * T^4$$

We extract the emitted heat of every pixel using the data of the camera. Then, using the value of emitted heat, we extract the real emissivity of every pixel knowing the ambient temperature. We calculate the emitted heat when device is heated using the data of the camera. Finally, we calculate the real temperature.

$$Q_{E_Tamb} = E_{Camera} * k * T_{C_Tamb}^4$$

$$E_{real} = \frac{Q_{E_Tamb}}{k * T_{amb}^4} = \frac{E_{Camera} * k * T_{C_Tamb}^4}{k * T_{amb}^4} = \frac{E_{Camera} * T_{C_Tamb}^4}{T_{amb}^4}$$

$$Q_{E_Theated} = E_{Camera} * k * T_C^4$$

$$T_{real}^4 = \frac{Q_{E_Theated}}{k * E_{real}} = \frac{E_{Camera} * k * T_C^4}{k * \left(\frac{E_{Camera} * T_{C_Tamb}^4}{T_{amb}^4} \right)} = \frac{T_{amb}^4 * T_C^4}{T_{C_Tamb}^4}$$

$$T_{real} = \frac{T_{amb} * T_C}{T_{C_Tamb}}$$

Where:

Q_{E_Tamb} = emitted heat at ambient temperature

$E_{Camera} = 0.9$

k = Constant of Boltzman

T_{C_Tamb} = Temperature measured by the camera at ambient temperature

$Q_{E_Theated}$ = emitted heat when device is heated

T_C = Temperature measured by the camera when device is heated

T_{amb} = Ambient temperature = 20 °C = 293 K

We can see in Figure IV-7 that once post-processed image is adjusted at ambient temperature.

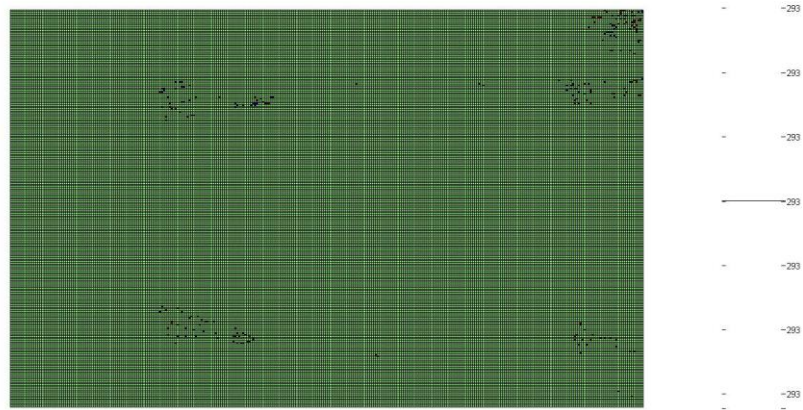


Figure IV-7: Initial design. Post-processed image at ambient temperature

IV.2. Comparison with simulations

Electrical resistivity and its temperature dependence have been adjusted using experimental measurements. Electrical resistivity has been estimated measuring the resistance at ambient temperature with a very small voltage and knowing the geometry of the heater. Average resistance is 250.2Ω for the initial design, 1031.3Ω for 4 heaters design and 710.2Ω for 15-30-60-80 design. Electrical resistivity has been calculated $2.56 \cdot 10^{-7} \Omega \cdot m$. To measure temperature dependence, membranes have been introduced in an oven and changes in resistance when increasing temperatures have been measured (See Figure IV-8). Temperature dependence has been estimated $2 \cdot 10^{-3} 1/K$ from the slope of the resistance-temperature graph. Both values have been introduced in our simulations.



Figure IV-8: Experimental set up for temperature dependence extraction

Membranes have been characterized in two ways:

- encapsulated in a T8 using a circuit for electric connection (See Figure IV-5)
- without encapsulation using point probes

In Annex are shown all infrared images and electric measurements. In this chapter we compare experimental results (dotted line) with simulations (continuous line). In tables of electric characterization in Annex are shown ranges of measure. Some steps due to the change of range are clearly visible in figures (for example in Figure IV-10 this change of range at 6 V for 15-30-60-80 heater or at 7 V for 4 heater design)

IV.2.1. Electro thermal characterization

Next figures show resistance change versus voltage and temperature versus voltage for 1 mm x 3 mm membranes encapsulated and non encapsulated. Measurements and simulations agree using a heat transfer coefficient of $60 \text{ W}/(\text{m}^2 \cdot \text{K})$.

In both cases resistance is very well adjusted. Temperature is more fitted in non encapsulated membranes. In both cases we are simulating just the heater (without measurement wires and

internal resistance of the measurement device), these added resistances are not taken into account in simulations.

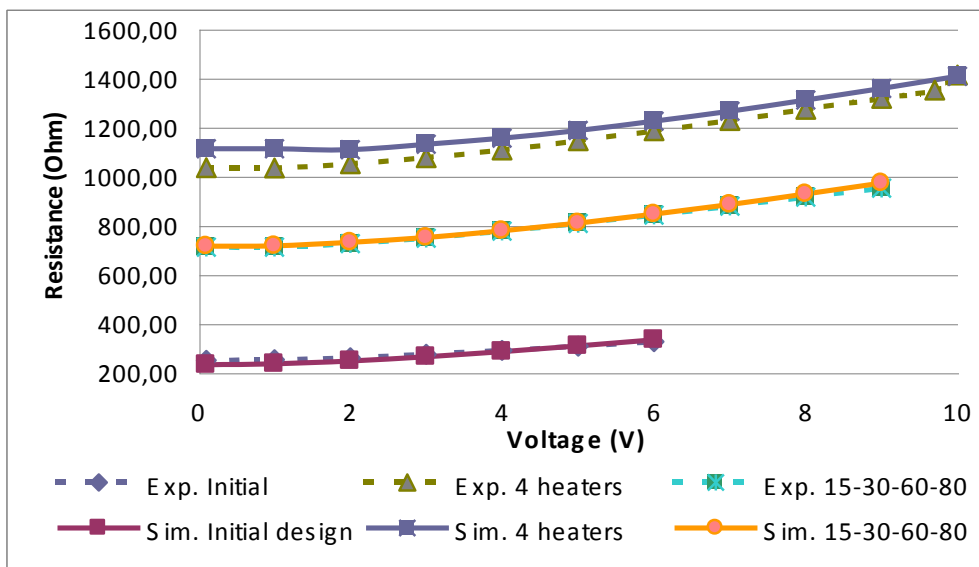


Figure IV-9: Membrane 1 mm x 3 mm encapsulated. Resistance versus voltage.

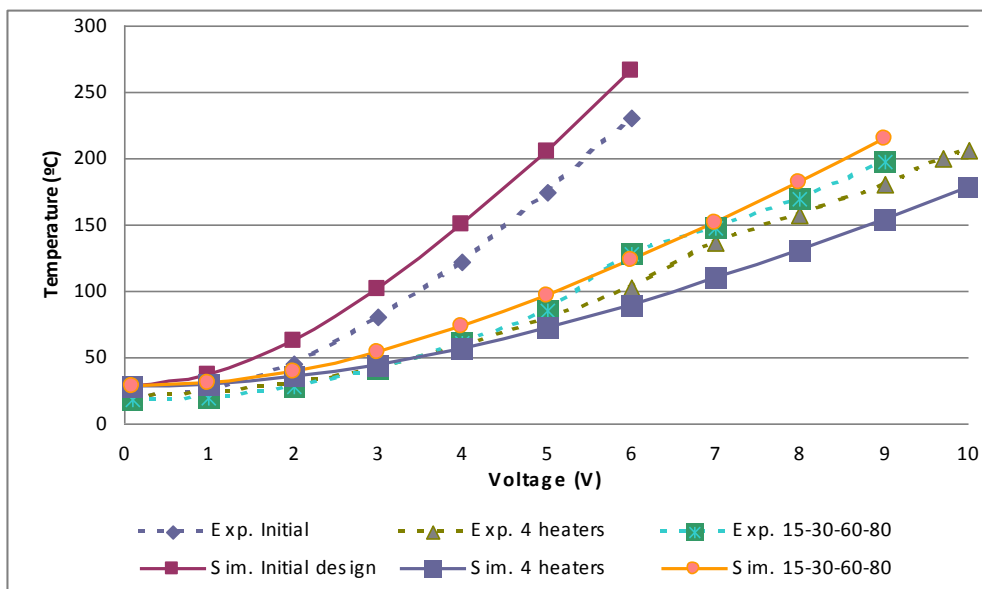


Figure IV-10: Membrane 1 mm x 3 mm encapsulated. Maximum temperature versus voltage.

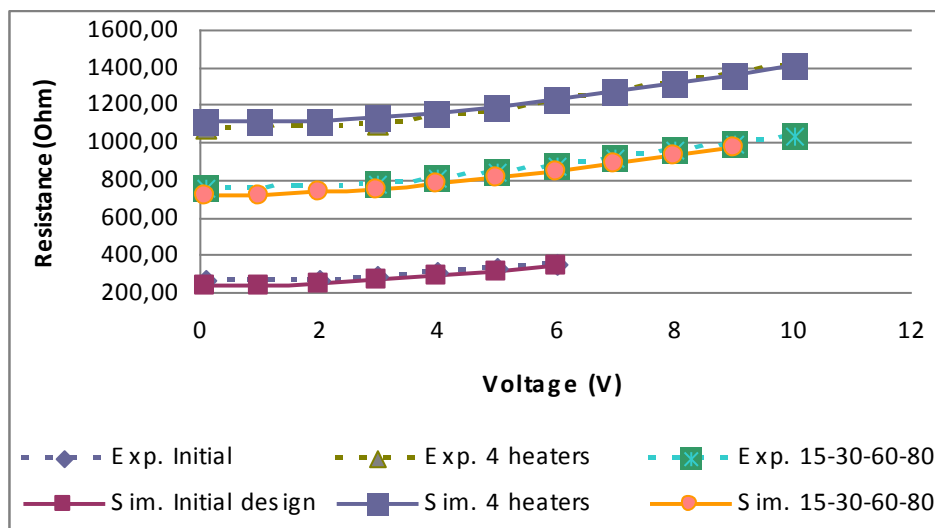


Figure IV-11: Membrane 1 mm x 3 mm non encapsulated. Resistance versus voltage.

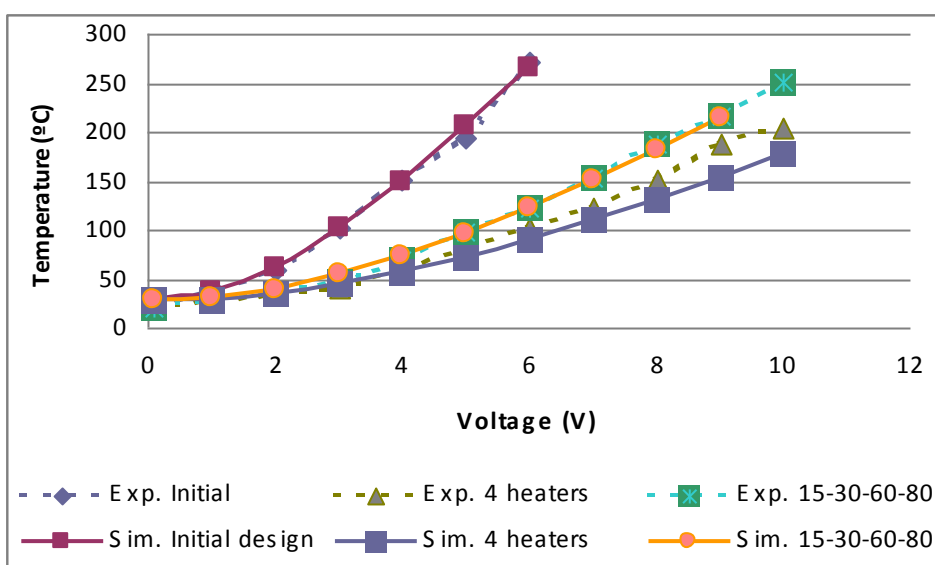


Figure IV-12: Membrane 1 mm x 3 mm non encapsulated. Maximum temperature versus voltage.

Next figures show graphs of large membranes. There is a good agreement between measurements and simulations using a heat flux of $30 \text{ W}/(\text{m}^2 \cdot \text{K})$.

There is an offset in the resistance-voltage curve (Figure IV-13) but simulations reproduce well the experimental trend.

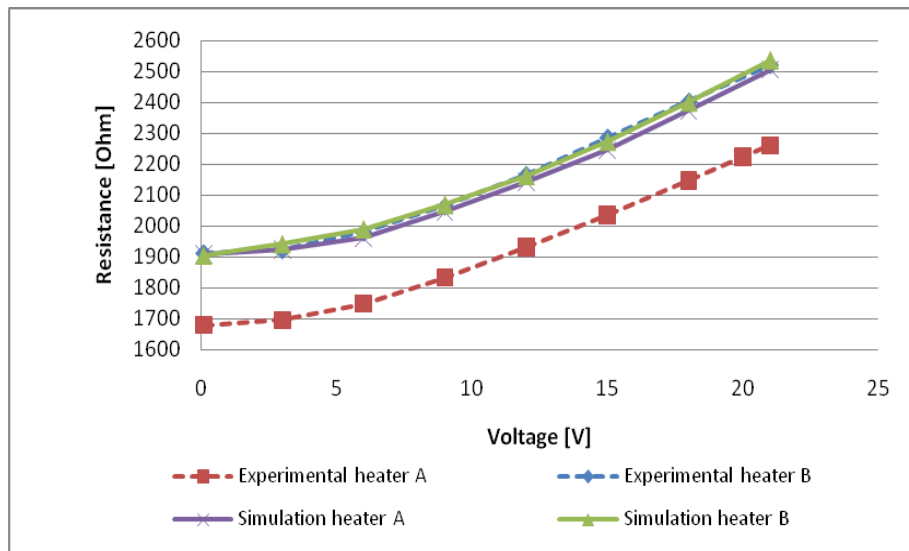


Figure IV-13: Membrane 1.5 mm x 5 mm encapsulated. Resistance versus voltage

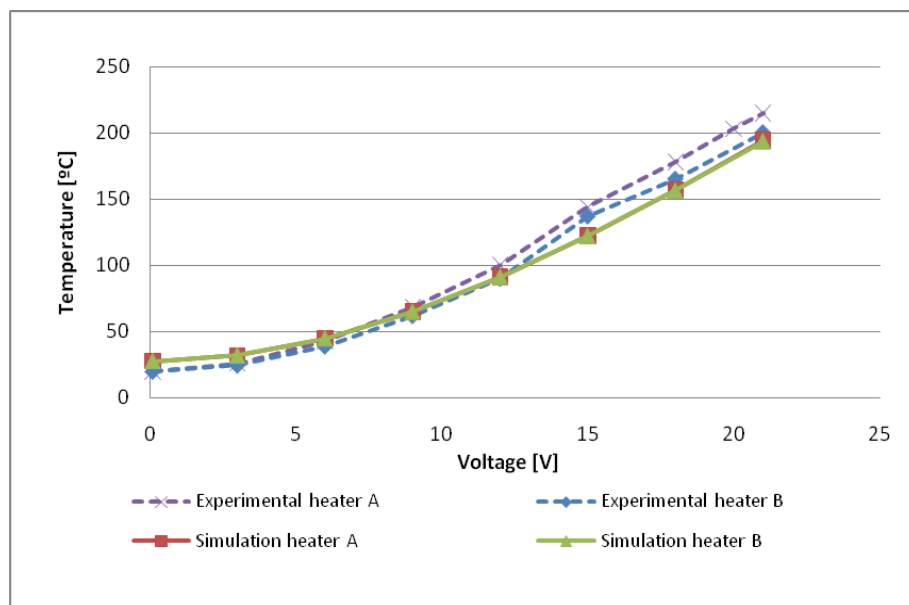


Figure IV-14: Membrane 1.5 mm x 5 mm encapsulated. Maximum temperature versus voltage.

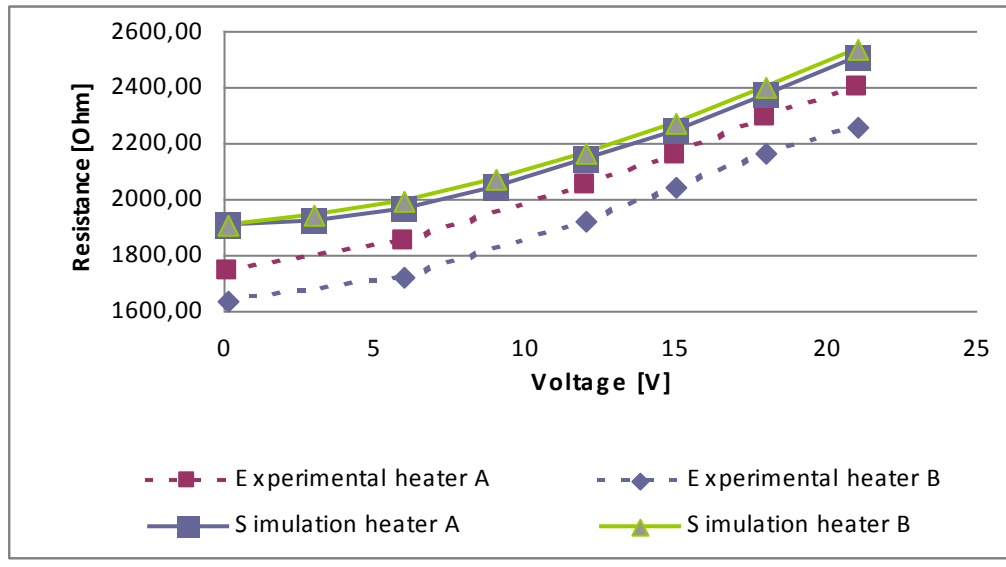


Figure IV-15: Membrane 1.5 mm x 5 mm non encapsulated. Resistance versus voltage

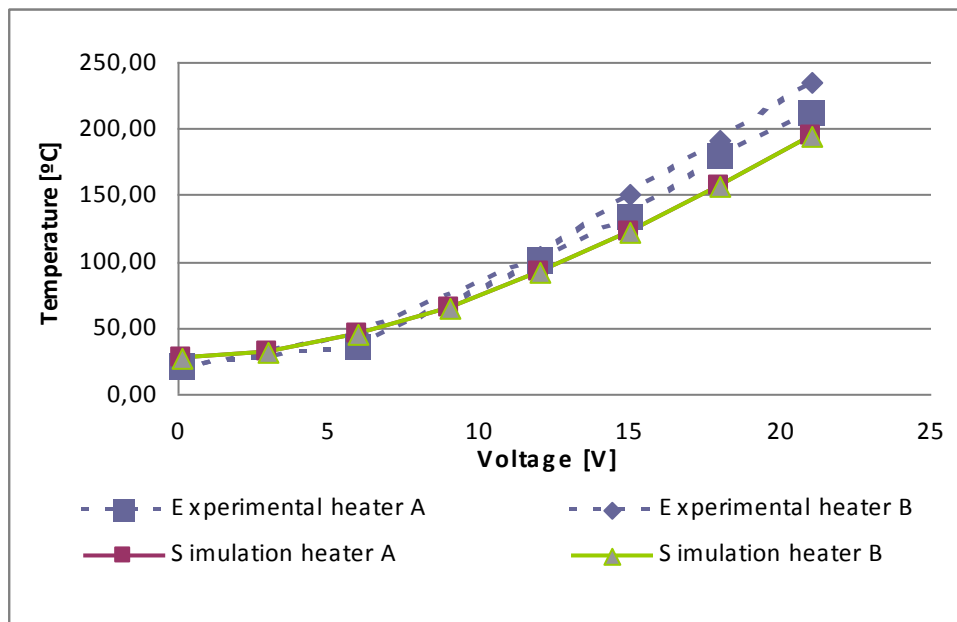


Figure IV-16: Membrane 1.5 mm x 5 mm non encapsulated. Maximum temperature versus voltage.

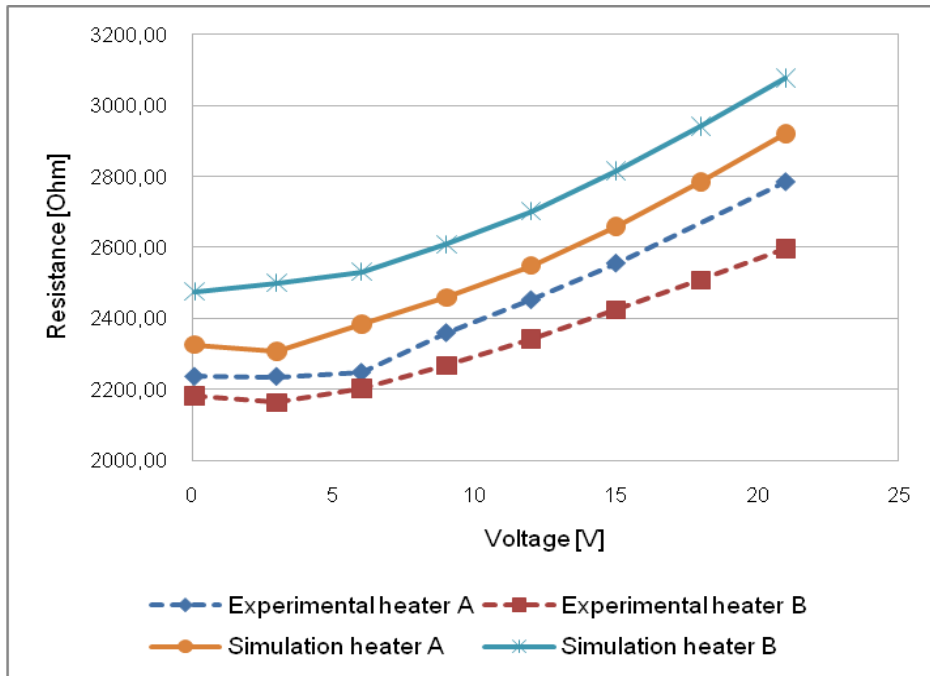


Figure IV-17: Membrane 2 mm x 4.5 mm encapsulated. Resistance versus voltage

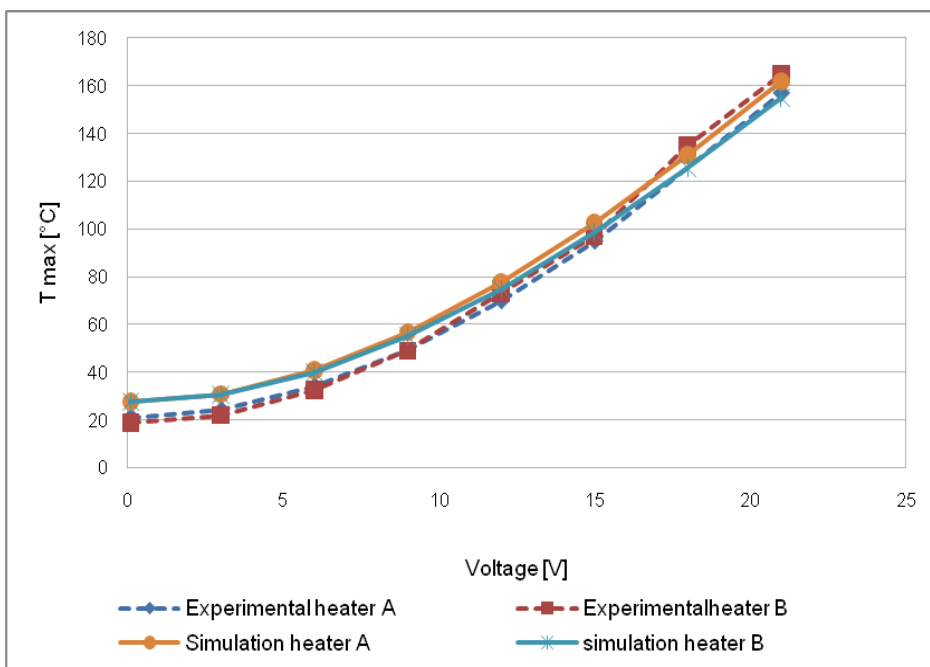


Figure IV-18: Membrane 2 mm x 4.5 mm encapsulated. Maximum temperature versus voltage.

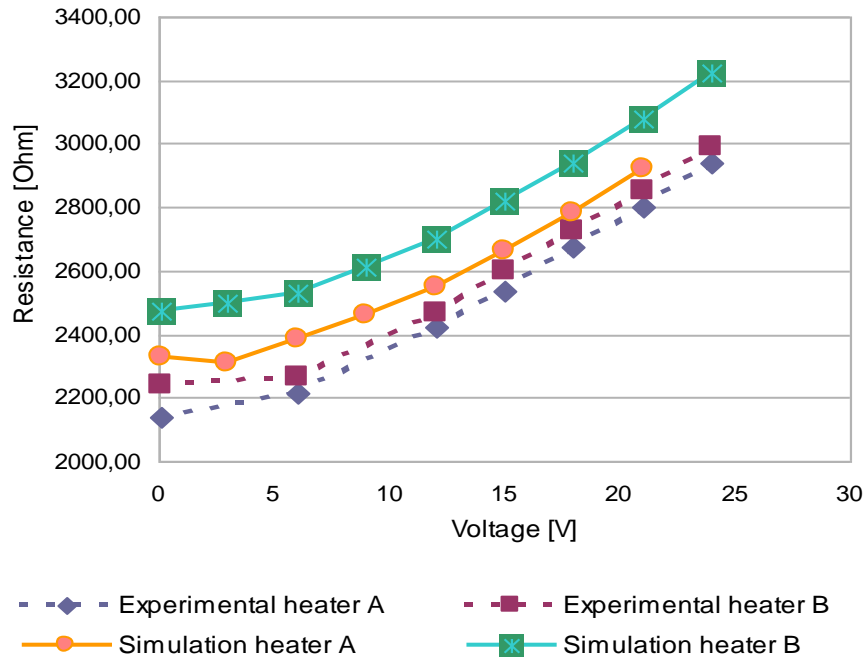
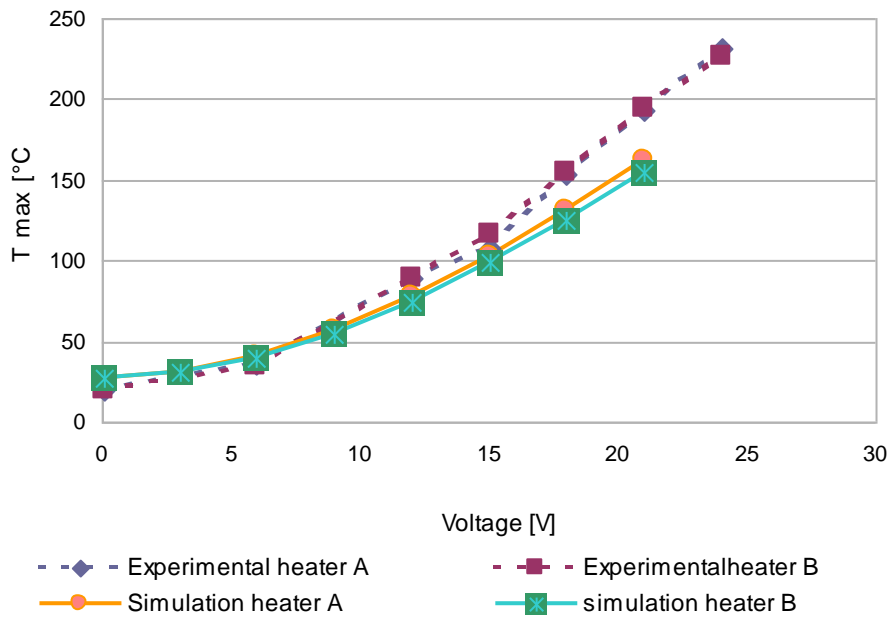


Figure IV-19: Membrane 2 mm x 4.5 mm non encapsulated. Resistance versus voltage



IV.2.2. Temperature profiles

In this chapter we show temperature profiles to compare simulations and experimental results. We show two axis x and y defined in Figure IV-20. Y is always crossing the heater parallel to the long side.

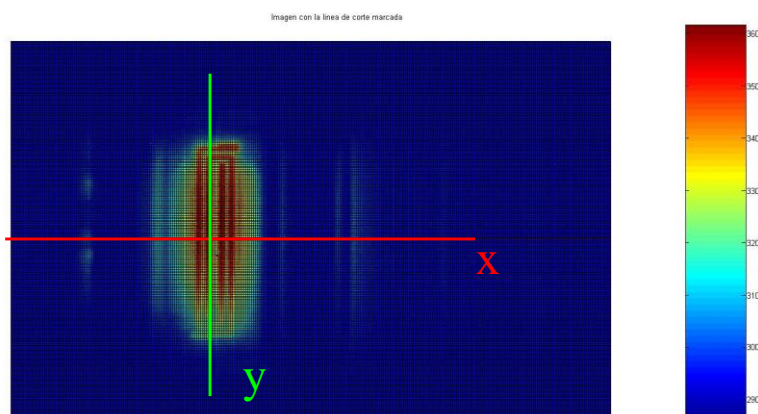


Figure IV-20: Definition of x and y axis

Figure IV-21 shows the temperature profile along the x axis defined in Figure IV-20. Taking into account distances we have realized that minimum peaks in the graph correspond to heater tracks. Despite being postprocessed image, platinum is “cheating” the infra red camera. We know platinum must be at least at the same temperature than adjacent membrane, because it is the heater element. So, we mustn’t take into account these minimums.

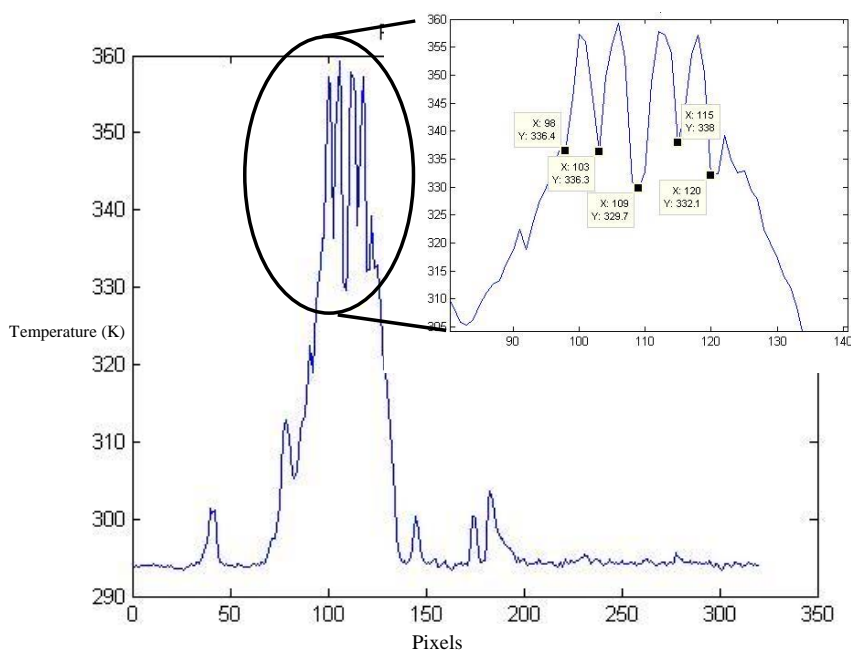


Figure IV-21: Temperature profile along x axis

In Annex all profiles are shown. In this chapter just most representatives ones are shown, they are profiles along x. Profiles along y are going parallel or just in the pixels between platinum and membrane (may be minimums ruled out in profiles along x) and for this reason y profiles images show more measurement noise.

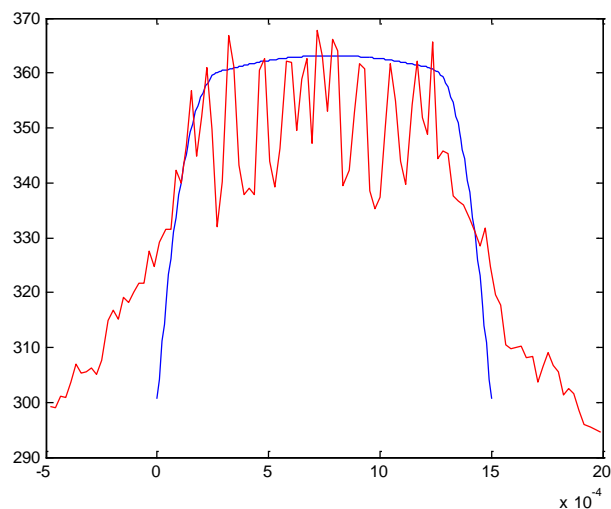


Figure IV-22: Chip 2 heater A. Temperature profile x applying 12 V.

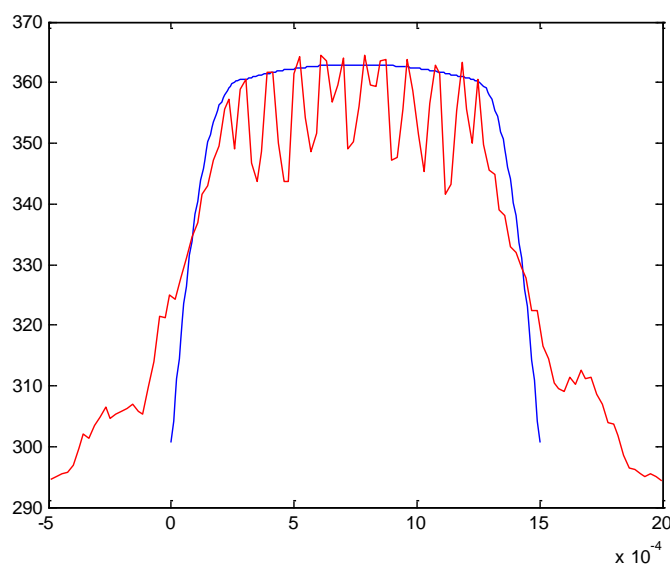


Figure IV-23: Chip 2 heater B. Temperature profile x applying 12 V.

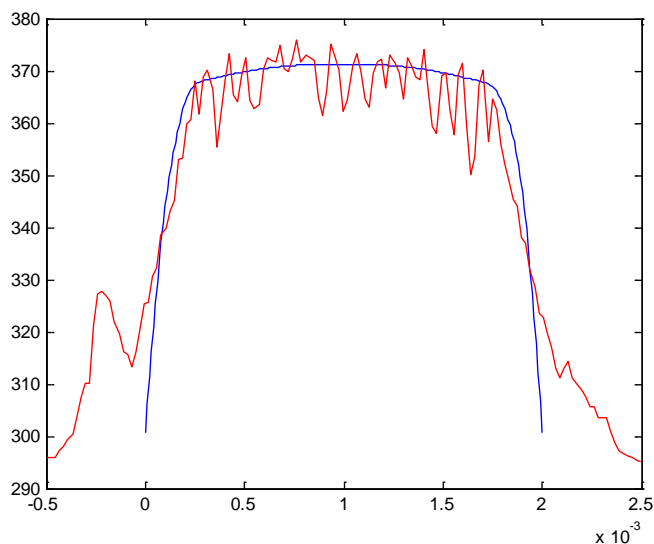


Figure IV-24: Chip 3 heater B. Temperature profile y applying 15 V.

In these images, if we don't take into account the minimums, experimental profiles and simulation ones fit very well. Temperature profiles and 2D images validate thermal distribution on simulations.

IV.2.3. Power consumption

Table IV-2 shows the power consumption per area unit and temperature degree. As we saw by means of simulation, large membranes are more efficient than small ones. So, if a big area is desired, it is better to use a large membrane than some small ones.

Membrane	Heater design	Simulation (mW/mm ² °C)	Encapsulated (mW/mm ² °C)	Non encapsulated (mW/mm ² °C)
1*3	initial	0,32	0,39	0,32
1*3	4 heaters	0,32	0,28	0,30
1*3	15-30-60-80	0,30	0,35	0,35
1,5*5	A	0,20	0,20	0,23
1,5*5	B	0,20	0,19	0,23
2*4,5	A	0,16	0,17	0,22
2*4,5	B	0,16	0,17	0,19

Table IV-2: Power consumption per unit area and degree.

IV.3. Conclusions

Membranes have been fabricated and tested. We have shown that simulations fit well with experimental results.

We have developed a model simulation which is well adjusted at experimental results and let us to try new ideas and study them avoiding fabrication cost and time which is higher than simulation cost and time. Taking into account a run could introduce a delay of some months it is completely non assumable in an investigation process.

V. CONCLUSIONS

We have developed a model simulation which reproduces quite well experimental results.

We have studied heater design and we have designed new heaters which improve temperature homogenisation. We have seen that a platinum double spiral resistor is not an optimum heater design. A double spiral shape with variable width exhibits better temperature uniformity than constant width. With this we have improved the membrane area usable for adsorbent material. We have studied also the distance between the heater and the edge membrane. We will use a distance of 250 μm , because a smaller one needs higher power consumption. So, in this way it is not possible increase area usable.

A silicon plug introduced under the heater area improves temperature homogeneity. Rising time is also increased but it's not determinant for us, tacking into account that the sensor has response time in order of seconds. Power consumption with a silicon plug doubles respects one without it, because we are heating much more area at high temperature which increases heat losses. A 5 μm depth silicon plug will be used, because it homogenizes enough to our application and it is less costly than one deeper. Despite homogenisation carried out by the silicon plug, best heater design should be used.

Big membranes are more effectives than some small ones in terms of silicon area used, tacking into account active area and tacking into account power consumption by unit. To obtain the same active area is better to use a big membrane than some small ones. Square membranes are more effectives in terms of silicon area used than rectangular ones. In terms of active area and power consumption by unit efficiency depends on the heater design.

Using a silicon plug 5 μm depth in big membranes homogenisation temperature is increased reaching a difference of temperature inside the heater area less than 15 K. Power consumption is increased respect to membranes without silicon plug.

Membranes have been fabricated and tested. We have shown that simulations fit well with experimental results. We have developed a model simulation which is well adjusted at experimental results and let us to try new ideas and study them avoiding fabrication cost and time.

As future work, in my opinion continue with heater design is not a good idea because new designs could improve just a few. A good configuration is reached using double spiral heater shapes with variable width.

An interesting investigation could be carried out in the fluid flow model including the adsorption-desorption process. Study of the preconcentrator in a real scenario could be interesting because temperature will be modified by the fluid. Fluids model could help in the preconcentrator and sensors cameras design, because fluid behaviour inside these cameras was completely unknown and we have seen this is important. Finally, in order to compare experimental and simulation desorption peaks, it is important to include the detector in the model. In our case, a gas chromatograph was

used as detector. This device introduces pressure and fluid modifications that were difficult to model. I think using a PID sensor could be easily modelled and it will be a more realistic measurement when the preconcentrator was included in the sensor system.

ANNEX

Experimental measurements: Chip 2 (1.5 mm x 5 mm)

Post-processed images

Now we shown the images before and after being post processed for an encapsulated device:

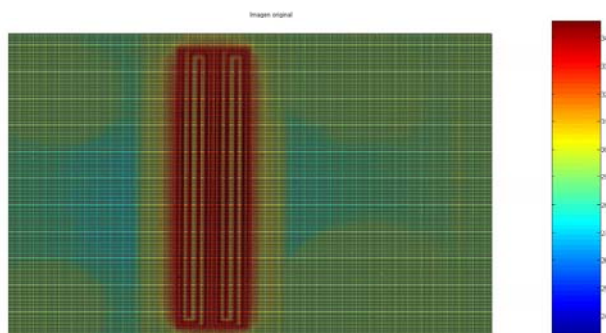


Figure Annex -1: Chip 2 heater A. Infrared camera image applying 10 V.

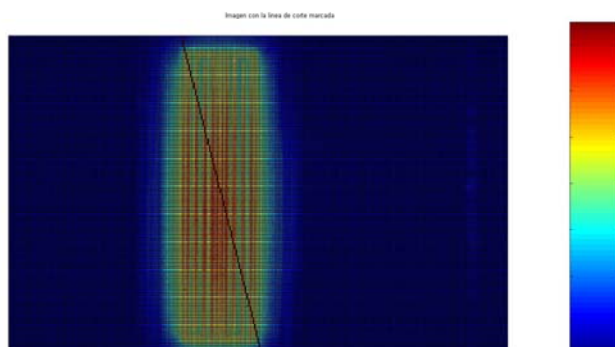


Figure Annex -2: Chip 2 heater A. Post-processed image applying 10 V.

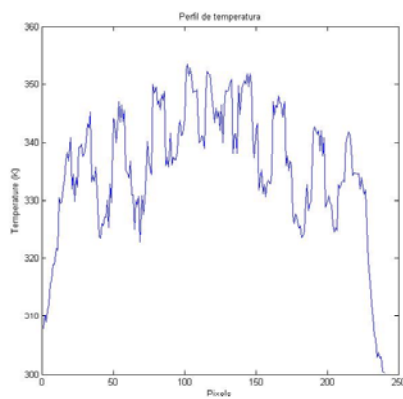


Figure Annex -3: Chip 2 heater A. Diagonal profile.

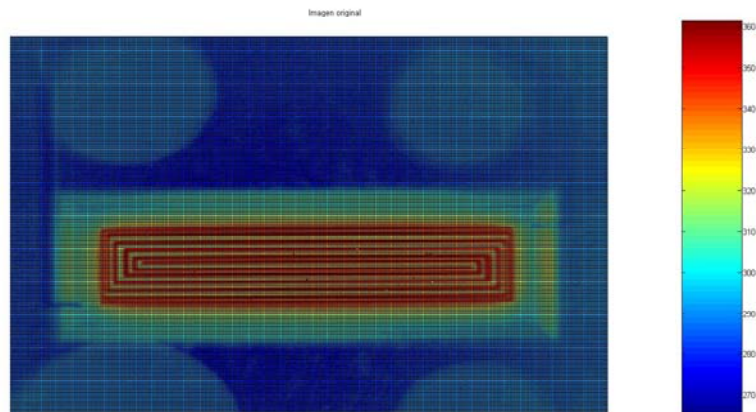


Figure Annex -4: Chip 2 heater B. Infrared camera image applying 12 V.

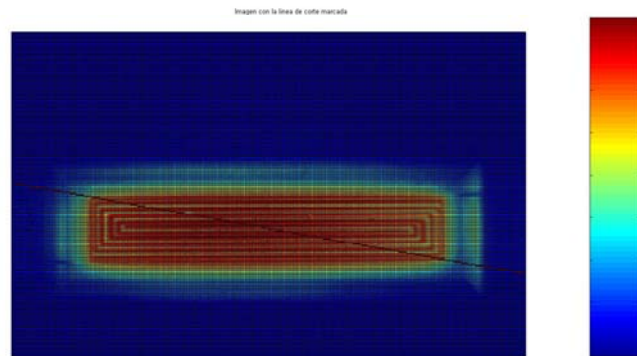


Figure Annex -5: Chip 2 heater B. Post-processed image applying 12 V.

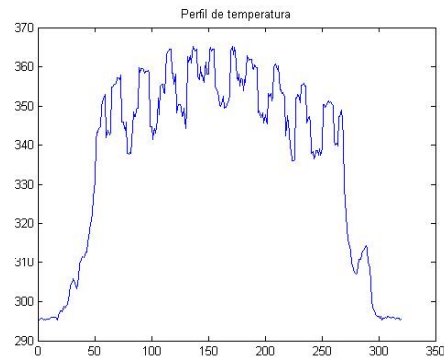


Figure Annex -6: Chip 2 heater B. Diagonal profile.

Electric characterization

Heater	V[V]	I[A]	R [ohm]	delta R	T max [°C]	delta T	Range
Design A	0,1	5,96E-005	1678,70	0,00	20	0	5-95
	3	1,77E-003	1694,92	16,22	26	6	5-95
	6	3,43E-003	1748,25	69,55	43	23	5-95
	9	4,91E-003	1832,99	154,30	68	48	5-95
	12	6,22E-003	1930,81	252,12	100	80	5-95
	15	7,37E-003	2035,28	356,58	144	124	125-250
	18	8,39E-003	2146,18	467,48	178	158	125-250
	20	8,99E-003	2224,69	546,00	203	183	125-250
	21	9,29E-003	2260,50	581,80	215	195	125-250
Degign B	V[V]	I[A]	R [ohm]	delta R	T max [°C]	delta T	Range
	0,1	5,23E-005	1913,14	0,00	20	20	5-95
	3	1,56E-003	1923,08	9,93	24,6	24,6	5-95
	6	3,03E-003	1980,20	67,05	39	39	5-95
	9	4,36E-003	2064,22	151,08	62	62	5-95
	12	5,54E-003	2166,06	252,92	90	90	5-95
	15	6,56E-003	2286,59	2286,59	137	137	125-250
	18	7,49E-003	2403,20	2403,20	165	165	125-250
	21	8,33E-003	2521,01	2521,01	200	200	125-250

Table Annex -1: Chip 2 encapsulated in T8

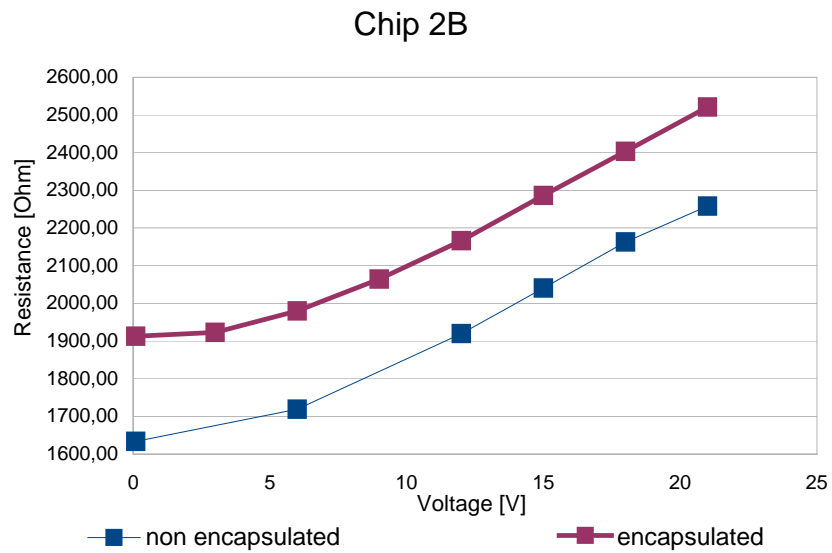
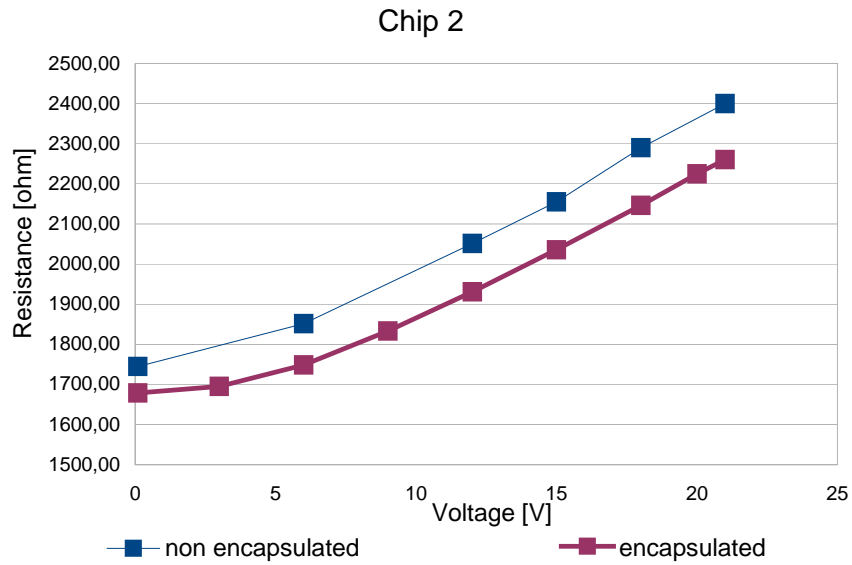


Figure Annex -7: Resistance versus voltage chip 2

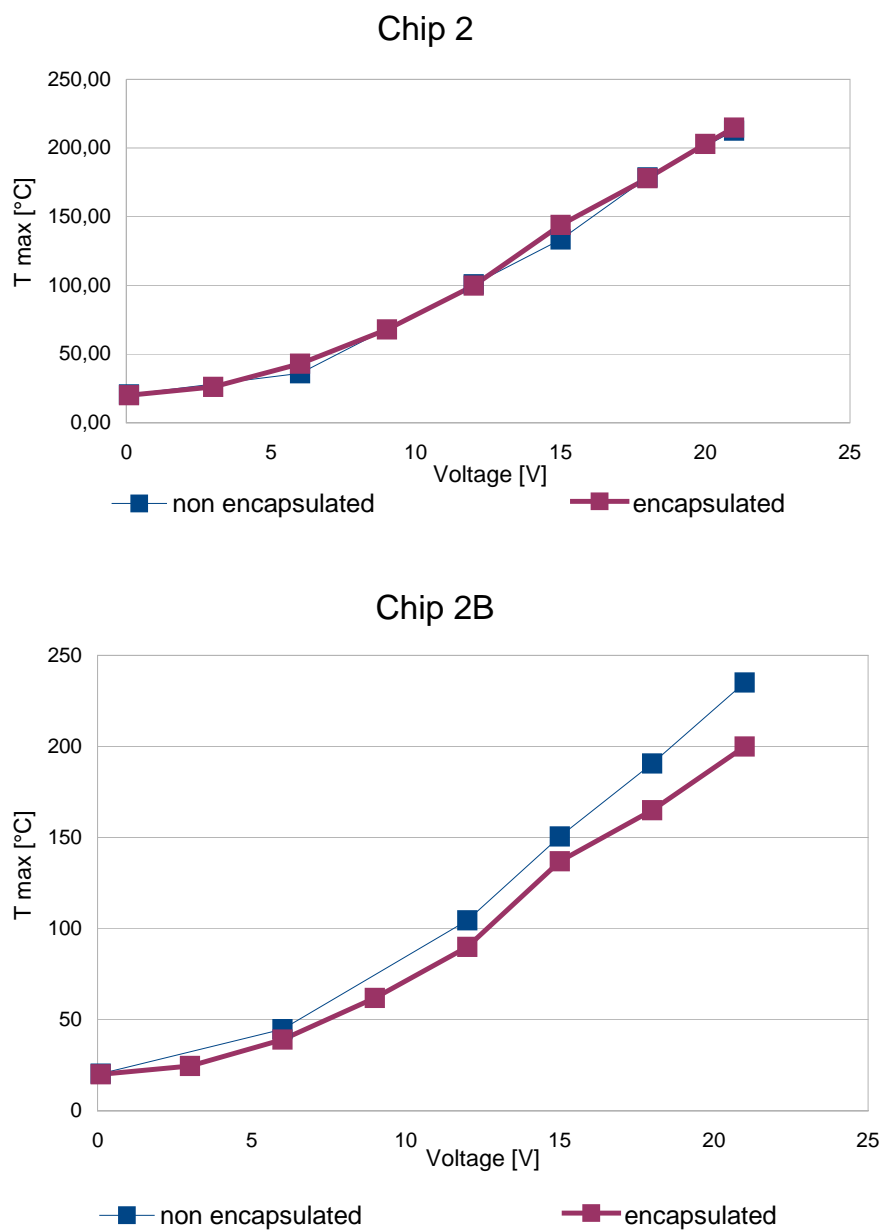


Figure Annex -8: Maximum temperature versus voltage chip 2

Temperature profiles

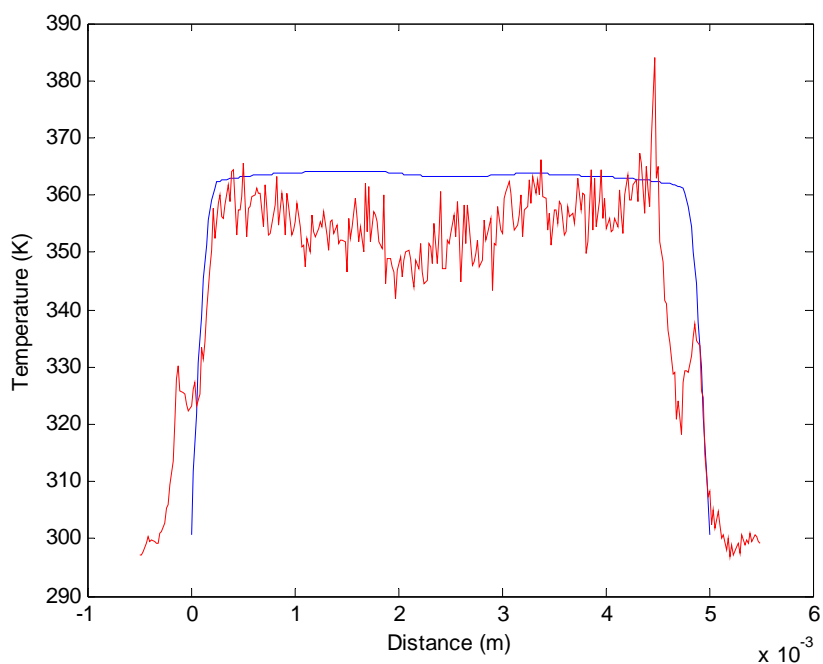


Figure Annex -9: Chip 2 heater A. Temperature profile y applying 12 V.

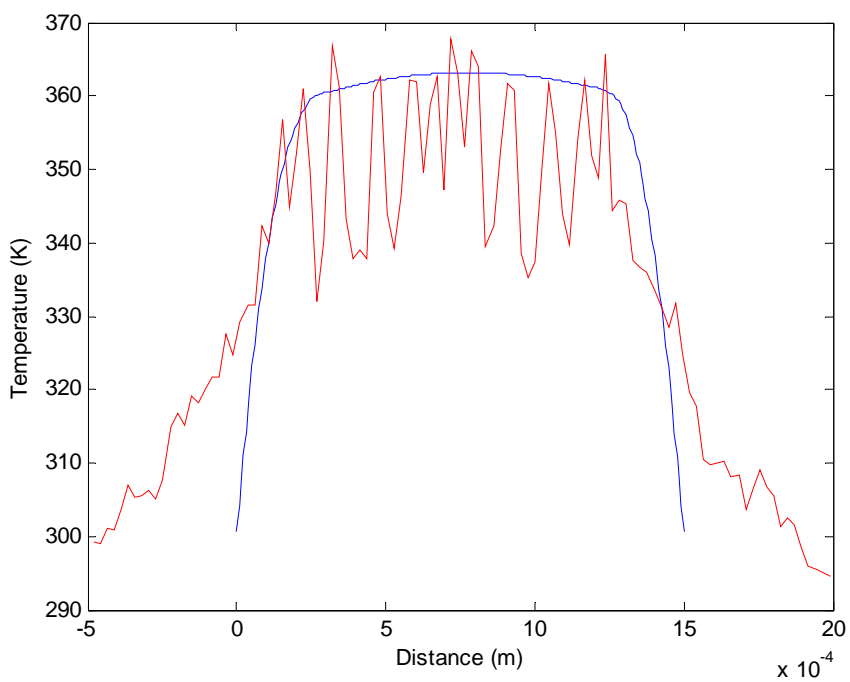


Figure Annex -10: Chip 2 heater A. Temperature profile x applying 12 V.

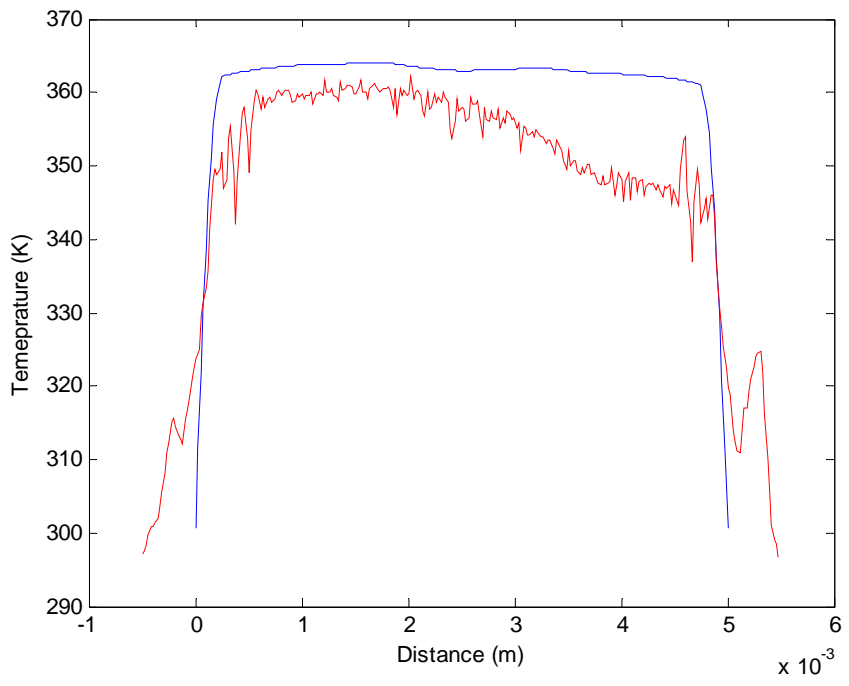


Figure Annex -11: Chip 2 heater B. Temperature profile y applying 12 V

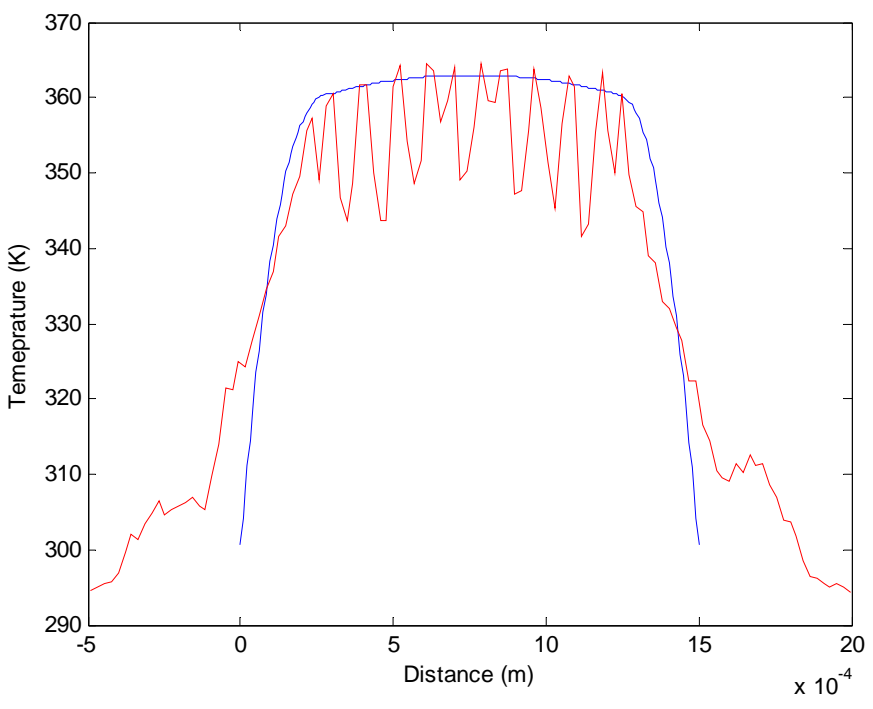


Figure Annex -12: Chip 2 heater B. Temperature profile x applying 12 V.

Experimental measurements: Chip 3 (2 mm x 4.5 mm)

Post-processed images

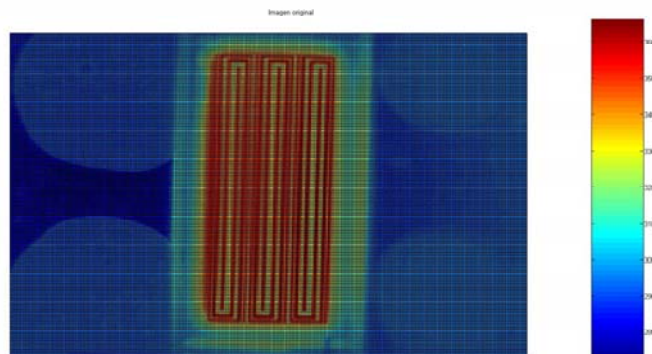


Figure Annex -13: Chip 3 heater A. Infrared camera image applying 15 V.

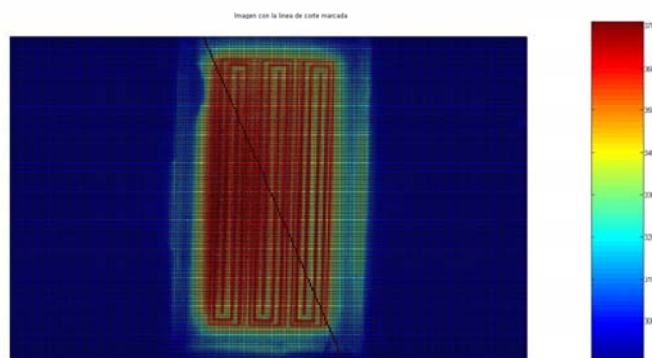


Figure Annex -14: Chip 3 heater A. Post-processed image applying 15 V.

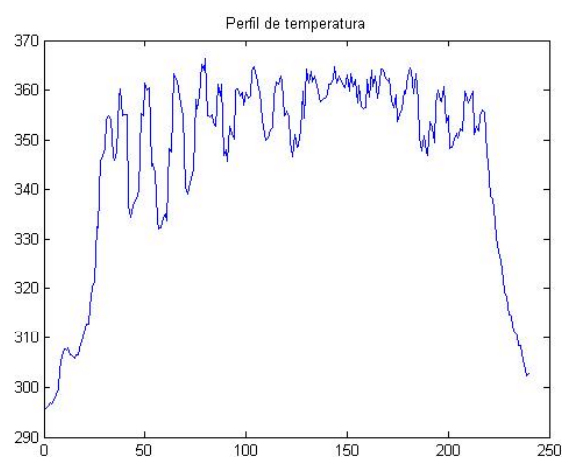


Figure Annex -15: Chip 3 heater A. Diagonal profile.

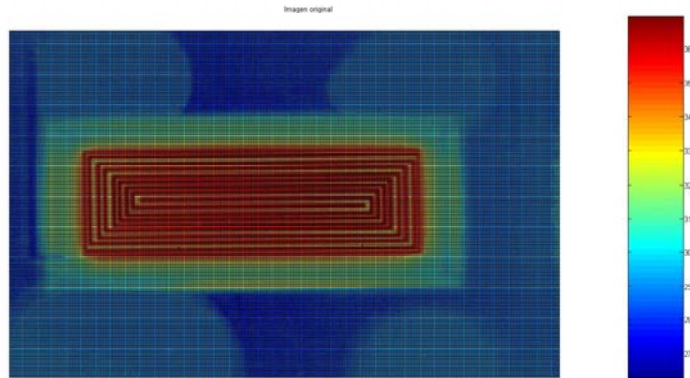


Figure Annex -16: Chip 3 heater B. Infrared camera image applying 15 V.

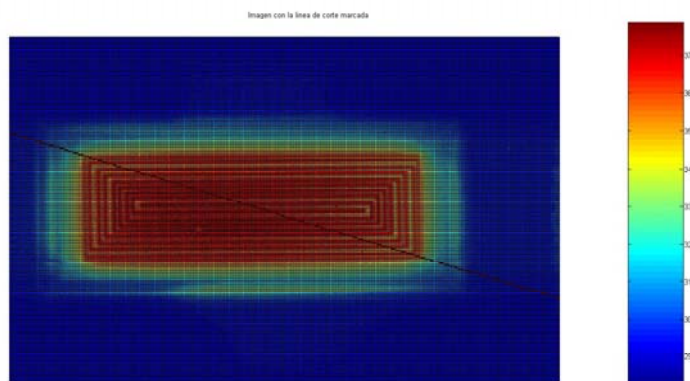


Figure Annex -17: Chip 3 heater B. Post-processed image applying 15 V.

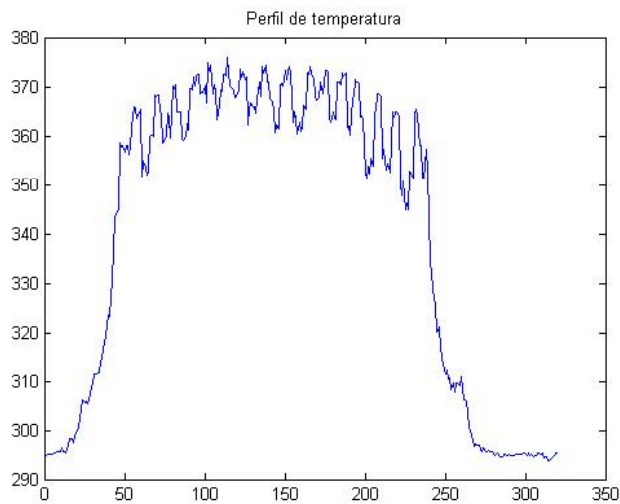


Figure Annex -18: Chip 3 heater B. Diagonal profile.

Electric characterization

Heater	V[V]	I[A]	R [ohm]	delta R	T max [°C]	delta T	Range
Design A	0,1	4,47E-005	2235,64	0,00	21	0	5-95
	3	1,34E-003	2235,47	-0,17	24	3	5-95
	6	2,67E-003	2247,19	11,55	34	13	5-95
	9	3,82E-003	2359,11	123,47	49	28	5-95
	12	4,89E-003	2451,98	216,35	70	49	5-95
	15	5,87E-003	2555,37	319,73	95	74	5-95
	21	7,54E-003	2785,15	549,51	157	136	125-250
Design B	V[V]	I[A]	R [ohm]	delta R	T max [°C]	delta T	Range
	0,1	4,58E-005	2181,98	0,00	18,8	-2,2	5-95
	3	1,39E-003	2162,94	-19,04	22	1	5-95
	6	2,72E-003	2202,64	20,67	32,5	11,5	5-95
	9	3,97E-003	2267,00	85,03	49	28	5-95
	12	5,12E-003	2341,92	159,94	73	52	5-95
	15	6,19E-003	2424,44	242,46	97	76	5-95
	18	7,18E-003	2507,66	272,03	135	114	125-250
21	8,09E-003	2595,80	360,16	165	144	125-250	

Table Annex -2: Chip 3 encapsulated in T8

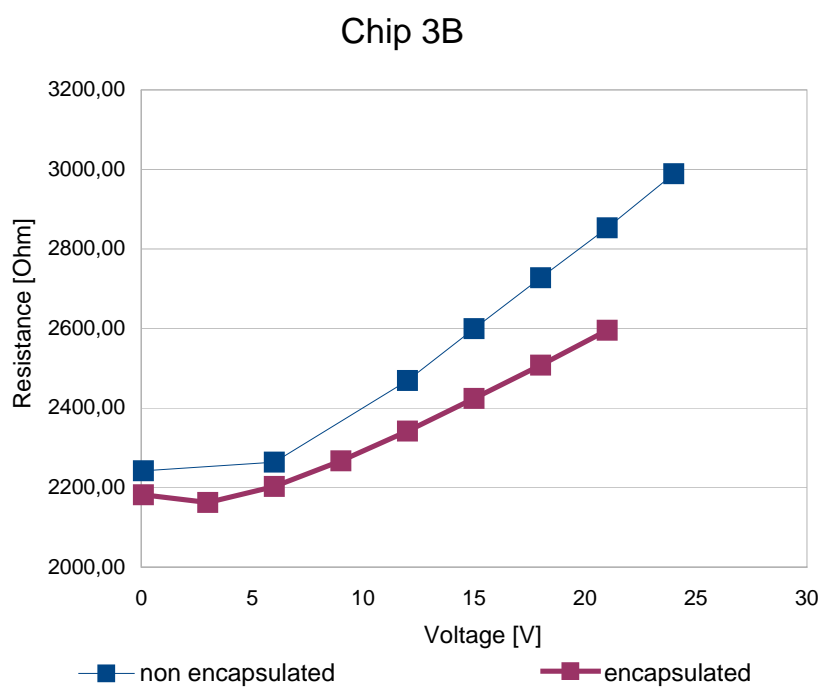
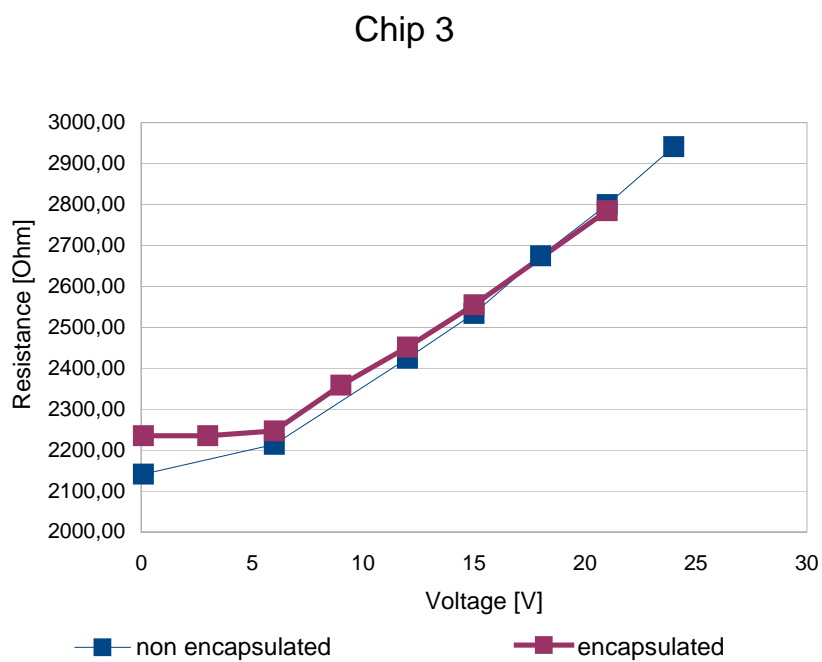


Figure Annex-19: Resistance versus voltage chip 3

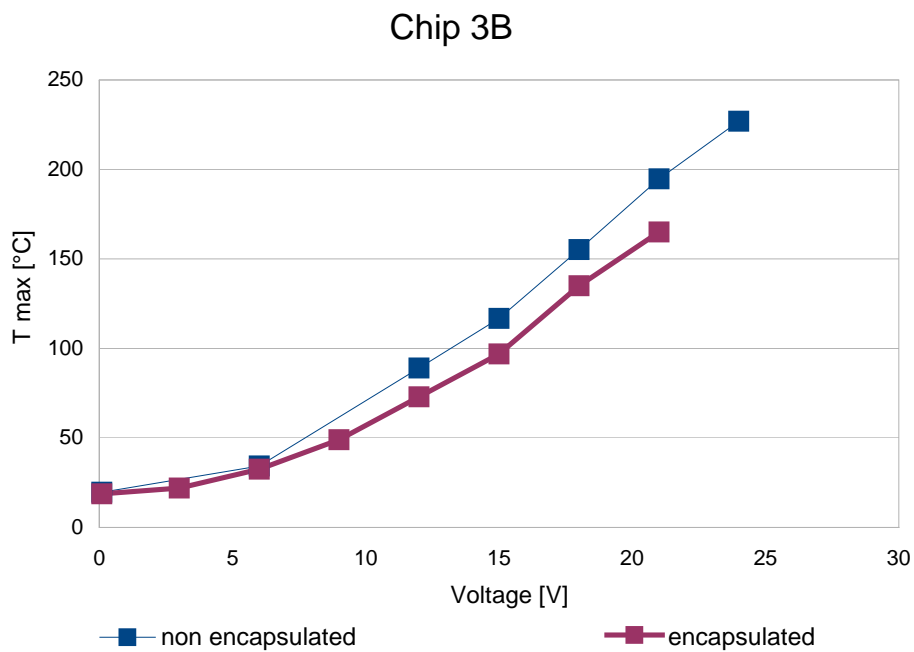
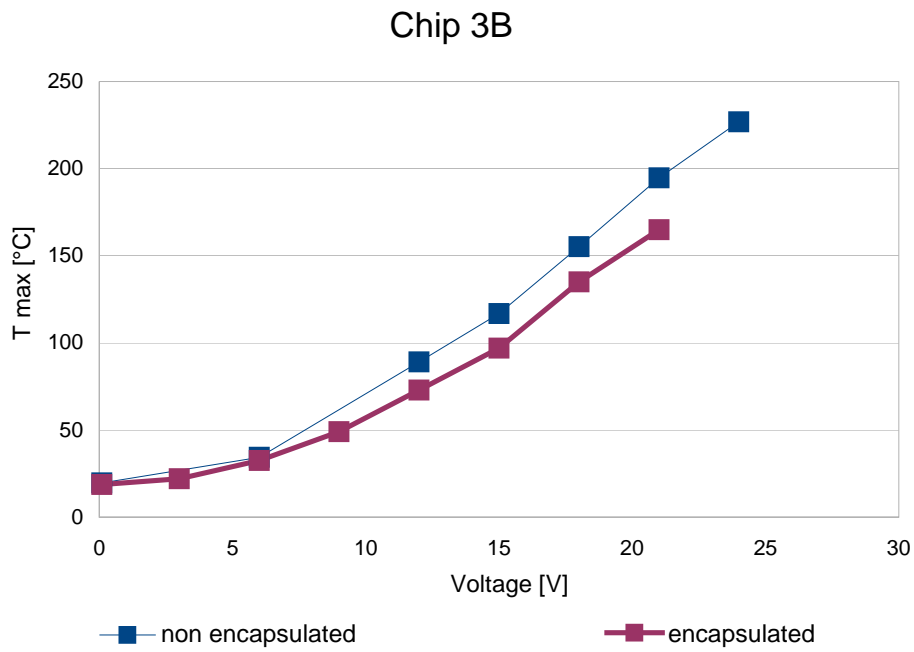


Figure Annex -20: Maximum temperature versus voltage chip 3

Temperature profiles

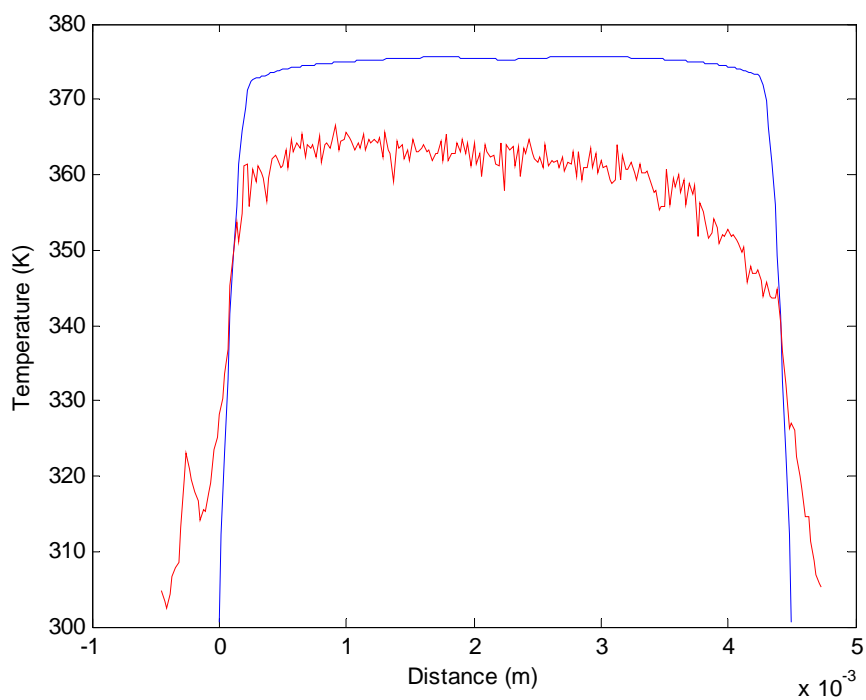


Figure Annex -21: Chip 3 heater A. Temperature profile x applying 15 V.

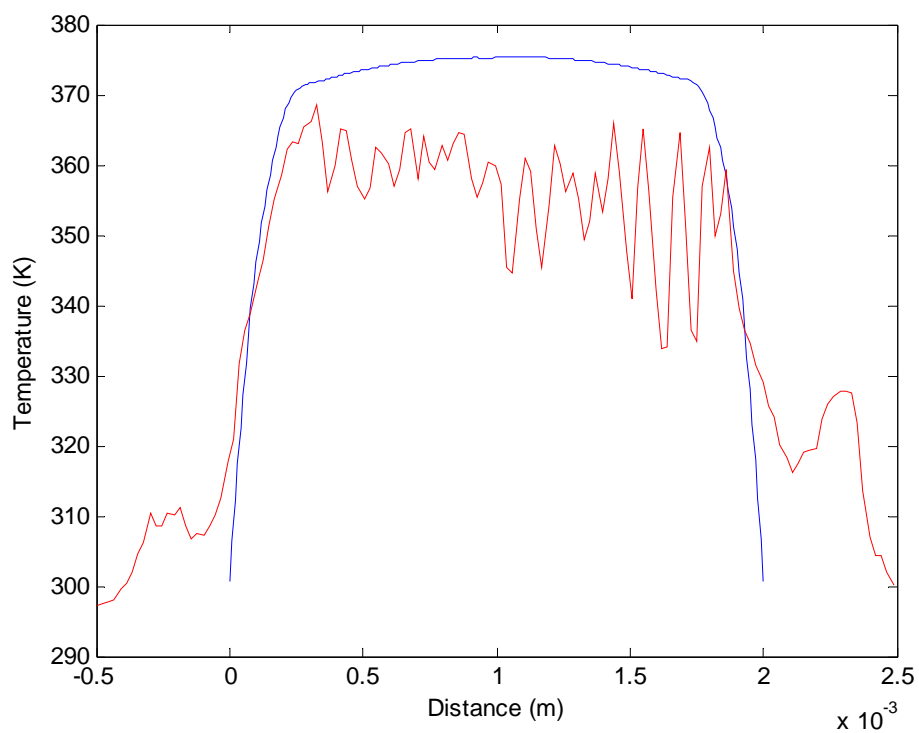


Figure Annex -22: Chip 3 heater A. Temperature profile y applying 15 V.

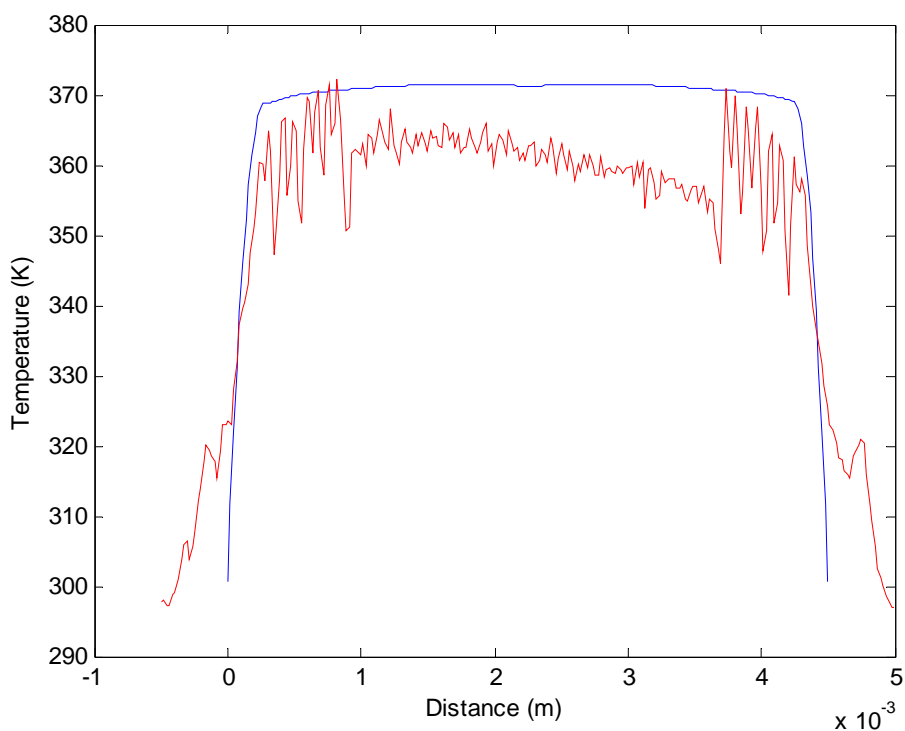


Figure Annex -23: Chip 3 heater B. Temperature profile x applying 15 V.

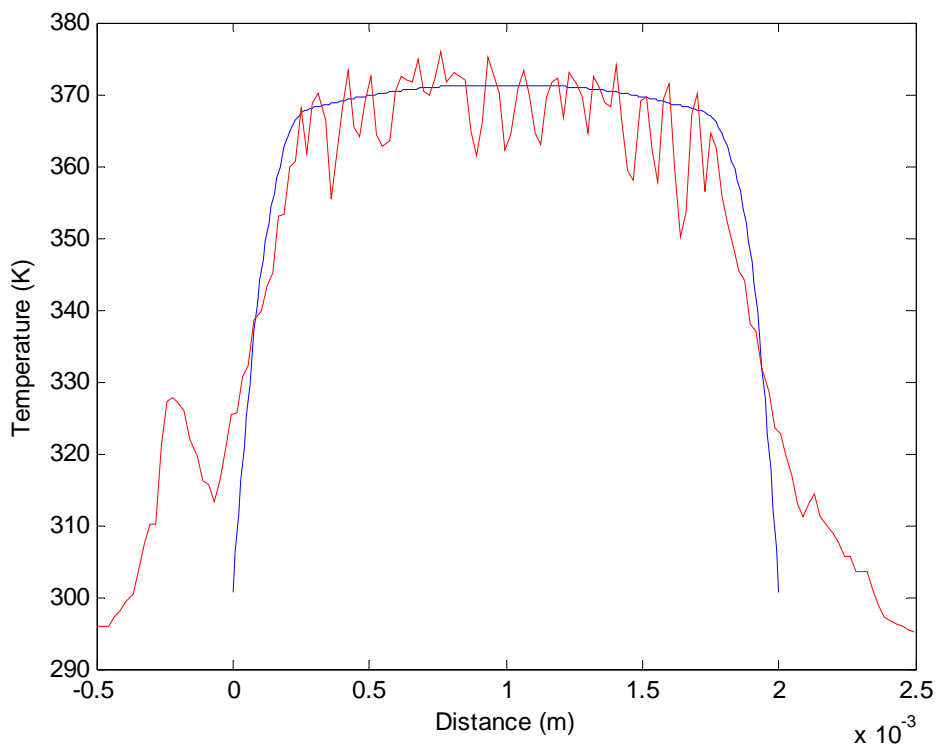


Figure Annex -24: Chip 3 heater B. Temperature profile y applying 15 V.

Experimental measurements: Chip 4 (1 mm x 3 mm)

Post-processed images

Now we will shown the images before and after being post processed for an encapsulated device:

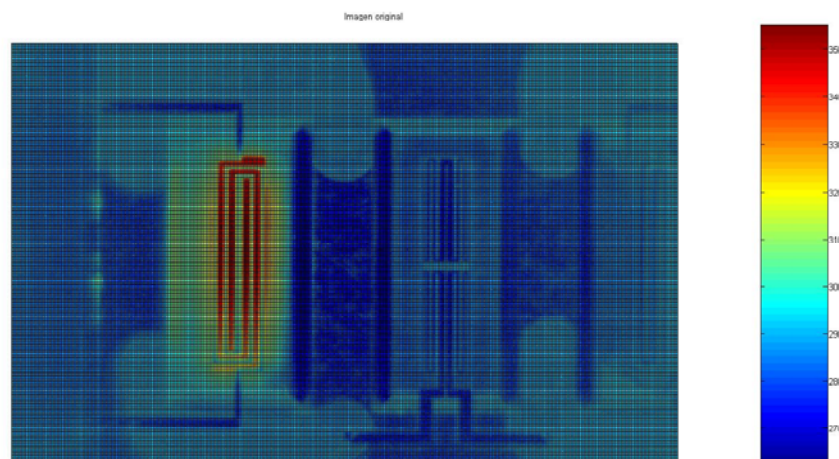


Figure Annex -25: Initial design T8. Infrared camera image applying 3V.

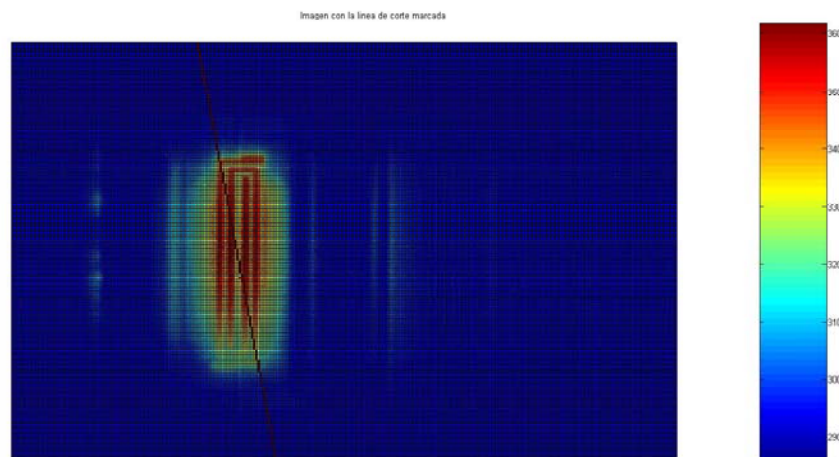


Figure Annex -26: Initial design T8. Post-processed image applying 3V.

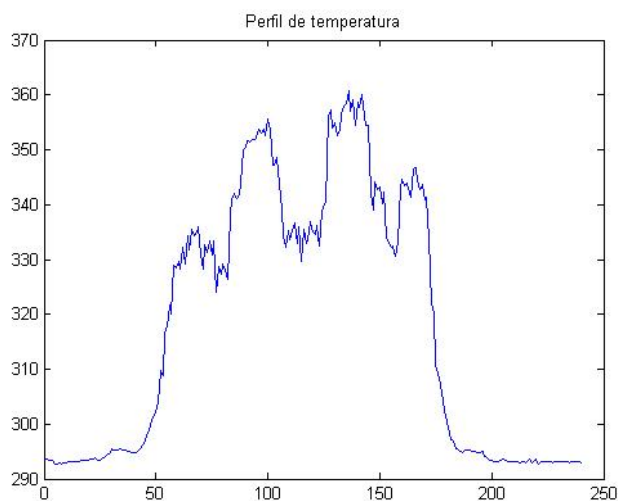


Figure Annex -27: Diagonal profile. Membrane 1 mm x 3 mm. Initial design heater.

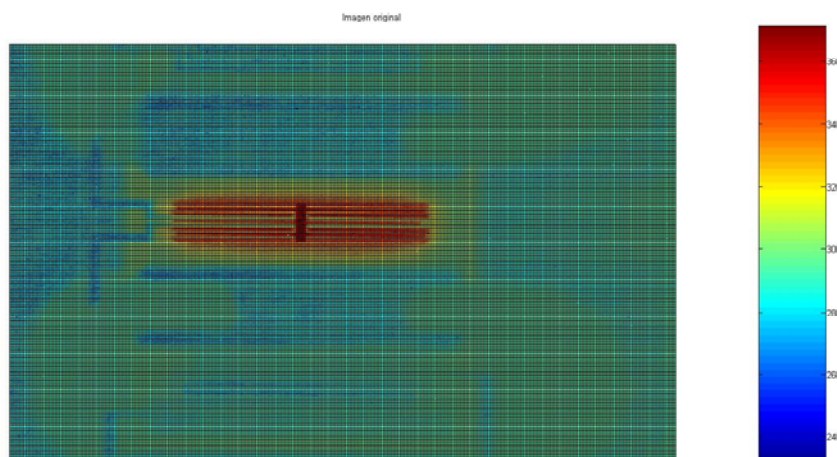


Figure Annex -28: 4 heaters design T8. Infrared camera image applying 6 V.

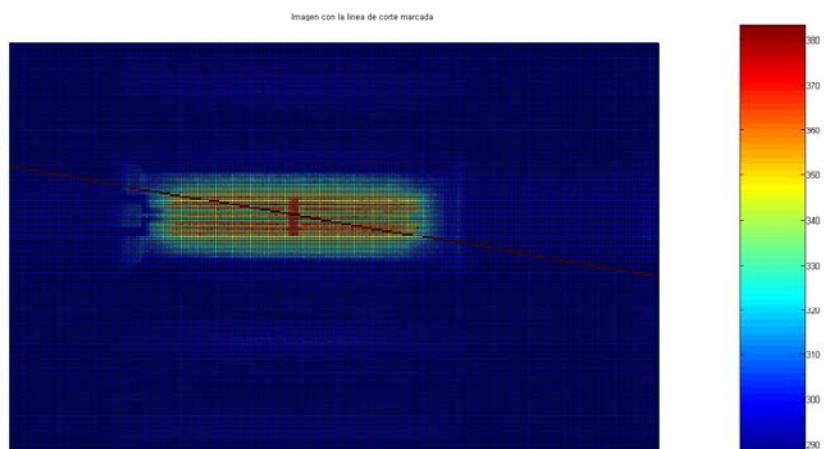


Figure Annex -29: 4 heaters design T8. Post-processed image applying 6 V.

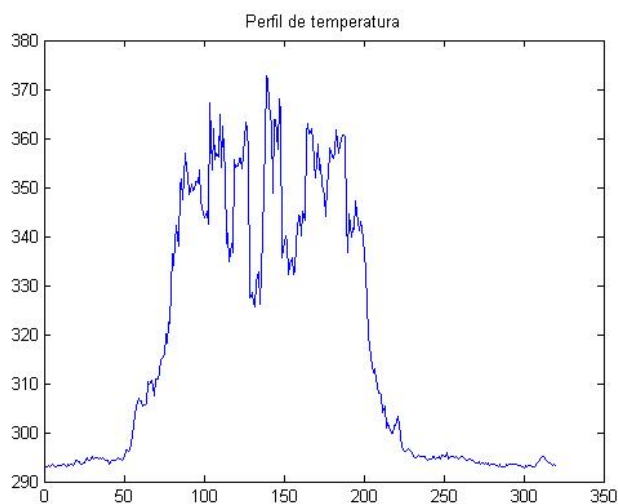


Figure Annex -30: Diagonal profile. Membrane 1 mm x 3 mm. 4 heaters design.

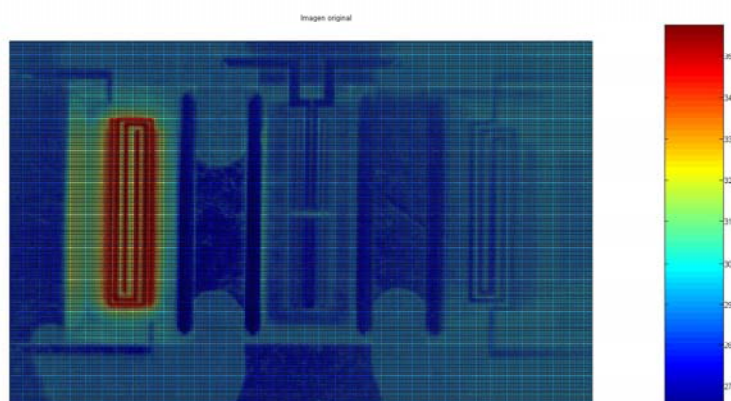


Figure Annex -31: 15-30-60-80 design T8. Infrared camera image applying 5 V.

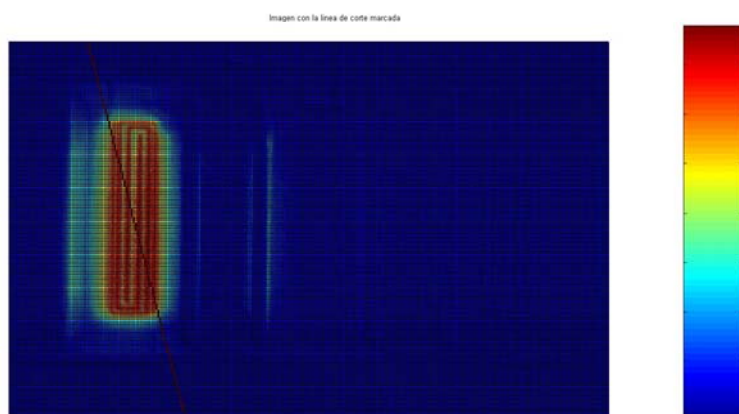


Figure Annex -32: 15-30-60-80 design T8. Post-processed image applying 5 V.

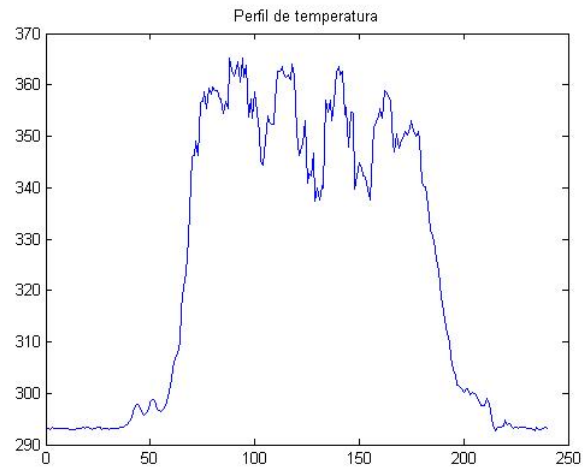


Figure Annex -33: Diagonal profile. Membrane 1 mm x 3 mm. 15-30-60-80 design.

Electric characterization

Heater	V[V]	I[A]	R [ohm]	delta R	T max [°C]	delta T	Range
15-30-60-80	0,1	1,41E-004	710,23	0,00	17,8	0	5-95
	1	1,41E-003	710,73	0,50	19,8	2	5-95
	2	2,76E-003	725,43	15,20	27,5	9,7	5-95
	3	4,01E-003	747,76	37,53	41	23,2	5-95
	4	5,16E-003	775,64	65,42	61	43,2	5-95
	5	6,19E-003	807,88	97,66	85	67,2	5-95
	6	7,13E-003	841,87	131,64	128	110,2	125-250
	7	7,97E-003	877,85	167,63	148	130,2	125-250
	8	8,75E-003	913,87	203,64	170	152,2	125-250
	9	9,47E-003	950,47	240,24	197	179,2	125-250
	9,1	9,53E-003	954,98	244,75	200	182,2	125-250
	9,2	9,60E-003	958,33	248,11	203	185,2	125-250
4 heaters	0,1	9,67E-005	1034,34	0,00	21	0	5-95
	1	9,68E-004	1033,48	-0,86	23	2	5-95
	2	1,91E-003	1049,87	15,53	30	9	5-95
	3	2,79E-003	1074,88	40,54	41,5	20,5	5-95
	4	3,62E-003	1106,50	72,16	58	37	5-95
	5	4,37E-003	1144,69	110,35	79	58	5-95
	6	5,06E-003	1184,83	150,49	102	81	5-95
	7	5,71E-003	1226,78	192,44	137	116	125-250
	8	6,29E-003	1272,06	237,72	157	136	125-250
	9	6,84E-003	1316,17	281,83	180	159	125-250
	9,7	7,18E-003	1351,16	316,82	200	179	125-250
	10	7,08E-003	1412,43	378,09	206	185	125-250
Initial design	0,1	4,00E-004	250,19	0,00	21	0	5-95
	1	3,97E-003	251,70	1,51	26	5	5-95
	2	7,67E-003	260,72	10,53	45,5	24,5	5-95
	3	1,09E-002	274,05	23,86	81	60	5-95
	4	1,38E-002	289,94	39,75	122	101	80-175
	5	1,63E-002	307,47	57,28	175	154	80-175
	6	1,85E-002	324,83	74,65	230	209	125-250

Table Annex -3: Chip 4 encapsulated in T8

Heater	V[V]	I[A]	R [ohm]	delta R	T max [°C]	delta T	Range
15-30-60-80	0,1	1,33E-004	753,01	0,00	20,5	0	5-95
	3	3,87E-003	775,19	22,18	46,7	26,2	5-95
	4	4,96E-003	806,45	53,44	68,6	48,1	5-95
	5	5,95E-003	840,34	87,32	97	76,5	5-95
	6	6,85E-003	875,91	122,90	121,5	101	80-175
	7	7,64E-003	916,23	163,22	153,2	132,7	80-175
	8	8,37E-003	955,79	202,78	188,3	167,8	80-175
	9	9,05E-003	994,69	241,68	215,9	195,4	125-250
	10	9,68E-003	1033,06	280,05	250,5	230	125-250
4 heaters	0,1	9,26E-005	1079,91	0,00	20	0	5-95
	3	2,73E-003	1098,90	18,99	40,6	20,6	5-95
	4	3,52E-003	1136,36	56,45	58,5	38,5	5-95
	5	4,25E-003	1176,47	96,56	80	60	5-95
	6	4,91E-003	1222,00	142,08	101,4	81,4	80-175
	7	5,52E-003	1268,12	188,20	123	103	80-175
	8	6,07E-003	1317,96	238,04	151,7	131,7	80-175
	9	6,58E-003	1367,78	287,87	187	167	80-175
	10	7,04E-003	1420,45	340,54	204	184	125-250
	11	7,35E-003	1496,60	416,69	225	205	125-250
	12	7,75E-003	1548,39	468,47	258,6	238,6	125-250
Initial design	0,1	3,85E-004	259,74	0,00	20,5	0	5-95
	2	7,43E-003	269,18	9,44	58,34	37,84	5-95
	3	1,05E-002	286,53	26,79	102,82	82,32	5-95
	4	1,31E-002	306,28	46,54	151,3	130,8	80-175
	5	1,53E-002	327,65	67,91	194,71	174,21	80-175
	6	1,73E-002	347,83	88,09	270,97	250,47	125-250

Table Annex -4: Chip 4 non encapsulated

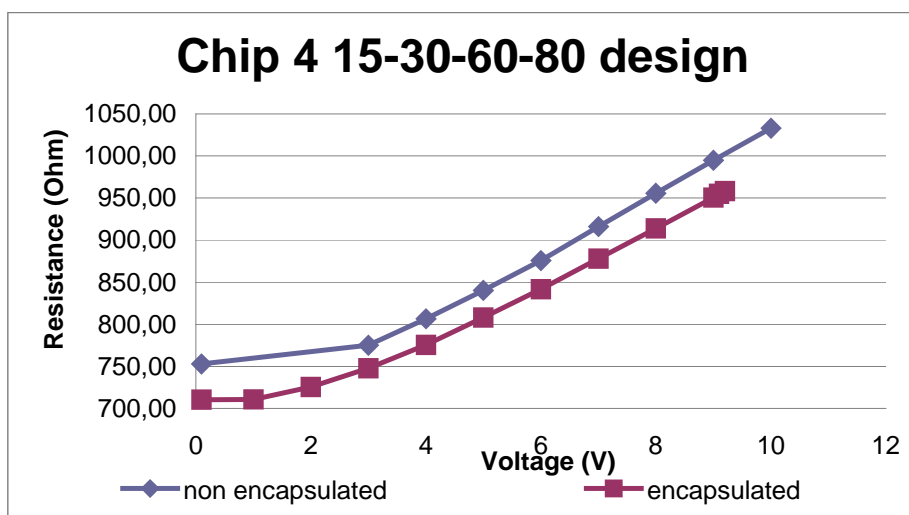
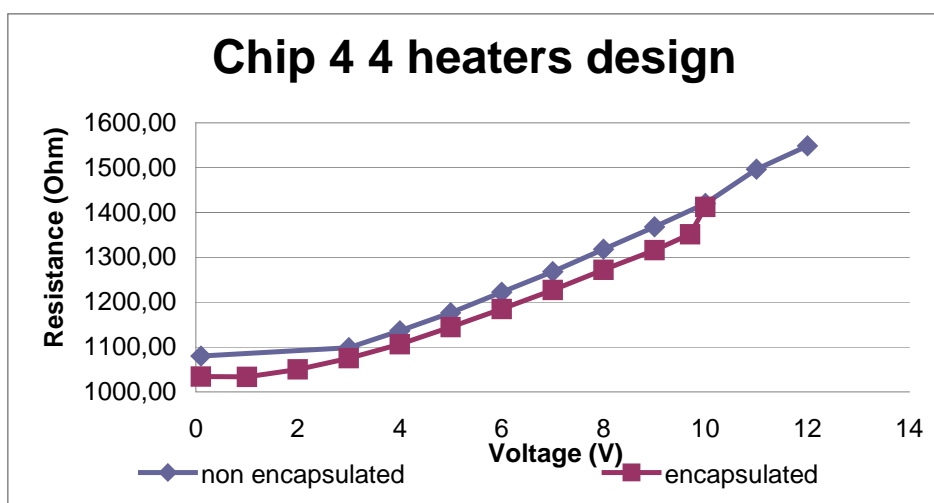
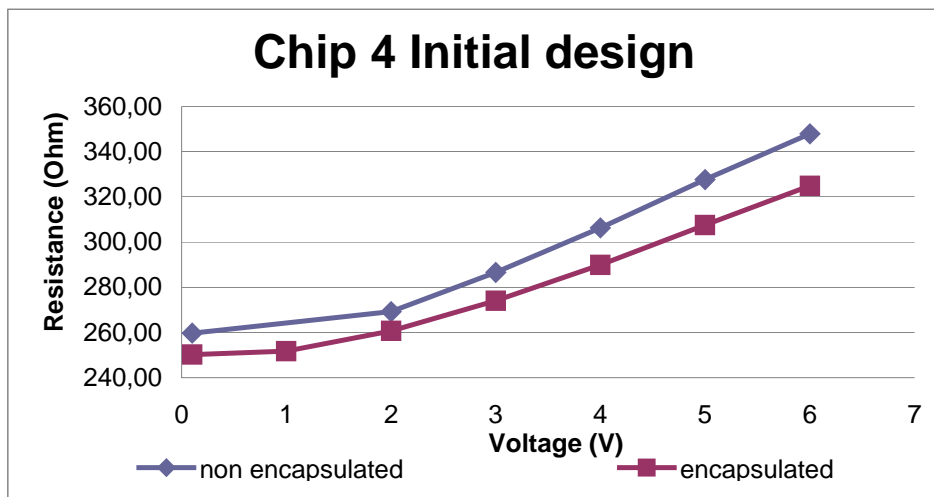


Figure Annex -34: Resistance versus voltage chip 4

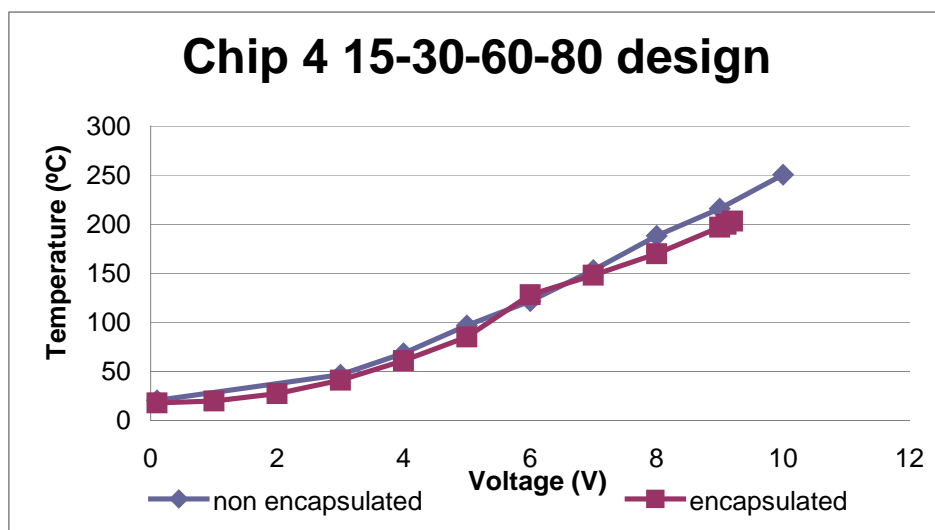
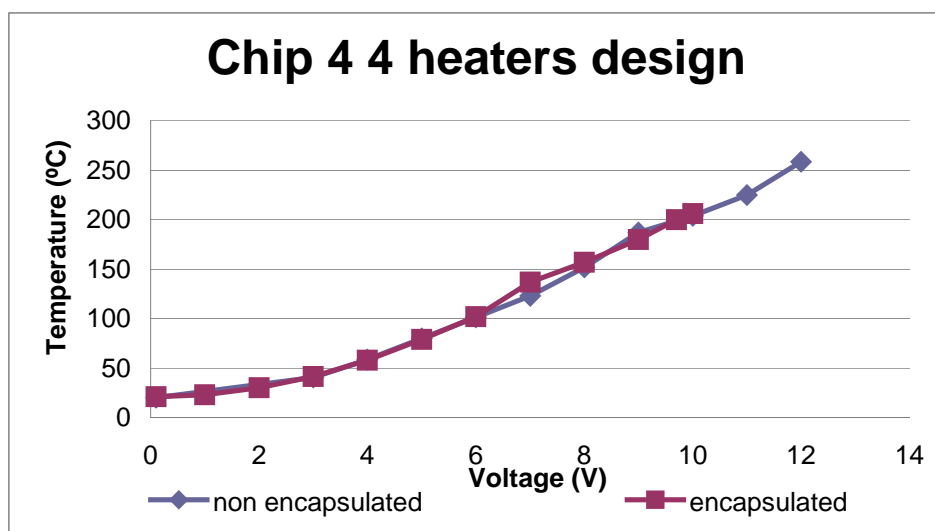
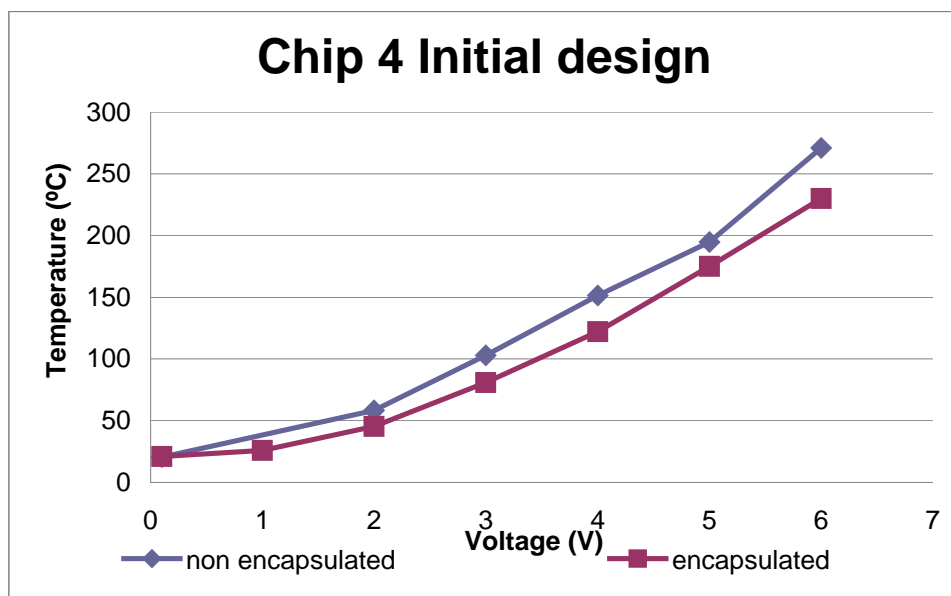


Figure Annex -35: Maximum temperature versus voltage chip 4

Temperature profiles

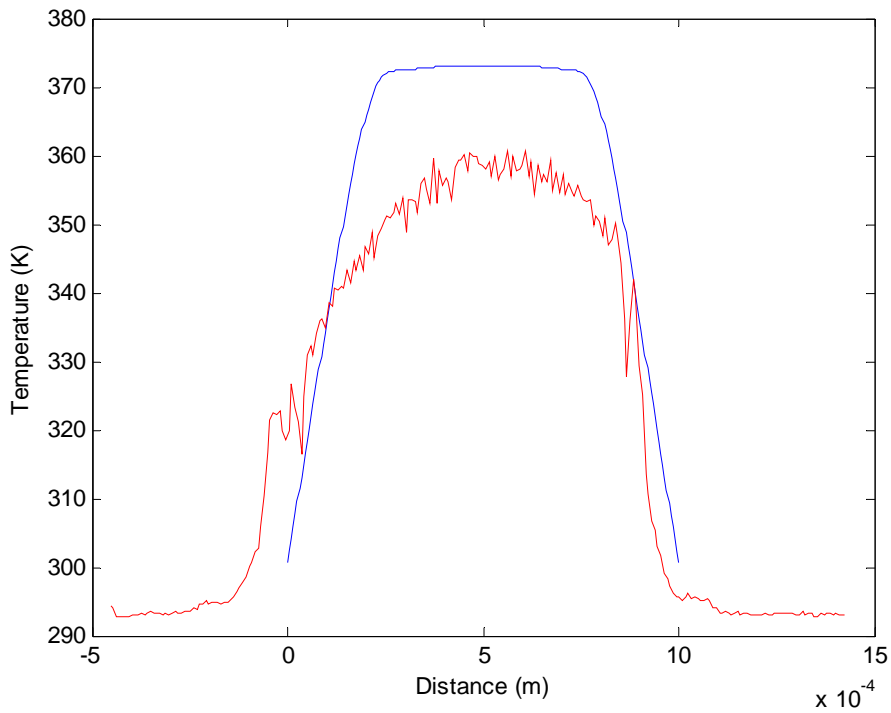


Figure Annex -36: Initial design. Temperature profile y applying 3V.

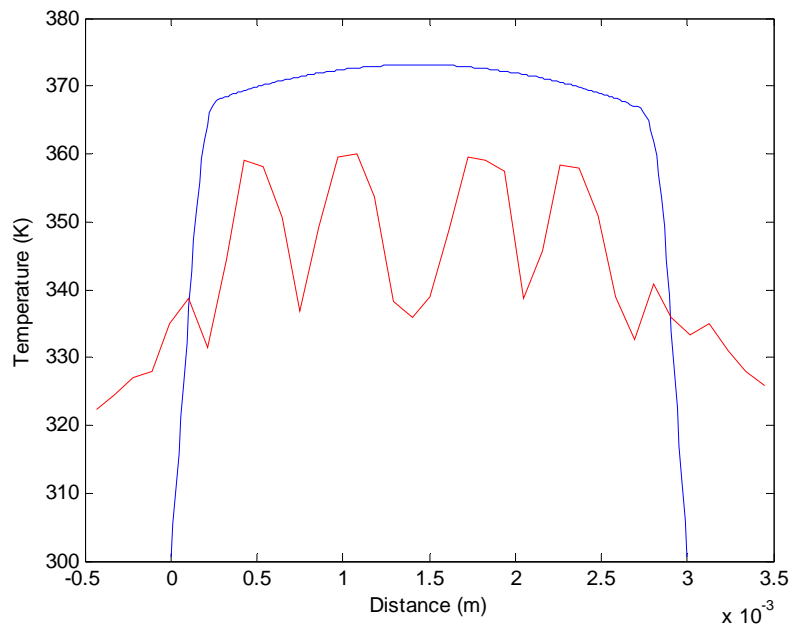


Figure Annex -37: Initial design. Temperature profile x applying 3V.

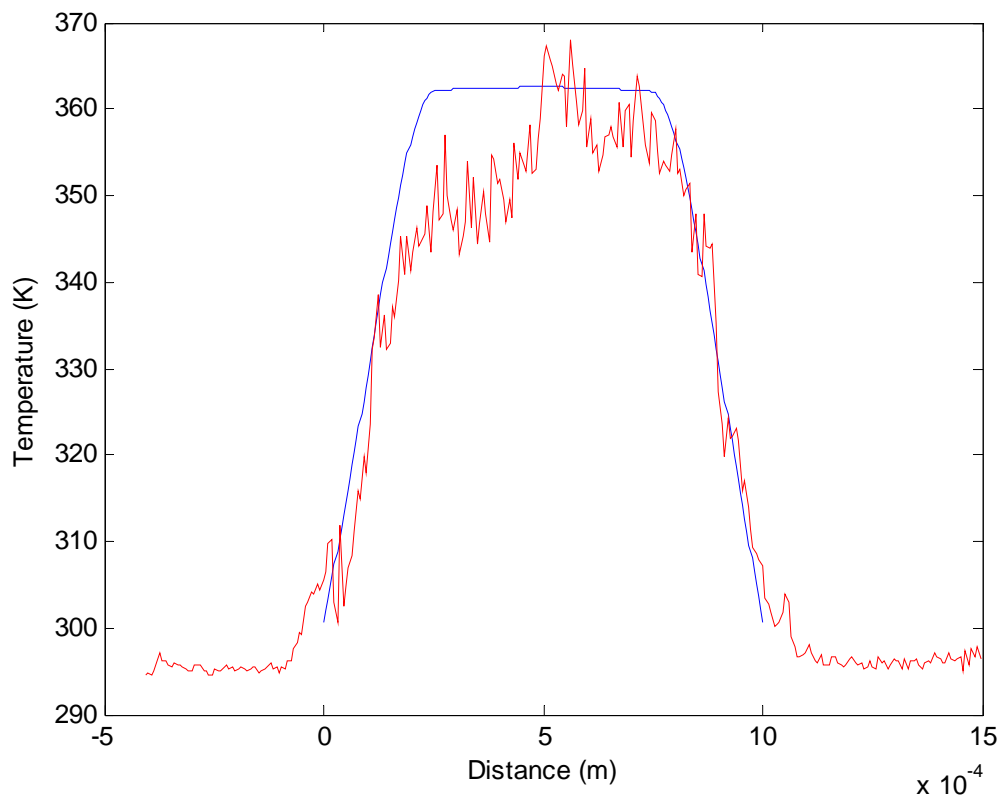


Figure Annex -38: 4 heater design. Temperature profile y applying 6V.

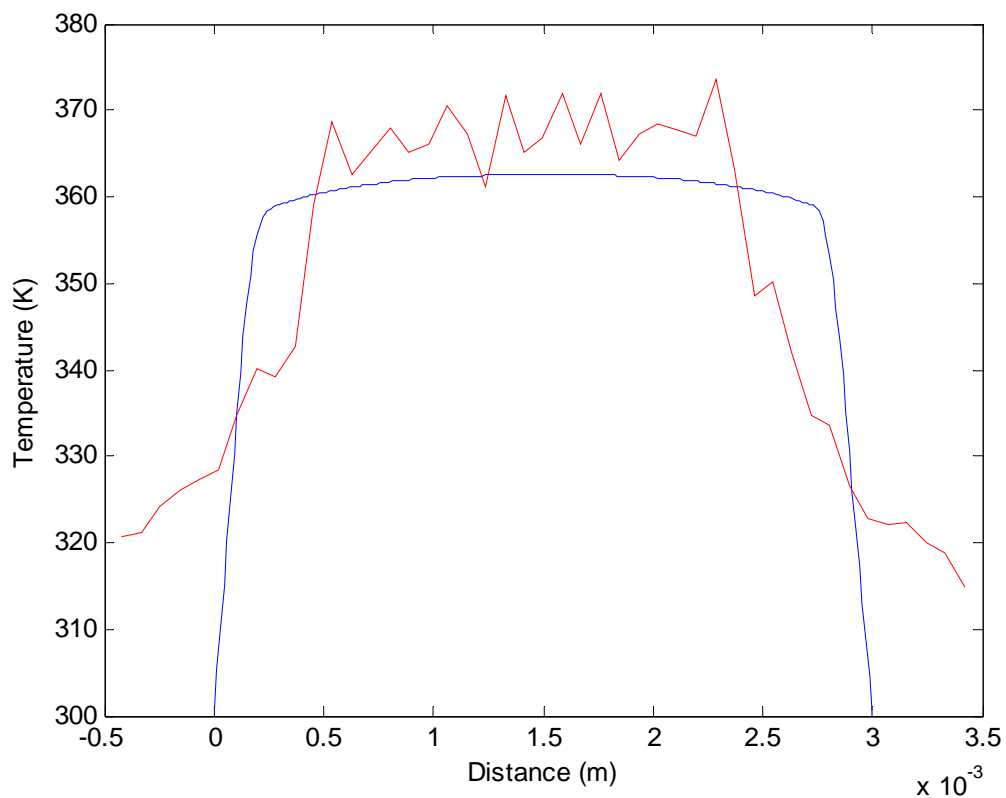


Figure Annex -39: 4 heater design. Temperature profile x applying 6V.

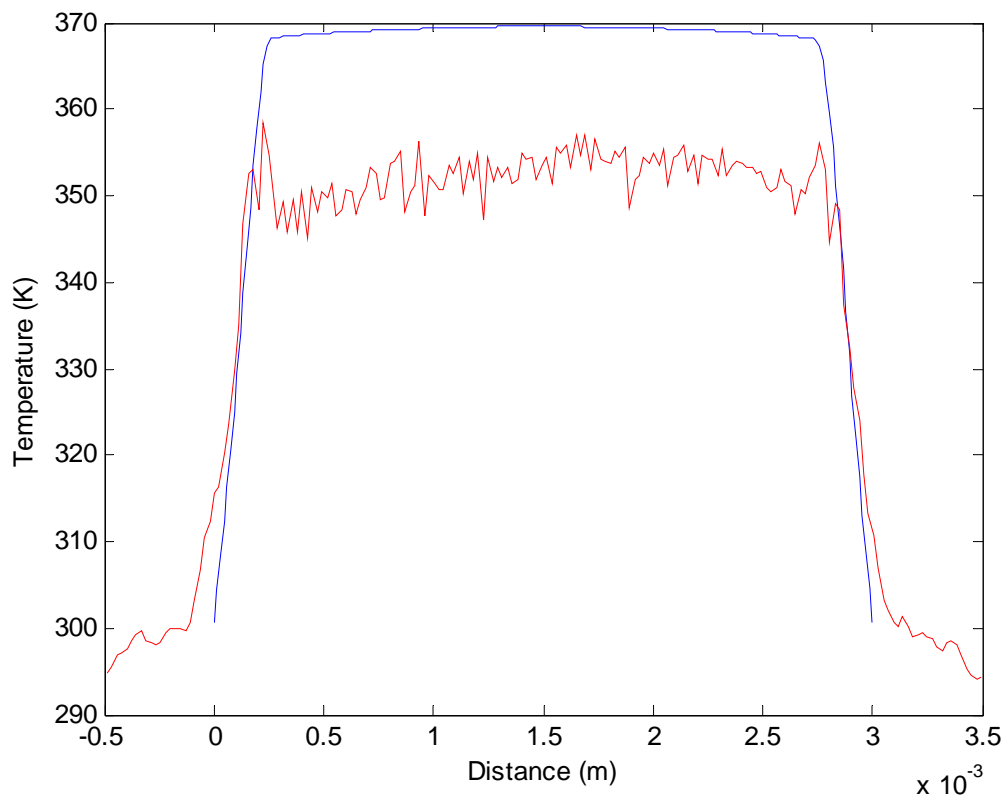


Figure Annex -40: 15-30-60-80 design. Temperature profile y applying 5V.

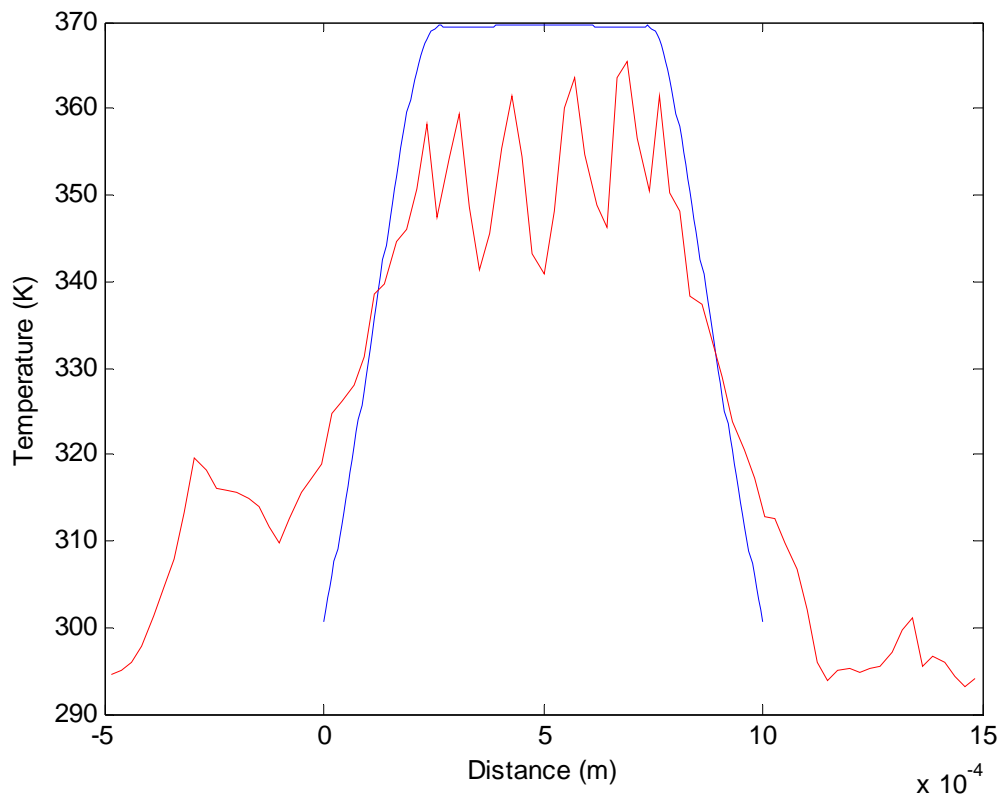


Figure Annex -41: 15-30-60-80 design. Temperature profile x applying 5V.